arXiv:1610.09634v1 [cond-mat.mes-hall] 30 Oct 2016

Theory of surface Andreev bound states and tunneling spectroscopy in three-dimensional chiral superconductors

Shun Tamura[1], Shingo Kobayashi[1,2], Lu Bo[3,4], Yukio Tanaka[1]
[1]*Department of Applied Physics, Nagoya University, Nagoya 464-8603, Japan*
[2]*Institute for Advanced Research, Nagoya University, Nagoya 464-8601, Japan*
[3]*National Graphene Institute, University of Manchester, Manchester, M13 9PL, UK*
[4]*School of Physics and Astronomy, University of Manchester, Manchester, M13 9PL, UK*

We study the surface Andreev bound states (SABSs) and quasiparticle tunneling spectroscopy of three-dimensional (3D) chiral superconductor by changing the surface (interface) misorientation angle of chiral superconductors. We obtain analytical formula of the energy dispersion of SABS for general pair potential when an original 4×4 BdG Hamiltonian can be reduced to be two 2×2 blocks. The resulting SABS for 3D chiral superconductors with pair potential given by $k_z(k_x + ik_y)^\nu$ ($\nu = 1, 2$) has a complicated energy dispersion due to the coexistence of both point and line nodes. We focus on the tunneling spectroscopy of this pairing in the presence of applied magnetic field which induces Doppler shift of quasiparticle spectra. By contrast to previous known Doppler effect in unconventional superconductors, zero bias conductance dip can change into zero bias conductance peak by external magnetic field. We also study SABSs and tunneling spectroscopy for possible pairing symmetries of UPt_3. For this purpose, we extend a standard formula of tunneling conductance of unconventional superconductor junctions in order to treat spin-triplet non-unitary pairings. The magneto tunneling spectroscopy, *i.e.*, tunneling spectroscopy in the presence of magnetic field, can serve as a guide to determine the pairing symmetry of this material.

I. INTRODUCTION

The surface Andreev bound state (SABS) is one of the key concepts to feature unconventional superconductors[1]. Various types of SABS have been revealed in two-dimensional (2D) unconventional superconductors up to now[2,3]. It is known that flat band SABS exists in a spin-singlet d-wave superconductor[4] which is protected by a topological invariant defined in bulk Hamiltonian[2,5]. The ubiquitous presence of this zero energy SABS manifests itself as a zero bias conductance peak (ZBCP) in the tunneling spectroscopy of high T_c cuprate[6–12]. There has been interest in the spin-triplet p-wave superconductor[13,14] with flat band SABS and sharp ZBCP, similar to the d-wave case[15–17]. Apart from flat bands, it is known that chiral p-wave superconductor hosts SABS with a linear dispersion as a function of momentum parallel to the edge, resulting in a much broad ZBCP[17–21].

To distinguish among pairing symmetries, the magneto tunneling spectroscopy, *i.e.*, the tunneling spectroscopy in the presence of applied magnetic field provides a powerful tool. Under applied magnetic field, the shift of quasiparticle energy spectrum which is proportional to the the transverse momentum is generally known as Doppler effect[9,22]. It has been shown that the splitting of ZBCP occurs in d-wave superconductor junctions due to this[9,22]. In contrast, for spin-triplet p-wave cases, ZBCP does not split into two[16] since the perpendicular injection of quasiparticle contributes to the tunneling conductance dominantly. For the perpendicular injection, the component of the Fermi velocity parallel to the interface is zero and there is no energy shift of the quasiparticles. Therefore we can distinguish between d and p-wave pairing with the magneto tunneling spectroscopy[23]. For chiral p-wave superconductor, the magnitude of ZBCP is enhanced or suppressed depending on which direction magnetic field is applied[16]. It also exhibits different features of the magneto tunneling spectroscopy between chiral and helical superconductors, where both of these superconductors have similar broad ZBCP without magnetic field[24]. In any case, ZBCP generated from zero bias conductance dip by applying magnetic field has not been found.

For three-dimensional (3D) unconventional superconductors, the energy dispersion of SABS becomes more complicated[13,25–36]. Recently, SABS of 3D chiral superconductors has been studied[37], where pair potential is given by $\Delta_0 k_z(k_x + ik_y)^\nu / k_{\rm F}^{\nu+1}$ with nonzero integer ν. These pairing symmetries are relevant to typical heavy fermion superconductors with $\nu = 1$ and $\nu = 2$, corresponding to the candidate pairing symmetry of URu_2Si_2[38–41] and UPt_3[42–47] respectively. The simultaneous presence of line and point nodes gives rise to exotic SABS. It has been shown that flat band SABS is found to be fragile against the surface misorientation angle α as shown in Fig. 1. Although the topological natures of flat band SABS has been clarified[37], the overall features of the energy dispersion as SABS has not been systematically analyzed. Thus, it is a challenging issue to identify 3D pairing states theoretically in terms of magneto tunneling spectroscopy.

In this paper, we study the SABS and quasiparticle tunneling spectroscopy of 3D chiral superconductors by changing the surface (interface) misorientation angle α. For this purpose, we analytically derive a formula of the energy dispersion of SABS available for general pair potential when original 4×4 matrix of a Bogoliubov-de Gennes (BdG) Hamiltonian can be decomposed into two blocks of 2×2 matrices. We apply this formula for

3D chiral superconductor with pair potential given by $\Delta_0 k_z(k_x+ik_y)^\nu/k_{\rm F}^{\nu+1}$ ($\nu=1,2$). The resulting SABS has a complex momentum dependence due to the coexistence of point and line nodes. SABSs arising from topological and non-topological are found to be coexisted. The number of branches of the energy dispersion of SABS with topological origin can be classified by ν for various α. On the other hand, if we apply our formula for 2D-like chiral superconductor with pair potential given by $\Delta_0(k_x+ik_y)^\nu/k_{\rm F}^\nu$ ($\nu=1,2$), the number of branches of SABS is equal to 2ν, where pair potential has only point nodes.

In order to distinguish two 3D chiral superconductors with different ν, we calculate the tunneling conductance of normal metal / insulator / chiral superconductor junctions in the presence of applied magnetic field which induces Doppler shift. The obtained angle resolved conductance has a complicated momentum dependence reflecting on the dispersion of SABS for nonzero α. Differently from previous studies of Doppler effect on tunneling conductance, zero bias conductance dip can evolve into zero bias conductance peak by applying magnetic field. This unique feature stems from the complex nodal structures of the pair potential where both line and point nodes coexist. Furthermore, we focus on four possible candidates of the pairing symmetry of UPt_3, where momentum dependence of the pair potentials are proportional to $k_z(k_x+ik_y)^2 d_z$, $(5k_z^2-k_{\rm F}^2)(k_x+ik_y)d_z$, $(5k_z^2-k_{\rm F}^2)(d_y k_x+d_z k_y)$, and $f+p$-wave belonging to E_{2u} representation. Here, we derive a general formula of tunneling conductance which is available even for non-unitary spin-triplet superconductors. We show that these four pairings can be classified by using magneto tunneling spectroscopy. Thus, our theory serves as a guide to determine the pairing symmetry of UPt_3.

The organization of this paper is as follows. In section II, we explain the model and formulation. We analytically derive a formula of the energy dispersion of SABS available for general pair potential when original 4×4 matrix of BdG Hamiltonian is decomposed into two blocks of 2×2 matrices. We also derive a general conductance formula available even for non-unitary spin-triplet pairing cases. Besides these, to understand the topological origin of SABS, we calculate winding number. In section III A, based on above formula, we calculate SABS and tunneling conductance for 3D chiral superconductor for various α. As a reference, we also calculate SABS for 2D-like chiral superconductor. In section III B, we calculate tunneling conductance in the presence of external magnetic field so called magneto tunneling spectroscopy. In section III C, we study SABS and tunneling conductance for promising pairing symmetries of UPt_3. In section IV, we summarize our results.

II. MODEL AND METHOD

In this section, we introduce the mean field Hamiltonian of 3D chiral superconductors. We derive an analytical formula for SABS when the original 4×4 BdG Hamiltonian can be reduced to be two blocks of 2×2 matrices. We calculate the tunneling conductance in the presence of an external applied magnetic field. In order to study the case of non-unitary spin-triplet pairings, we derive an analytical formula for the tunneling conductance. The bulk BdG Hamiltonian is given as follows,

$$\mathcal{H}=\sum_{\mathbf{k}}\Psi^\dagger(\mathbf{k})H(\mathbf{k})\Psi(\mathbf{k}), \tag{1}$$

$$H(\mathbf{k})=\begin{pmatrix}\hat{\varepsilon}(\mathbf{k}) & \Delta(\mathbf{k})\\ \Delta^\dagger(\mathbf{k}) & -\hat{\varepsilon}(-\mathbf{k})\end{pmatrix}, \tag{2}$$

$$\Psi(\mathbf{k})=(c_{\mathbf{k},\uparrow},c_{\mathbf{k},\downarrow},c^\dagger_{-\mathbf{k},\uparrow},c^\dagger_{-\mathbf{k},\downarrow})^{\rm T}, \tag{3}$$

where $\hat{\varepsilon}(\mathbf{k})=\mathrm{diag}[\varepsilon(\mathbf{k}),\varepsilon(\mathbf{k})]$ and $\Delta(\mathbf{k})$ are 2×2 matrices. Here, $\varepsilon(\mathbf{k})$ denotes the energy dispersion $\hbar^2\mathbf{k}^2/(2m)-\mu$ in the normal state. For spin-triplet pairing, pair potential is given by

$$\Delta=\mathbf{d}\cdot\boldsymbol{\sigma}i\sigma_2, \tag{4}$$

by using a $\mathbf{d}$-vector, where $(\sigma_1,\sigma_2,\sigma_3)=\boldsymbol{\sigma}$ are the pauli matrices. We consider normal metal ($z<0$)/superconductor ($z>0$) junctions with a flat interface shown in Fig. 1. The momentum parallel to the interface $\mathbf{k}_\parallel=(k_x,k_y)$ becomes a good quantum number.

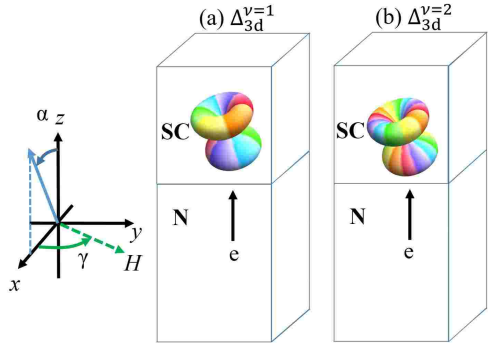

FIG. 1. We mainly consider above two types of normal (N) -superconductor (SC) junctions. Here α is the misorientation angle from k_z axis. Magnetic field is applied in $x-y$ plane rotated from x axis by γ.

In the following, we explain eight-types of pair potentials and corresponding formula for tunneling conductance and SABS. In Sec. II A, we explain the case when the BdG Hamiltonian can be reduced to be 2×2 form [$\Delta_{3d}^{\nu=0,1,2}$, $\Delta_{2d}^{\nu=1,2}$ and $\Delta_{E_{1u}}^{\rm chiral}$]. In Sec. II B, we explain the case where 4×4 BdG Hamiltonian can not be reduced to be two 2×2 blocks [$\Delta_{E_{1u}}^{\rm planar}$ and $\Delta_{E_{2u}}^{f+p}$]. In Sec. II C, we briefly summarize the zero-energy SABS (ZESABS) stemming from topological numbers.

A. 2×2 BdG Hamiltonian

In this subsection, we introduce pair potentials for 3D and 2D-like chiral superconductors. We derive a formula of SABS where the BdG Hamiltonian can be reduced to be 2×2 matrices. $\Delta(\mathbf{k})$ takes

$$\Delta^{\nu}_{\rm 3d}(\mathbf{k}) = \begin{cases} \tilde{\Delta}^{\nu}_{\rm 3d} i\sigma_2 & \nu : \text{odd}, \\ \tilde{\Delta}^{\nu}_{\rm 3d}\sigma_3 i\sigma_2 & \nu : \text{even}, \end{cases} \tag{5}$$

$$\Delta^{\nu}_{\rm 2d}(\mathbf{k}) = \begin{cases} \tilde{\Delta}^{\nu}_{\rm 2d}\sigma_3 i\sigma_2 & \nu : \text{odd}, \\ \tilde{\Delta}^{\nu}_{\rm 2d} i\sigma_2 & \nu : \text{even}, \end{cases} \tag{6}$$

$$\Delta^{\rm chiral}_{E_{1u}}(\mathbf{k}) = \tilde{\Delta}^{\rm chiral}_{E_{1u}}\sigma_3 i\sigma_2, \tag{7}$$

$$\tilde{\Delta}^{\nu}_{\rm 3d} = \frac{\Delta_0}{r_{{\rm 3d},\nu}k_{\rm F}^{\nu+1}} k'_z (k'_x + ik'_y)^{\nu}, \tag{8}$$

$$\tilde{\Delta}^{\nu}_{\rm 2d} = \frac{\Delta_0}{k_{\rm F}^{\nu}} (k'_x + ik'_y)^{\nu}, \tag{9}$$

$$\tilde{\Delta}^{\rm chiral}_{E_{1u}} = \frac{\Delta_0}{r_{E_{1u}}k_{\rm F}^3}\left(5{k'_z}^2 - k_{\rm F}^2\right)(k'_x + ik'_y), \tag{10}$$

$$k'_x = k_x\cos\alpha - k_z\sin\alpha, \tag{11}$$

$$k'_y = k_y, \tag{12}$$

$$k'_z = k_x\sin\alpha + k_z\cos\alpha, \tag{13}$$

where α is the misorientation angle from k_z axis and $(r_{{\rm 3d},\nu=0}, r_{{\rm 3d},\nu=1}, r_{{\rm 3d},\nu=2}, r_{E_{1u}}) = (1,\ 1/2,\ 2/\sqrt{27},\ 16/(3\sqrt{15}))$ are the normalization factors so that the maximum value of the pair potential becomes Δ_0. Because the direction of the **d**-vector in spin-space does not affect conductance, *i.e.*, conductance is invariant under the spin rotation (Appendix C 4), we fix the direction of the **d**-vector given in Eqs. (5), (6) and (7) for the spin-triplet cases. $\Delta^{\nu}_{\rm 3d}$ and $\Delta^{\nu}_{\rm 2d}$ are chosen in Sec. III A and Sec: III B. We study $\Delta^{\nu=2}_{\rm 3d}$ and $\Delta^{\rm chiral}_{E_{1u}}$ in Sec. III C. Under quasiclassical approximation, the magnitude of wave vector is pinned to the value on the Fermi surface, $k_z = \sqrt{k_{\rm F}^2 - k_x^2 - k_y^2}$. As shown in Fig. 2, $\Delta^{\nu=0}_{\rm 3d}$ has a line node, $\Delta^{\nu}_{\rm 3d}(\nu=1,2)$ has two point nodes and one line node and $\Delta^{\nu}_{\rm 2d}$ $(\nu>0)$ has two point nodes. $\Delta^{\rm chiral}_{E_{1u}}$ has two point nodes and two line nodes. Then,

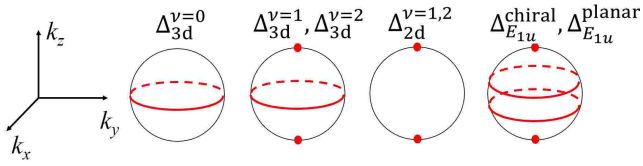

FIG. 2. Schematic illustration of nodal structures of $\Delta(\mathbf{k})$ with $\alpha = 0$. Red points and lines indicate nodes.

we show that the BdG Hamiltonian can be reduced to be 2×2 form for all the cases. For spin-singlet cases ($\Delta^{\nu=1}_{\rm 3d}$ and $\Delta^{\nu=2}_{\rm 2d}$), Eq. (2) is reduced to be

$$\begin{aligned}\mathcal{H}(\mathbf{k}) =& \sum_{\mathbf{k}} \Psi^{\dagger} \begin{pmatrix} \varepsilon(\mathbf{k}) & 0 & 0 & D \\ 0 & \varepsilon(\mathbf{k}) & -D & 0 \\ 0 & -D^* & -\varepsilon(\mathbf{k}) & 0 \\ D^* & 0 & 0 & -\varepsilon(\mathbf{k}) \end{pmatrix} \Psi \\ =& \sum_{\mathbf{k}} (c^{\dagger}_{\mathbf{k},\uparrow}\, c_{-\mathbf{k},\downarrow}) \begin{pmatrix} \varepsilon(\mathbf{k}) & D \\ D^* & -\varepsilon(\mathbf{k}) \end{pmatrix} \begin{pmatrix} c_{\mathbf{k},\uparrow} \\ c^{\dagger}_{-\mathbf{k}\downarrow} \end{pmatrix} \\ &+ \sum_{\mathbf{k}} (c^{\dagger}_{\mathbf{k},\downarrow}\, c_{-\mathbf{k},\uparrow}) \begin{pmatrix} \varepsilon(\mathbf{k}) & -D \\ -D^* & -\varepsilon(\mathbf{k}) \end{pmatrix} \begin{pmatrix} c_{\mathbf{k},\downarrow} \\ c^{\dagger}_{-\mathbf{k}\uparrow} \end{pmatrix}, \end{aligned} \tag{14}$$

with $Di\sigma_2 = \Delta^{\nu=1}_{\rm 3d}$ or $\Delta^{\nu=2}_{\rm 2d}$. For spin-triplet cases ($\Delta^{\nu=0,2}_{\rm 3d}$, $\Delta^{\nu=1}_{\rm 2d}$ and $\Delta^{\rm chiral}_{E_{1u}}$), with a **d**-vector, Eq. (2) becomes

$$\begin{aligned}\mathcal{H}(\mathbf{k}) =& \sum_{\mathbf{k}} \Psi^{\dagger} \begin{pmatrix} \varepsilon(\mathbf{k}) & 0 & 0 & d_3 \\ 0 & \varepsilon(\mathbf{k}) & d_3 & 0 \\ 0 & d_3^* & -\varepsilon(\mathbf{k}) & 0 \\ d_3^* & 0 & 0 & -\varepsilon(\mathbf{k}) \end{pmatrix} \Psi \\ =& \sum_{\mathbf{k}} (c^{\dagger}_{\mathbf{k},\uparrow}\, c_{-\mathbf{k},\downarrow}) \begin{pmatrix} \varepsilon(\mathbf{k}) & d_3 \\ d_3^* & -\varepsilon(\mathbf{k}) \end{pmatrix} \begin{pmatrix} c_{\mathbf{k},\uparrow} \\ c^{\dagger}_{-\mathbf{k}\downarrow} \end{pmatrix} \\ &+ \sum_{\mathbf{k}} (c^{\dagger}_{\mathbf{k},\downarrow}\, c_{-\mathbf{k},\uparrow}) \begin{pmatrix} \varepsilon(\mathbf{k}) & d_3 \\ d_3^* & -\varepsilon(\mathbf{k}) \end{pmatrix} \begin{pmatrix} c_{\mathbf{k},\downarrow} \\ c^{\dagger}_{-\mathbf{k}\uparrow} \end{pmatrix}, \end{aligned} \tag{15}$$

with $(d_3\sigma_3)(i\sigma_2) = \Delta^{\nu=2}_{\rm 3d}$, $\Delta^{\nu=1}_{\rm 2d}$ or $\Delta^{\rm chiral}_{E_{1u}}$.

In the following, we calculate the charge conductance by using the extended version[1,6,48] of Blonder-Tinkham-Klapwijk (BTK) formula[49] for unconventional superconductors[50]. Since we assume that the penetration depth of the magnetic field λ is much larger than the coherence length of the pair potential[22,51], we can neglect the spatial dependence of the magnetic field. Therefore, we can take the vector potential as

$$\mathbf{A} = (-H\lambda\sin\gamma, H\lambda\cos\gamma, 0). \tag{16}$$

Solving the BdG equation with the quasiclassical approximation where μ is much larger than the energy of an injected electron $|eV|$ and $|\Delta(\mathbf{k}_{\parallel})|$, the wave function in the normal metal (N) and the superconductor (S) are obtained

$$\begin{aligned}\Psi^{\rm N}_{\sigma}(z<0,\mathbf{k}_{\parallel}) =& \psi^{\rm N}_{e,\sigma} e^{i\mathbf{k}\cdot\mathbf{r}} \\ &+ \sum_{\sigma'=\pm}\left(a_{\sigma,\sigma'}\psi^{\rm N}_{h,\sigma'}e^{i\mathbf{k}\cdot\mathbf{r}} + b_{\sigma,\sigma'}\psi^{\rm N}_{e,\sigma'}e^{i\tilde{\mathbf{k}}\cdot\mathbf{r}}\right), \end{aligned} \tag{17}$$

$$\Psi^{\rm S}(z>0,\mathbf{k}_{\parallel}) = \sum_{\sigma'=\pm}\left(c_{\sigma'}\psi^{\rm S}_{e,\sigma'}e^{i\mathbf{k}\cdot\mathbf{r}} + d_{\sigma'}\psi^{\rm S}_{h,\sigma'}e^{i\tilde{\mathbf{k}}\cdot\mathbf{r}}\right), \tag{18}$$

and

$$\psi^{\rm N}_{e,\sigma} =(1+\sigma,1-\sigma,0,0)^{\rm T}/2, \tag{19}$$
$$\psi^{\rm N}_{h,\sigma} =(0,0,1+\sigma,1-\sigma)^{\rm T}/2, \tag{20}$$
$$\psi^{\rm S}_{e,\sigma} =[1+\sigma,1-\sigma,(1-\sigma)\rho\Gamma_+,(1+\sigma)\Gamma_+]^{\rm T}/2, \tag{21}$$
$$\psi^{\rm S}_{h,\sigma} =[(1+\sigma)\Gamma_-,(1-\sigma)\rho\Gamma_-,1-\sigma,1+\sigma]^{\rm T}/2, \tag{22}$$
$$\Gamma_+ =\frac{\Delta^*(\mathbf{k})}{\tilde{E}+\sqrt{\tilde{E}^2-|\Delta(\mathbf{k})|^2}}, \tag{23}$$
$$\Gamma_- =\frac{\Delta(\tilde{\mathbf{k}})}{\tilde{E}+\sqrt{\tilde{E}^2-|\Delta(\tilde{\mathbf{k}})|^2}}, \tag{24}$$
$$\tilde{E} =eV-\frac{H}{H_0}\Delta_0\left(\frac{k_y}{k_{\rm F}}\cos\gamma-\frac{k_x}{k_{\rm F}}\sin\gamma\right), \tag{25}$$

with $\tilde{\mathbf{k}}=(k_x,k_y,-k_z)$ and $H_0=\Delta_0/(e\lambda v_{\rm F})$. $\Delta(\mathbf{k})=\tilde{\Delta}^{\nu}_{\rm 3d}(\mathbf{k})$, $\tilde{\Delta}^{\nu}_{\rm 2d}(\mathbf{k})$ or $\tilde{\Delta}^{\rm chiral}_{E_{1u}}(\mathbf{k})$. Here, $\rho=-1$ for $\Delta^{\nu=1}_{\rm 3d}$ and $\Delta^{\nu=2}_{\rm 2d}$ (even parity) and $\rho=1$ for $\Delta^{\nu=0,2}_{\rm 3d}$, $\Delta^{\nu=1}_{\rm 2d}$ and $\Delta^{\rm chiral}_{E_{1u}}$ (odd parity). The coefficients $(a_{\sigma,\sigma'},b_{\sigma,\sigma'},c_\sigma,d_\sigma)$ are determined by the boundary conditions:

$$\Psi^{\rm N}_\sigma(0_-,\mathbf{k}_\parallel) =\Psi^{\rm S}(0_+,\mathbf{k}_\parallel), \tag{26}$$
$$\left.\frac{d\Psi^{\rm S}}{dz}\right|_{z=0_+}-\left.\frac{d\Psi^{\rm N}_\sigma}{dz}\right|_{z=0_-} =\frac{2mU_0}{\hbar^2}\Psi^{\rm N}_\sigma(0_-,\mathbf{k}_\parallel), \tag{27}$$

where the insulating barrier at $z=0$ is simplified as $V(z)=U_0\delta(z)$. The angle resolved conductance is given by[6,48]

$$\sigma_{\rm S}(eV,\mathbf{k}_\parallel) =1+\frac{1}{2}\sum_{\sigma,\sigma'=\pm}\left[|a_{\sigma,\sigma'}|^2-|b_{\sigma,\sigma'}|^2\right]$$
$$=\sigma_{\rm N}\frac{1+\sigma_{\rm N}|\Gamma_+|^2+(\sigma_{\rm N}-1)|\Gamma_+\Gamma_-|^2}{|1+(\sigma_{\rm N}-1)\Gamma_+\Gamma_-|^2}, \tag{28}$$
$$\sigma_{\rm N}(\mathbf{k}_\parallel) =\frac{4\cos^2\theta}{4\cos^2\theta+Z^2}, \tag{29}$$

with $\cos\theta=k_z/k_{\rm F}$ and $Z=2mU_0/(\hbar^2k_{\rm F})$.

In Sec. III A, we discuss SABS with $H=0$ which is determined by requiring the condition that the denominator of Eq. (28) is zero for $Z\to\infty$ ($\sigma_{\rm N}\to 0$). Then, at the energy level of SABS, the denominator of Eq. (28) must satisfy following conditions

$$\mathrm{Re}(\Gamma_+\Gamma_-) =1, \tag{30}$$
$$\mathrm{Im}(\Gamma_+\Gamma_-) =0. \tag{31}$$

In this case, $\sigma_{\rm S}$ becomes two which is the maximum value of angle resolved conductance due to the perfect resonance. We define $E(\mathbf{k}_\parallel)=\tilde{E}$ which satisfies Eq. (30) and Eq. (31).

Here, we derive a general formula of SABS for pair potentials with arbitrary momentum dependence (detailed is explained in Appendix B). There are two cases. For $\mathrm{Im}\left[\Delta^*(\mathbf{k})\Delta(\tilde{\mathbf{k}})\right]\neq 0$, the energy dispersion of SABS $E(\mathbf{k}_\parallel)$ is given by

$$E(\mathbf{k}_\parallel)=\frac{\mathrm{Im}\left[\Delta^*(\mathbf{k})\Delta(\tilde{\mathbf{k}})\right]}{\left|\Delta(\mathbf{k})-\Delta(\tilde{\mathbf{k}})\right|} \tag{32}$$

where $\Delta(\mathbf{k})$ and $\Delta(\tilde{\mathbf{k}})$ must satisfy

$$\left\{|\Delta(\mathbf{k})|^2-\mathrm{Re}\left[\Delta^*(\mathbf{k})\Delta(\tilde{\mathbf{k}})\right]\right\}$$
$$\times\left\{\left|\Delta(\tilde{\mathbf{k}})\right|^2-\mathrm{Re}\left[\Delta^*(\mathbf{k})\Delta(\tilde{\mathbf{k}})\right]\right\}\geq 0. \tag{33}$$

For $\mathrm{Im}\left[\Delta^*(\mathbf{k})\Delta(\tilde{\mathbf{k}})\right]=0$,

$$E(\mathbf{k}_\parallel) =0, \tag{34}$$
$$\text{with } \frac{\Delta(\mathbf{k})}{|\Delta(\mathbf{k})|}=-\frac{\Delta(\tilde{\mathbf{k}})}{|\Delta(\tilde{\mathbf{k}})|}. \tag{35}$$

This formula reproduces all of the known results of SABSs in 2D unconventional superconductors like d-wave[1,4], p-wave[14,17], $d+is$-wave[52,53], chiral p-wave[54] and chiral d-wave ones.

In Sec. III B and Sec. III C, we discuss the normalized conductance given by

$$\sigma(eV)=\frac{\int_{|k_x^2+k_y^2|<k_{\rm F}}dk_xdk_y\sigma_{\rm S}(eV,k_x,k_y)}{\int_{|k_x^2+k_y^2|<k_{\rm F}}dk_xdk_y\sigma_{\rm N}(k_x,k_y)}, \tag{36}$$

which can be measured experimentally[1].

B. 4×4 BdG Hamiltonian

In this subsection, let us explain the case that the BdG Hamiltonian is in the 4×4 form. In Sec. III C, in addition to $\Delta^{\nu=2}_{\rm 3d}$ and $\Delta^{\rm chiral}_{E_{1u}}$, we choose $\Delta^{\rm planar}_{E_{1u}}$ (Fig. 2) and $\Delta^{f+p}_{E_{2u}}$. $\Delta^{\rm planar}_{E_{1u}}$ is a spin-triplet pair potential in unitary state *i.e.* $\mathbf{q}=i\mathbf{d}\times\mathbf{d}^*=0$, while $\Delta^{f+p}_{E_{2u}}$ can incorporate non-unitary case ($\mathbf{q}\neq 0$). $\Delta^{\rm planar}_{E_{1u}}$ is given by

$$\Delta^{\rm planar}_{E_{1u}}(\mathbf{k}) =\frac{\Delta_0}{r_{E_{1u}}k_{\rm F}^3}\left(5{k'_z}^2-k_{\rm F}^2\right)(ik'_x\sigma_0+k'_y\sigma_1). \tag{37}$$

It is noted that time-reversal symmetry is not broken for $\Delta^{\rm planar}_{E_{1u}}$ but $\Delta^{\rm chiral}_{E_{1u}}$ does not have time reversal symmetry.

$\Delta^{f+p}_{E_{2u}}$ is the combination of chiral p-wave and f-wave pairings. The $\mathbf{d}$-vector of $\Delta^{f+p}_{E_{2u}}$ is given by

$$\mathbf{d} =\frac{\Delta_0}{r^{f+p}}\left\{\delta\frac{1}{k_{\rm F}}\left[\left(k'_x+i\eta k'_y\right)d_x+i\left(\eta k'_x+ik'_y\right)d_y\right]\right.$$
$$\left.+\frac{1}{k_{\rm F}^3}\left[k'_z({k'_x}^2-{k'_y}^2)+2i\eta k'_zk'_xk'_y\right]d_z\right\}, \tag{38}$$

where δ is considered to be small[55] and r^{f+p} is a normalized factor which is determined numerically so that

the maximum value of the pair potential becomes Δ_0. If $(\eta, \delta) = (1, 0)$ is satisfied, we obtain $\Delta^{f+p}_{E_{1u}} = \Delta^{\nu=2}_{3\mathrm{d}}$. The position of nodes of this f+p-wave pairing depends on the value of η and δ. If $\delta = 0$ is satisfied (Fig. 3), there are two cases. In the case of $\eta = 0$ [Fig. 3 (a-i)-(a-iii)], there are three line nodes. For $\eta > 0$ [Fig. 3 (b-i)-(b-iii)], there is a line node and two point nodes. For $\delta > 0$ (Fig. 4), there are three cases. For $\eta < 1$ [Fig. 4 (a-i)-(a-iii)], there are 16 point nodes on $k_y = \pm k_x$ lines [Fig. 4 (a-ii)]. In the case of $\eta = 1$ [Fig. 4 (b-i)-(b-iii)], the position of nodes are the same as that in the case of $\eta > 0$ and $\delta = 0$ [Fig. 3 (b-i)-(b-iii)]. For $\eta > 1$ [Fig. 4 (c-i)-(c-iii)], there are 16 point nodes on lines $k_x k_y = 0$ as shown in Fig. 4 (c-ii).

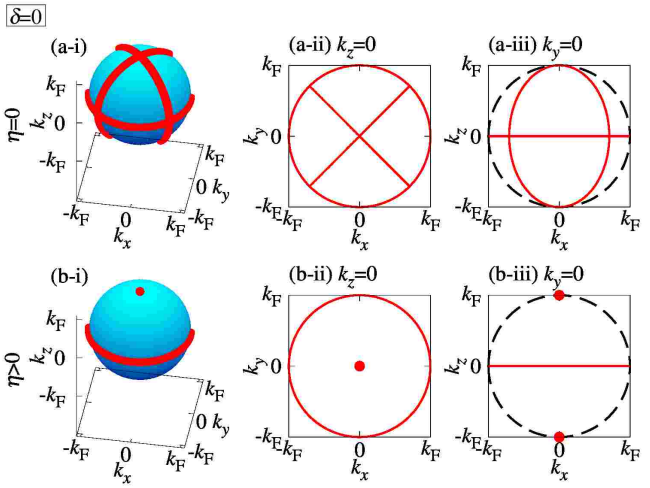

FIG. 3. Red lines and dots express the positions of nodes of the pair potential $\Delta^{f+p}_{E_{2u}}$ for $\delta = 0$. $\eta = 0$ for (a-i)-(a-iii). $\eta > 0$ for (b-i)-(b-iii). (a-ii) and (b-ii) are nodes projected on $k_z = 0$ plane. (a-iii) and (b-iii) are nodes projected on $k_y = 0$ plane. Dashed line in (a-iii) and (b-iii) indicates projected Fermi surface on $k_y = 0$ plane.

The wave function for normal metal side is shown in Eq. (17) with Eq. (19) and Eq. (20) and that for superconducting side is given in Eq. (18) with

$$\left(\psi^{\mathrm{S}}_{e,\uparrow} \;\; \psi^{\mathrm{S}}_{e,\downarrow} \;\; \psi^{\mathrm{S}}_{h,\uparrow} \;\; \psi^{\mathrm{S}}_{h,\downarrow}\right) = \begin{pmatrix} u_e & v_h \\ v_e & u_h \end{pmatrix}, \tag{39}$$

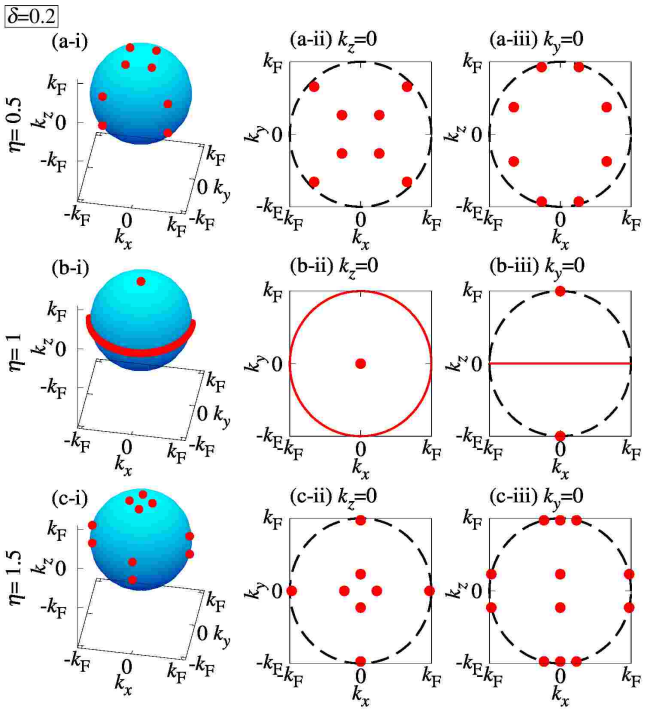

FIG. 4. Red lines and dots express the position of nodes of the pair potential $\Delta^{f+p}_{E_{2u}}$ for $\delta = 0.2$. $\eta = 0.5$ for (a-i)-(a-iii). $\eta = 1$ for (b-i)-(b-iii). $\eta = 1.5$ for (c-i)-(c-iii). (a-ii), (b-ii) and (c-ii) are nodes projected on $k_z = 0$ plane. (a-iii), (b-iii) and (c-iii) are nodes projected on $k_y = 0$ plane. Dashed line in (a-ii), (a-iii), (b-iii), (c-ii) and (c-iii) indicates projected Fermi surface on $k_z = 0$ or $k_y = 0$ plane.

with

$$u_{e(h)} = \frac{[\tilde{E} + \omega_{+(-)}]\sigma_0}{\sqrt{(\tilde{E} + \omega_{+(-)})^2 + \frac{1}{2}\mathrm{Tr}\Delta_{+(-)}\Delta^\dagger_{+(-)}}}, \tag{40}$$

$$v_e = \frac{\Delta^\dagger_+}{\sqrt{(\tilde{E} + \omega_+)^2 + \frac{1}{2}\mathrm{Tr}\Delta_+\Delta^\dagger_+}}, \tag{41}$$

$$v_h = \frac{\Delta_-}{\sqrt{(\tilde{E} + \omega_-)^2 + \frac{1}{2}\mathrm{Tr}\Delta_-\Delta^\dagger_-}}, \tag{42}$$

$$\omega_\pm = \sqrt{\tilde{E}^2 - \frac{1}{2}\mathrm{Tr}\Delta_\pm\Delta^\dagger_\pm}, \tag{43}$$

$$\Delta_+ = \Delta^{\mathrm{planar}}_{E_{1u}}(\mathbf{k}), \tag{44}$$

$$\Delta_- = \Delta^{\mathrm{planar}}_{E_{1u}}(\tilde{\mathbf{k}}), \tag{45}$$

for $\Delta^{\rm planar}_{E_{1u}}(\mathbf{k})$ and

$$
\begin{aligned}
u_e =& a_+[|\mathbf{q}_+|\sigma_0+\mathbf{q}_+\cdot\boldsymbol{\sigma}](\sigma_0+\sigma_3)\\
&+b_+[|\mathbf{q}_+|\sigma_0-\mathbf{q}_+\cdot\boldsymbol{\sigma}](\sigma_0-\sigma_3), \qquad (46)\\
u_h =& a_-[|\mathbf{q}_-|\sigma_0+\mathbf{q}_-\cdot\boldsymbol{\sigma}^*](\sigma_0+\sigma_3)\\
&+b_-[|\mathbf{q}_-|\sigma_0-\mathbf{q}_-\cdot\boldsymbol{\sigma}^*](\sigma_0-\sigma_3), \qquad (47)\\
a_\pm =& \frac{1}{\sqrt{16|\mathbf{q}_\pm|[|\mathbf{q}_\pm|+(\mathbf{q}_\pm)_3]}}\sqrt{\frac{\tilde{E}+\omega_{\pm,p}}{\tilde{E}}}, \qquad (48)\\
b_\pm =& \frac{1}{\sqrt{16|\mathbf{q}_\pm|[|\mathbf{q}_\pm|+(\mathbf{q}_\pm)_3]}}\sqrt{\frac{\tilde{E}+\omega_{\pm,m}}{\tilde{E}}}, \qquad (49)\\
v_e =& \Delta_+^\dagger u_e(\tilde{E}\sigma_0+\hat{\omega}_{+,pm})^{-1}, \qquad (50)\\
v_h =& \Delta_- u_h(\tilde{E}\sigma_0+\hat{\omega}_{-,pm})^{-1}, \qquad (51)\\
\hat{\omega}_{\pm,pm} =& \begin{pmatrix}\omega_{\pm,p} & 0\\ 0 & \omega_{\pm,m}\end{pmatrix}, \qquad (52)\\
\omega_{\pm,p} =& \sqrt{\tilde{E}^2-(|\mathbf{d}_\pm|^2+|\mathbf{q}_\pm|)}, \qquad (53)\\
\omega_{\pm,m} =& \sqrt{\tilde{E}^2-(|\mathbf{d}_\pm|^2-|\mathbf{q}_\pm|)}, \qquad (54)\\
\mathbf{q}_\pm =& i\mathbf{d}_\pm\times\mathbf{d}_\pm^*, \qquad (55)\\
\mathbf{d}_+ =& \mathbf{d}(\mathbf{k}), \qquad (56)\\
\mathbf{d}_- =& \mathbf{d}(\tilde{\mathbf{k}}), \qquad (57)
\end{aligned}
$$

for $\Delta^{f+p}_{E_{2u}}$. The boundary conditions are given in Eq. (26) and Eq. (27). We derive a general formula of conductance which includes the non-unitary case. This formula is similar to that derived in the context of doped topological insulator[56]. In the present case, $\Gamma_\pm$ is available for general pair potential including non-unitary spin-triplet pairing. The derivation of conductance for general pair potential is given in Appendix C.

$$
\begin{aligned}
\sigma_{\rm S} =& \frac{\sigma_{\rm N}}{2}{\rm Tr}\left[\sigma_0-(1-\sigma_{\rm N})\hat{\Gamma}_+^\dagger\hat{\Gamma}_-^\dagger\right]^{-1}\\
&\times\left[1+\sigma_{\rm N}\hat{\Gamma}_+^\dagger\hat{\Gamma}_+ +(\sigma_{\rm N}-1)\,\hat{\Gamma}_+^\dagger\hat{\Gamma}_-^\dagger\hat{\Gamma}_-\hat{\Gamma}_+\right]\\
&\times\left[\sigma_0-(1-\sigma_{\rm N})\hat{\Gamma}_-\hat{\Gamma}_+\right]^{-1}, \qquad (58)
\end{aligned}
$$

with

$$
\begin{aligned}
\hat{\Gamma}_+ =& \frac{\Delta_+^\dagger}{\tilde{E}+\omega_+}, \qquad (59)\\
\hat{\Gamma}_- =& \frac{\Delta_-}{\tilde{E}+\omega_-}, \qquad (60)
\end{aligned}
$$

for $\Delta^{\rm planar}_{E_{1u}}$, and

$$
\begin{aligned}
\hat{\Gamma}_+ =& \frac{\Delta_+^\dagger}{2}\left[\left(\frac{1}{\tilde{E}+\omega_{+,p}}+\frac{1}{\tilde{E}+\omega_{+,m}}\right)\right.\\
&\left.+\left(\frac{1}{\tilde{E}+\omega_{+,p}}-\frac{1}{\tilde{E}+\omega_{+,m}}\right)\frac{\mathbf{q}_+}{|\mathbf{q}_+|}\cdot\boldsymbol{\sigma}\right], \qquad (61)\\
\hat{\Gamma}_- =& \frac{\Delta_-}{2}\left[\left(\frac{1}{\tilde{E}+\omega_{-,p}}+\frac{1}{\tilde{E}+\omega_{-,m}}\right)\right.\\
&\left.+\left(\frac{1}{\tilde{E}+\omega_{-,p}}-\frac{1}{\tilde{E}+\omega_{-,m}}\right)\frac{\mathbf{q}_-}{|\mathbf{q}_-|}\cdot\boldsymbol{\sigma}^*\right], \qquad (62)
\end{aligned}
$$

for $\Delta^{f+p}_{E_{2u}}$. It is noted that the charge conductance for $\Delta^{\rm planar}_{E_{1u}}$ can be written by using $\Delta^{\rm chiral}_{E_{1u}}$.

$$
\begin{aligned}
\sigma_{\rm S}(eV,\mathbf{k}_\parallel) =& \frac{\sigma_{\rm N}}{2}\left[1+\sigma_{\rm N}|\Gamma_+|^2+(\sigma_{\rm N}-1)|\Gamma_+\Gamma_-|^2\right]\\
&\times\left(\frac{1}{S_1}+\frac{1}{S_2}\right), \qquad (63)\\
S_1 =& \frac{1}{|1+(\sigma_{\rm N}-1)\Gamma_+\Gamma_-|^2}, \qquad (64)\\
S_2 =& \frac{1}{|1+(\sigma_{\rm N}-1)\Omega_+\Omega_-|^2}, \qquad (65)\\
\Omega_+ =& \frac{\tilde{\Delta}^{\rm chiral}_{E_{1u}}(\mathbf{k})}{\tilde{E}+\sqrt{\tilde{E}^2-|\tilde{\Delta}^{\rm chiral}_{E_{1u}}(\mathbf{k})|^2}}, \qquad (66)\\
\Omega_- =& \frac{[\tilde{\Delta}^{\rm chiral}_{E_{1u}}(\tilde{\mathbf{k}})]^*}{\tilde{E}+\sqrt{\tilde{E}^2-|\tilde{\Delta}^{\rm chiral}_{E_{1u}}(\tilde{\mathbf{k}})|^2}}, \qquad (67)
\end{aligned}
$$

where $\Gamma_\pm$ in Eq. (64) is the same as Eq. (23) and Eq. (24) with replacing Δ by $\tilde{\Delta}^{\rm chiral}_{E_{1u}}$. SABS is given by Eq. (30), Eq. (31) and

$$
\begin{aligned}
{\rm Re}(\Omega_+\Omega_-) =& 1, \qquad (68)\\
{\rm Im}(\Omega_+\Omega_-) =& 0. \qquad (69)
\end{aligned}
$$

Due to the presence of time-reversal symmetry, the energy level of SABS is given by

$$E(\mathbf{k}_\parallel)=\pm E^{\rm chiral}(\mathbf{k}_\parallel), \qquad (70)$$

where $E^{\rm chiral}(\mathbf{k}_\parallel)$ is the energy level of SABS for $\Delta^{\rm chiral}_{E_{1u}}$. The normalized conductance is given in Eq. (36).

C. Topological number

In this subsection, we briefly summarize the main discussion about the number of the ZESABSs for $\Delta^\nu_{\rm 2d}$ and $\Delta^\nu_{\rm 3d}$ ($\nu\le 2$)[37]. This result is used in Sec. III A. The ZESABSs for $\Delta^\nu_{\rm 2d}$ are understood only from a two-dimensional topological number (Chern number) and those for $\Delta^\nu_{\rm 3d}$ are understood from a one-dimensional topological number (winding number) and the Chern

number. Similar discussions for $\Delta_{3\mathrm{d}}^{\nu>2}$ and $\Delta_{E_{1u}}^{\mathrm{chiral}}$ are given in Appendix A. For $\Delta_{3\mathrm{d}}^{\nu>2}$ with $0<\alpha<\pi/4$, cylindrical cuts must be used to calculate the Chern number.

Generally, if a Hamiltonian possesses the time reversal symmetry, the winding number can be defined by using a chiral operator $\Gamma=-iCT$ ($C=\sigma_0\tau_1K$: Charge conjugation, $T=i\sigma_2\tau_0K$: Time reversal. σ_i and τ_i are the pauli matrices in spin and Nambu spaces, respectively.) which anticommutes with the Hamiltonian. The winding number is given by[57,58],

$$W(\mathbf{k}_\parallel,\Gamma)=\frac{-1}{4\pi i}\int_{-\infty}^{\infty}dk_\perp \mathrm{Tr}\left[\Gamma H^{-1}(\mathbf{k})\partial_{k_\perp}H(\mathbf{k})\right], \quad (71)$$

where $\mathbf{k}_\parallel$ and $k_\perp$ are wave vectors parallel and perpendicular to a certain surface, respectively. Although $\Delta_{3\mathrm{d}}^{\nu}$ ($\nu\geq 1$) does not have the time reversal symmetry, the BdG Hamiltonian hosts a momentum dependent pseudo time reversal symmetry[37]:

$$U_{\varphi_{\mathbf{k}}}^\dagger T U_{\varphi_{\mathbf{k}}} H(\mathbf{k}) U_{\varphi_{\mathbf{k}}}^\dagger T^\dagger U_{\varphi_{\mathbf{k}}}=H(-\mathbf{k}), \quad (72)$$

with $U_{\varphi_{\mathbf{k}}}=\exp(-i\nu\varphi_{\mathbf{k}}\sigma_0\tau_3/2)$ and $\varphi_{\mathbf{k}}=\tan^{-1}(k_y/k_x)$. Replacing Γ with $\Gamma_{\varphi_{\mathbf{k}}}$, we can define the winding number where $\Gamma_{\varphi_{\mathbf{k}}}$ is given by

$$\Gamma_{\varphi_{\mathbf{k}}}=\begin{cases} U_{\varphi_{\mathbf{k}}}^\dagger\Gamma U_{\varphi_{\mathbf{k}}} & (\nu:\text{ odd}),\\ U_{\varphi_{\mathbf{k}}}^\dagger S_z C T U_{\varphi_{\mathbf{k}}} & (\nu:\text{ even}),\end{cases} \quad (73)$$

with $S_z=\sigma_3\tau_3$.

The Chern number[59] at a fixed $k_{\parallel,1}$ is defined by

$$N(k_{\parallel,1})=\frac{i}{2\pi}\sum_{n\in\mathrm{occ}}\int_{\mathrm{BZ}}dk_\perp dk_{\parallel,2}\epsilon^{ab}\partial_{k_a}\langle u_n(\mathbf{k})|\partial_{k_b}|u_n(\mathbf{k})\rangle, \quad (74)$$

where $|u_n(\mathbf{k})\rangle$ is an eigenstate of $H(\mathbf{k})$ and the summation is taken over all of the occupied states.

These topological numbers connect the number of the ZESABSs by the bulk-boundary correspondence. We show angle resolved zero voltage conductance calculated by using Eq. (28) in Fig. 5 ($\Delta_{2\mathrm{d}}^{\nu}$), Fig. 6 ($\Delta_{3\mathrm{d}}^{\nu=0}$) and Fig. 7 ($\Delta_{3\mathrm{d}}^{\nu=1,2}$). The corresponding energy dispersion of SABS calculated by using Eq. (32)-Eq. (35) are also shown in the same figures and we discuss them in Sec. III A.

TABLE I. Origin of ZESABSs for each pair potential. w and c indicate winding number and Chern number, respectively.

Δ	$\alpha=0$	$0<\alpha<\frac{\pi}{4}$	$\alpha=\frac{\pi}{4}$	$\frac{\pi}{4}<\alpha<\frac{\pi}{2}$	$\alpha=\frac{\pi}{2}$
$\Delta_{2\mathrm{d}}^{\nu}$	$-$	c	c	c	c
$\Delta_{3\mathrm{d}}^{\nu=0}$	w	w	w	w	$-$
$\Delta_{3\mathrm{d}}^{\nu=1}$	w	w	$-$	c	c
$\Delta_{3\mathrm{d}}^{\nu=2}$	w	w	w	w and c	c

The position of a line node or point nodes or both on the Fermi surface for each pair potential are shown in Fig. 5 (a-i)-(a-iii), Fig. 6 (b-i)-(b-v) and Fig. 7 (a-i)-(a-v) and those on the projected k_x-k_y (001) plane are shown in Fig. 5 (b-i)-(b-iii), Fig. 6 (c-i)-(c-v) and Fig. 7 (b-i)-(b-v). For Δ_{3d}^{ν}, the position of a projected line node is given by

$$\frac{k_x^2}{\cos^2\alpha}+k_y^2=k_{\mathrm{F}}^2. \quad (75)$$

The ZESABSs including the spin degrees of freedom for $\Delta_{3\mathrm{d}}^{\nu=0}$ are shown in Fig. 6 (d-i)-(d-v). Angle resolved conductance at zero-bias voltage reflects on the ZESABSs. They are shown in Fig. 5 (d-i)-(d-iii) for $\Delta_{2\mathrm{d}}^{\nu=1}$ and Fig. 5 (g-i)-(g-iii) for $\Delta_{2\mathrm{d}}^{\nu=2}$. They are also shown in Fig. 7 (d-i)-(d-v) for $\Delta_{3\mathrm{d}}^{\nu=1}$ and Fig. 7 (g-i)-(g-v) for $\Delta_{3\mathrm{d}}^{\nu=2}$.

In the case of $\Delta_{3\mathrm{d}}^{\nu=0}$, there are flat band SABSs within the ellipse of Eq. (75) originated from the winding number [Fig. 6 (d-i)-(d-v)]. There are two bands due to spin degrees of freedom. For $\Delta_{3\mathrm{d}}^{\nu\geq 1}$ with $\alpha=0$, there are flat band SABSs within $k_x^2+k_y^2\leq k_{\mathrm{F}}^2$ [See Fig. 7 (d-i) and (g-i)]. The origin of these flat bands are explained from the winding number. On the other hand, there is no ZESABS for $\Delta_{2\mathrm{d}}^{\nu}$ with $\alpha=0$ (not shown). In the case of $\alpha=\pi/4$ for $\Delta_{3\mathrm{d}}^{\nu=1}$ there is no ZESABS [Fig. 7 (d-iii)], while they exist on $k_y=0$ for $\alpha=\pi/4$ with $\Delta_{3\mathrm{d}}^{\nu=2}$ [Fig. 7 (g-iii)]. In other cases, (except for $\alpha=0,\pi/4$ for $\Delta_{3\mathrm{d}}^{\nu\geq 1}$ and $\alpha=0$ for $\Delta_{2\mathrm{d}}^{\nu}$), the number of the arc shaped ZESABSs which terminate at projected point nodes on k_x-k_y plane is 2ν where two comes from the spin degeneracy [see Fig. 5 (d-i)-(d-iii), (g-i)-(g-iii) and Fig. 7 (d-ii), (d-iv), (d-v), (g-ii), (g-iv) and (g-v)]. For $\Delta_{2\mathrm{d}}^{\nu}$, the number of ZESABSs connecting two projected point nodes is 2ν.

In addition to the ZESABSs which terminate at the projected point nodes, the ZESABSs located on $k_y=0$ and $\cos\alpha>|k_x|$ appears for $\pi/4<\alpha\leq\pi/2$ with $\Delta_{3\mathrm{d}}^{\nu=2}$.

For $0<\alpha<\pi/4$ with $\Delta_{3\mathrm{d}}^{\nu=1,2}$, the ZESABSs are originated from the winding number. For $\pi/4<\alpha<\pi/2$ with $\Delta_{3\mathrm{d}}^{\nu=2}$, the ZESABSs are originated from both the winding number and the Chern number. The ZESABSs for $\Delta_{2\mathrm{d}}^{\nu}$ are originated from the Chern number for arbitrary α (Table I).

III. RESULTS

A. Andreev bound state with $H=0$

In this subsection, we calculate the energy dispersion of SABS with $H=0$ for two cases of chiral superconductors where pair potentials are given by $(k_x'+ik_y')^\nu$ ($\nu=1,2$) and $k_z'(k_x'+ik_y')^\nu$ ($\nu=1,2$). Although the ZESABS has been discussed in the previous paper[37], the energy dispersion of SABS with nonzero energy has not been clarified at all. To resolve this problem, we calculate the energy spectrum of SABS from Eqs. (32) to (35).

Here, we apply this formula for normal metal / 3D chiral superconductor junctions. First, we calculate the energy dispersion and tunneling conductance of the 2D-like chiral superconductor where the pair potential is given

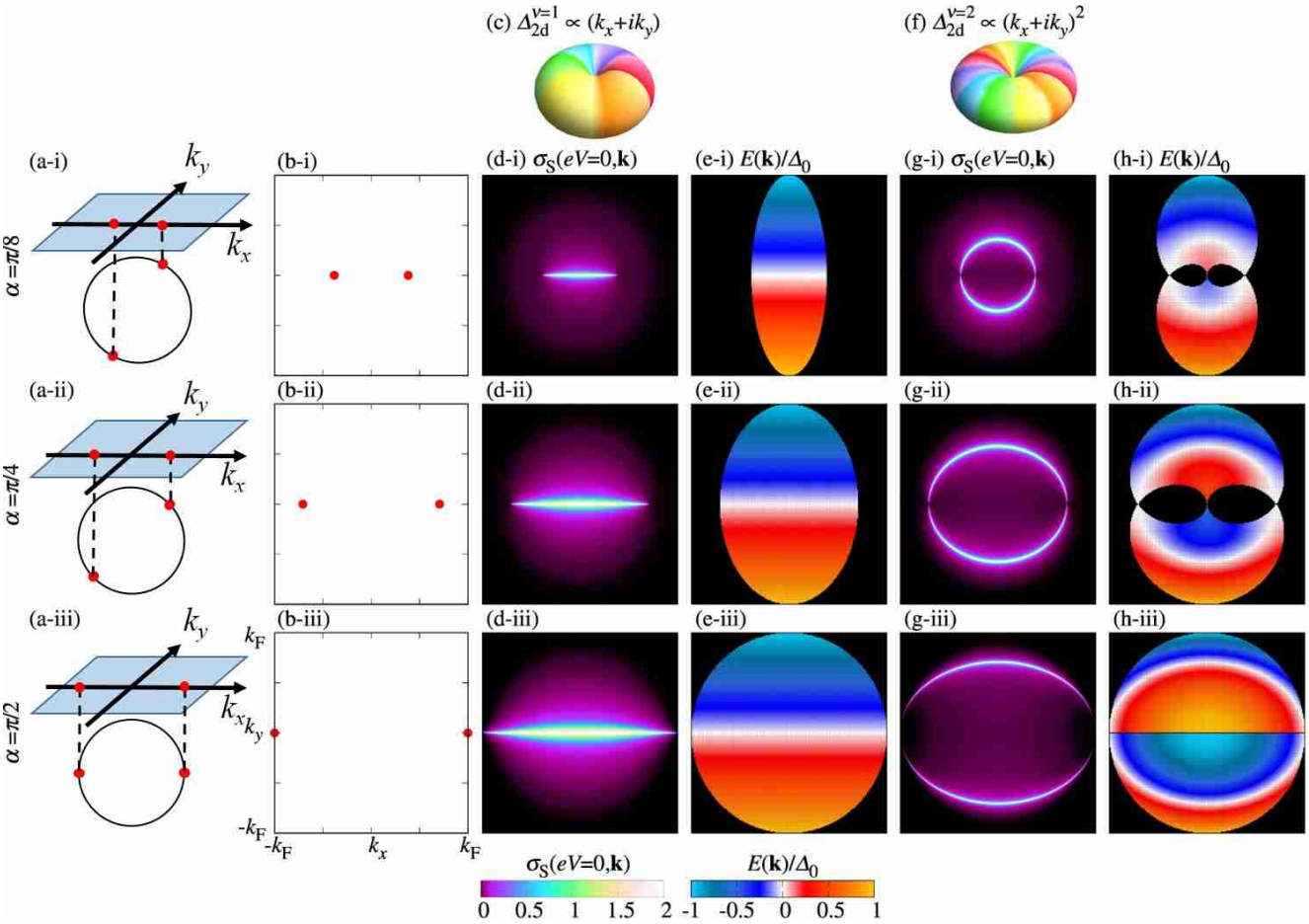

FIG. 5. Schematic illustration of point nodes (red dots) for (a-i) $\alpha = \pi/8$, (a-ii) $\alpha = \pi/4$ and (a-iii) $\alpha = \pi/2$. Point nodes on $k_x - k_y$ plane corresponding to (a-i)-(a-iii) are shown in (b-i)-(b-iii). Schematic picture of pair potential for (c) $\Delta_{2d}^{\nu=1}$ and (f) $\Delta_{2d}^{\nu=2}$. The angle resolved zero-bias conductance $\sigma_S(eV = 0, \mathbf{k})$ at $Z = 6$ are plotted as a function of k_x and k_y for $\Delta_{2d}^{\nu=1}$ (d-i) $\alpha = \pi/8$, (d-ii) $\alpha = \pi/4$, and (d-iii) $\alpha = \pi/2$. Similar plots for $\Delta_{2d}^{\nu=2}$ for (g-i) $\alpha = \pi/8$, (g-ii) $\alpha = \pi/4$, and (g-iii) $\alpha = \pi/2$. The energy dispersions of SABS $E(\mathbf{k}_\parallel)$ are plotted as a function of k_x and k_y for $\Delta_{2d}^{\nu=1}$ [(e-i)-(e-iii)] and for $\Delta_{2d}^{\nu=2}$ [(h-i)-(h-iii)].

by $\Delta_{2d}^{\nu} \propto (k'_x + ik'_y)^\nu$. The angle resolved zero bias conductance and the energy dispersion of SABS are shown in Fig. 5. For $\nu = 1$, angle resolved zero voltage conductance is plotted from Fig. 5 (d-i) to (d-iii). As explained in Sec. II C, we can see that the ZESABS appears on the line connecting two point nodes at $k_y = 0$. The region of the ZESABS spreads with the increase of α. The corresponding energy dispersion of SABS $E(\mathbf{k}_\parallel)$ is shown in Fig. 5 (e-i)-(e-iii). In this case, we can obtain analytical formula of SABS given by

$$E(\mathbf{k}_\parallel) = -\Delta_0 k_y/k_F \tag{76}$$

$$\text{with } k_x^2 + k_y^2 \sin^2\alpha \le k_F^2 \sin^2\alpha. \tag{77}$$

The number of SABSs including zero energy state is two (including the spin degeneracy). For $\nu = 2$, two branches of the ZESABS appear as arcs on the $k_x - k_y$ plane connecting two point nodes as shown from Fig. 5 (g-i) to (g-iii). The length of arcs increases with the increase of α. The corresponding $E(\mathbf{k}_\parallel)$ is shown from Fig. 5 (h-i) to (h-iii). The number of SABSs including zero energy state is four. Then, we can summarize that the number of SABSs stemming from topological origin including the ZESABS is 2ν.

Next, we focus on the 3D chiral superconductor case [$\Delta_{3d}^{\nu} \propto k'_z(k'_x + ik'_y)^\nu$ including p-wave case]. In p-wave ($\nu = 0$) case, (see Fig. 6), the energy dispersion of SABS is shown from Fig. 6 (d-i) to (d-v). It is located inside the ellipse given by Eq. (75) and there only appears the ZESABS.

In $\nu = 1$ and 2 cases, (see Fig. 7), angle resolved zero voltage conductance is plotted in Fig. 7 (d-i)-(d-v) for $\nu = 1$ and the corresponding energy dispersion of SABS $E(\mathbf{k}_\parallel)$ is shown in Fig. 7 (e-i)-(e-v). We can derive an analytical formula of $E(\mathbf{k}_\parallel)$ for $\alpha = \pi/4$ and $\alpha = \pi/2$

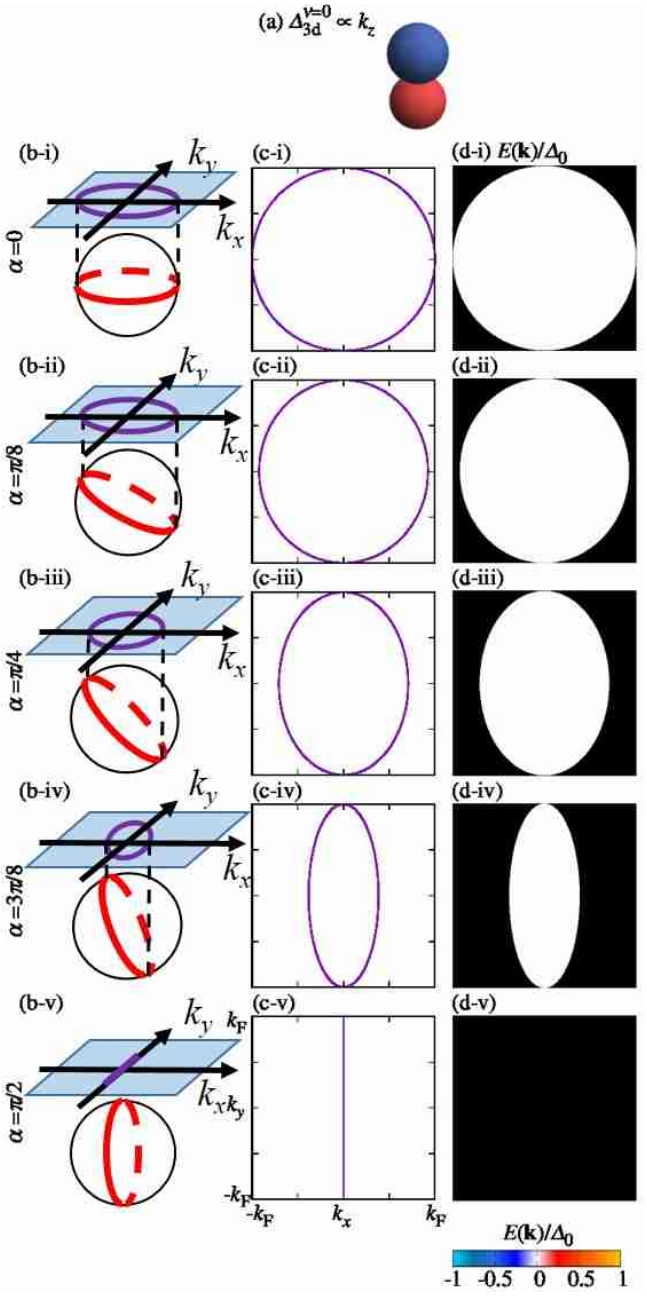

FIG. 6. Schematic illustration of pair potential for (a) $\Delta_{3d}^{\nu=0}$. Schematic illustration of a line node(red line) for (b-i) $\alpha = 0$, (b-ii) $\alpha = \pi/8$, (b-iii) $\alpha = \pi/4$, (b-iv) $\alpha = 3\pi/8$ and (b-v) $\alpha = \pi/2$. The line node on $k_x - k_y$ plane corresponding to (b-i)-(b-v) are shown in (c-i)-(c-v). The energy dispersion of SABS $E(\mathbf{k}_\parallel)$ for given α are plotted as a function of k_x and k_y [(d-i)-(d-v)].

given by

$$E(\mathbf{k}_\parallel) = -\frac{\Delta_0}{2\sqrt{2}r_{3\mathrm{d},\nu=1}}\left(\hat{k}_x + \sqrt{1-\hat{k}_x^2-\hat{k}_y^2}\right)^2 \times \left(\hat{k}_x - \sqrt{1-\hat{k}_x^2-\hat{k}_y^2}\right)\mathrm{sgn}(k_y), \tag{78}$$

$$\text{with } 2k_x^2 + k_y^2 \le k_\mathrm{F}^2, \tag{79}$$

where $\hat{k}_i = k_i/k_\mathrm{F}$ $(i = x, y, z)$ and

$$E(\mathbf{k}_\parallel) = -\frac{\Delta_0}{r_{3\mathrm{d},\nu=1}}\hat{k}_y \mid \hat{k}_x \mid, \tag{80}$$

respectively. The number of SABSs n_ABS which includes the ZESABS is classified whether (k_x, k_y) is inside the ellipse [Eq. (75)] or not. Inside the ellipse, n_ABS becomes two (including the spin degeneracy) for $\alpha < \pi/4$ and zero for $\alpha \ge \pi/4$. On the other hand, outside the ellipse, n_ABS becomes zero for $\alpha \le \pi/4$ and four for $\alpha > \pi/4$. Besides this SABS with topological origin, inside the ellipse nonzero non-topologically SABS which dons not include the zero-energy state exists.

Next, we focus on $\nu = 2$ case. Angle resolved zero voltage conductance is plotted in Fig. 7 (g-i)-(g-v) and the corresponding energy dispersion of SABS $E(\mathbf{k}_\parallel)$ is shown in Fig. 7 (h-i)-(h-v). We can derive an analytical formula of $E(\mathbf{k}_\parallel)$ for $\alpha = \pi/2$ given by

$$E(\mathbf{k}_\parallel) = \frac{\Delta_0}{r_{3\mathrm{d},\nu=2}}\mathrm{sgn}(\hat{k}_y)|\hat{k}_x|(1-\hat{k}_x^2-2\hat{k}_y^2). \tag{81}$$

n_ABS is also classified whether (k_x, k_y) is inside the ellipse or not. Inside the ellipse, n_ABS becomes two for $\alpha = 0$. For $0 < \alpha < \pi/4$, n_ABS is four and $n_\mathrm{ABS} = 2$ for $\alpha \ge \pi/4$. On the other hand, outside the ellipse, n_ABS becomes zero for $\alpha \le \pi/4$ and eight for $\alpha > \pi/4$. Beside this SABS with topological origin, nonzero non-topologically SABS also exists.

We further calculate n_ABS up to $\nu = 4$ (The ZESABSs for $0 < \alpha < \pi/4$ with $\nu = 3, 4$ are discussed in Appendix A 2). The summary of n_ABS is shown in Table. II as a function of ν. We can also obtain the analytical formula of $E(\mathbf{k}_\parallel)$ both for the 3D and 2D-like chiral superconductors for $\alpha = \pi/2$. The results are summarized in Table III.

B. Conductance with magnetic field

In this subsection, we discuss the magnetic field dependence of conductance. We consider the situation where magnetic field is applied in $x - y$ plane [Eq. (16)] and is rotated along z axis by γ (Fig. 8). It is known that the applied magnetic field shifts the energy of quasiparticle as a Doppler effect[22]. In usual case, ZBCP without magnetic field is split into two[22,51] or height of ZBCP is suppressed[16,60] by Doppler effect. For chiral p-wave superconductor, the height of ZBCP is controlled by the

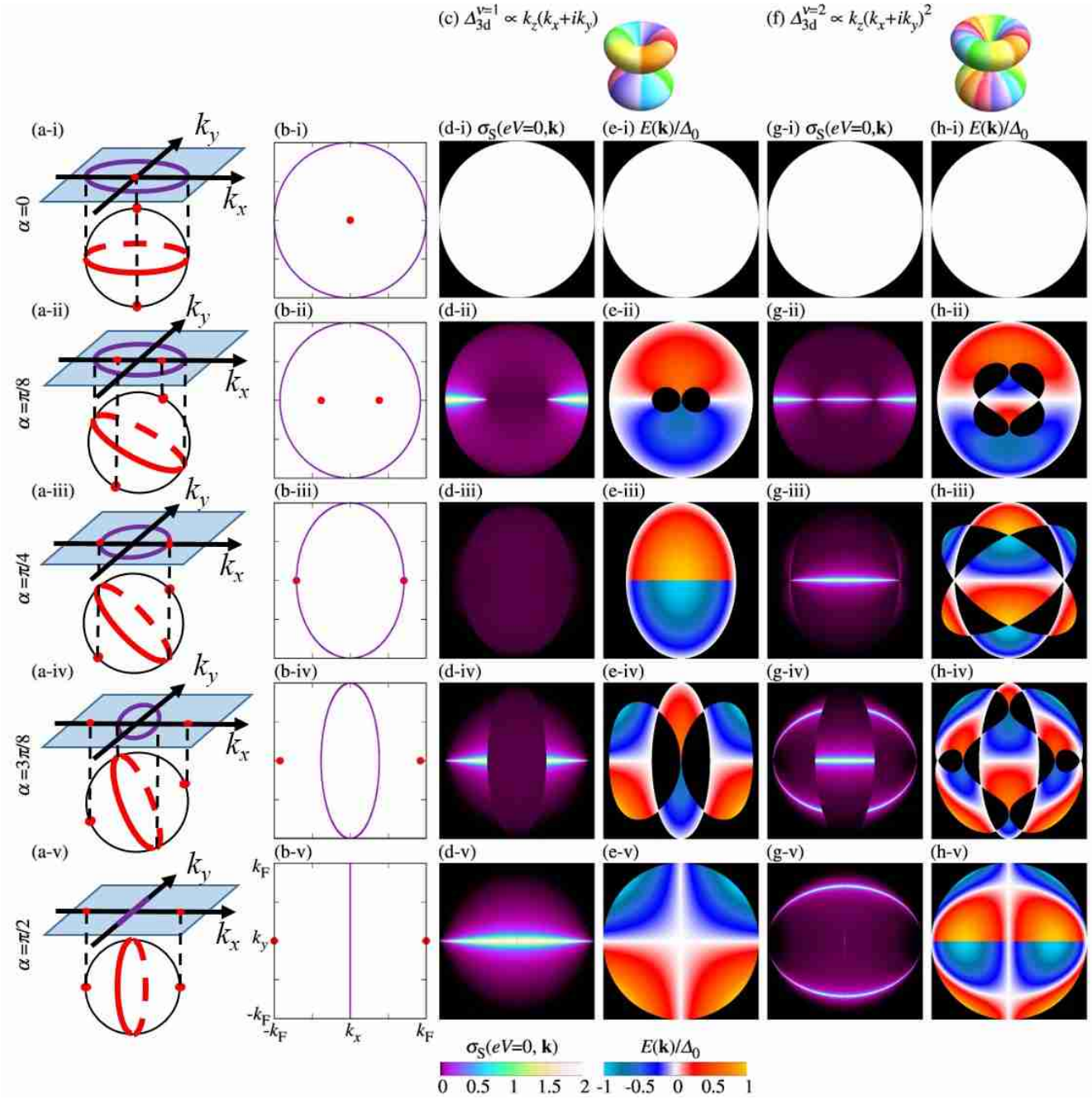

FIG. 7. Schematic illustration of point nodes and a line node(red dots and line) for (a-i) $\alpha = 0$, (a-ii) $\alpha = \pi/8$, (a-iii) $\alpha = \pi/4$, (a-iv) $\alpha = 3\pi/8$ and (a-v) $\alpha = \pi/2$. Point nodes and a line node on $k_x - k_y$ plane corresponding to (a-i)-(a-v) are shown in (b-i)-(b-v). Schematic illustration of pair potential for (c) $\Delta_{3d}^{\nu=1}$ and (f) $\Delta_{3d}^{\nu=2}$. The angle resolved zero bias conductance $\sigma_S(eV = 0, \mathbf{k})$ with $Z = 6$ is plotted as a function of k_x and k_y for $\Delta_{3d}^{\nu=1}$ [(d-i)-(d-v)] and for $\Delta_{3d}^{\nu=2}$ [(g-i)-(g-v)]. The energy dispersion of SABS $E(\mathbf{k}_\parallel)$ for given α are plotted as a function of k_x and k_y for $\Delta_{3d}^{\nu=1}$ [(e-i)-(e-v)] and for $\Delta_{3d}^{\nu=2}$ [(h-i)-(h-v)].

direction of the applied magnetic field[60]. By contrast to this standard knowledge, we show a unique behavior that Doppler effect can change the line shape of conductance from zero bias dip to zero bias peak as shown in Fig. 9 ($\Delta_{3d}^{\nu=1}$) and Fig. 11 ($\Delta_{3d}^{\nu=2}$).

For $\alpha = \pi/8$ with $H = 0$ [Fig. 9 (f), Fig. 11 (f)], σ near $eV = 0$ has a concave shape, and it changes into ZBCP for $H/H_0 = 0.1$ with $\gamma = \pi$ [Fig. 9 (c), Fig. 11 (c)]. Doppler effect shifts the energy dispersion of SABS along the vector $(\cos\gamma, \sin\gamma, 0)$ as shown in Fig. 8. SABS which is slightly above or below zero energy for $H = 0$ can contribute to zero bias conductance in the presence of the magnetic field. For $\nu = 1$, in Fig. 9 (e), there is no ZESABS. However, in the presence of the magnetic

TABLE II. The number of SABS ($n_{\rm ABS}$) which cross zero-energy for $\Delta^{\nu}_{\rm 3d}$. It is classified by inside or outside of the ellipse [Eq. (75)] corresponding to projected line node [Fig. 6 (c-i)-(c-v) and Fig. 7 (b-i)-(b-v)]. $n_{\rm ABS}$ is counted including the spin degeneracy. The dash "-" means there is no area inside or outside the ellipse [Fig. 6 (c-i) and (c-v)].

	$n_{\rm ABS}$	
α	Inside ellipse	Outside ellipse
0	2	–
$0<\alpha<\frac{\pi}{4}$	2ν	0
$\alpha=\pi/4$	$2(\nu-1)$	0
$\frac{\pi}{4}<\alpha<\frac{\pi}{2}$	$2(\nu-1)$	4ν
$\alpha=\pi/2$	–	4ν

TABLE III. The energy dispersion of SABS $E(\mathbf{k}_\parallel)/\Delta_0$ times normalization factor r ($r=r_{3{\rm d},\nu}$ for $\Delta^{\nu}_{\rm 3d}$ and $r=1$ for $\Delta^{\nu}_{\rm 2d}$) at $\alpha=\pi/2$ is shown for $\Delta^{\nu}_{\rm 3d}$ and $\Delta^{\nu}_{\rm 2d}$. $\hat{k}_i=k_i/k_{\rm F}(i=x,y,z)$. For the chiral 3D superconductor, the line k_x=0 does not express the energy dispersion of SABS since $\Delta^{\nu}_{\rm 3d}(k_x=0)=0$ is satisfied for $\nu=1,2,3$.

$\Delta(\mathbf{k})$	$E(\mathbf{k}_\parallel)r/\Delta_0$
$k_x(-k_z+ik_y)$	$-\hat{k}_y\lvert\hat{k}_x\rvert$
$(-k_z+ik_y)$	$-\hat{k}_y$
$k_x(-k_z+ik_y)^2$	$\mathrm{sgn}(\hat{k}_y)\lvert\hat{k}_x\rvert(1-\hat{k}_x^2-2\hat{k}_y^2)^{45}$
$(-k_z+ik_y)^2$	$\mathrm{sgn}(\hat{k}_y)(1-\hat{k}_x^2-2\hat{k}_y^2)$
$k_x(-k_z+ik_y)^3$	$-\lvert\hat{k}_x\rvert\hat{k}_y(3-3\hat{k}_x^2-4\hat{k}_y^2)\mathrm{sgn}(1-\hat{k}_x^2-2\hat{k}_y^2)$
$(-k_z+ik_y)^3$	$-\hat{k}_y(3-3\hat{k}_x^2-4\hat{k}_y^2)\mathrm{sgn}(1-\hat{k}_x^2-2\hat{k}_y^2)$

field for $\gamma=\pi$, SABS exists around zero energy near $(k_x,k_y)=(0,\pm k_{\rm F})$ [Fig. 9 (b)]. We can also see the circle near $k_x^2/\cos^2(\pi/8)+k_y^2=k_{\rm F}^2$ of ZESABS in Fig. 9 (a) which does not exist in Fig. 9 (d). On the other hand, if the direction of the magnetic field is opposite, *i.e.*, $\gamma=0$, SABS around zero energy remains to be absent. [Fig. 9 (g) and Fig. 9 (h)]. As seen from Fig. 9 (a), the angle resolved conductance near $(k_x,k_y)=(\pm k_{\rm F},0)$ is enhanced. In Fig. 10 (a), we can see how the ZBCP developes with increasing magnetic field. We can see the generation of ZBCP even for small magnitude of H with $H/H_0=0.01$. The magnitude of zero-bias conductance as a function of H is shown in Fig. 10 (b) and it is approximately linear function of H.

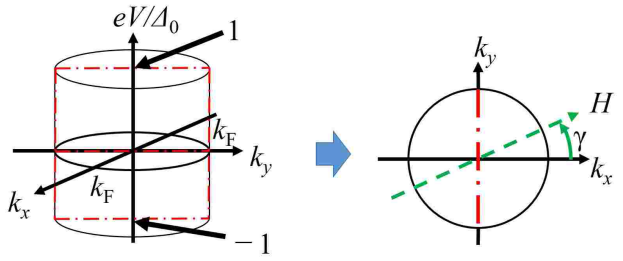

FIG. 8. Dash dotted line (red line) represents a rectangular located at $k_y/k_{\rm F}=[-1,1]$ and $eV/\Delta_0=[-1,1]$ on k_y-eV plane which are used for (b), (e) and (h) in Fig. 9, Fig. 11 and Fig. 13. Dashed line (green line) represents the direction of magnetic field which corresponds to the arrow in Fig. 1.

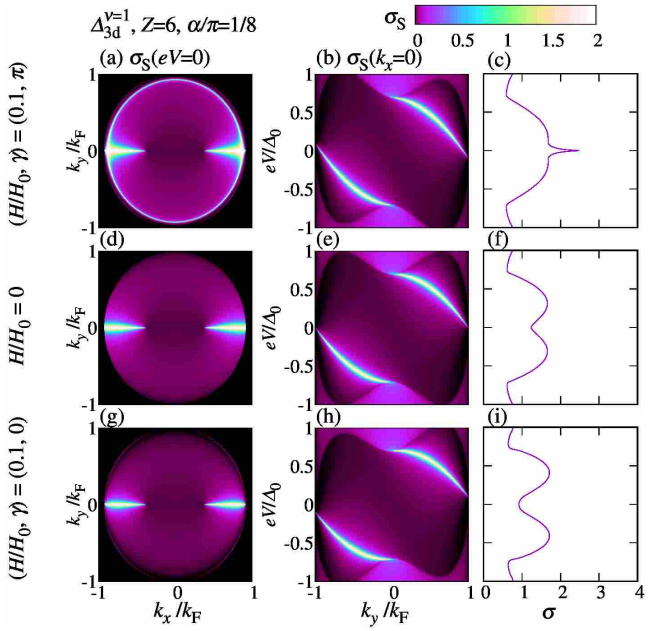

FIG. 9. Angle-resolved conductance $\sigma_{\rm S}(eV,k_x,k_y)$ for $\Delta^{\nu=1}_{\rm 3d}$ with $\alpha=\pi/8$ are plotted as a function of (k_x,k_y) with $eV=0$ [(a), (d), (g)] and (k_y,eV) with $k_x=0$ [(b), (e), (h)] (see Fig. 8) and normalized conductance plotted as a function of eV [(c), (f), (i)]. Normalized magnetic field H/H_0 is chosen to be 0.1 with $\gamma=\pi$ [(a), (b), (c)], 0 [(d), (e), (f)], 0.1 with $\gamma=0$ [(g), (h), (i)].

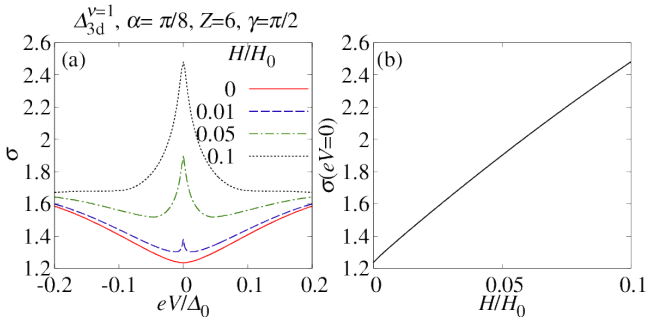

FIG. 10. (a) Conductance is plotted as a function of eV for $H/H_0=0$, 0.01, 0.05 and 0.1 with $\gamma=\pi/2$. (b) Conductance at $eV=0$ is plotted as a function of H/H_0. This plot is fitted by the linear function $f(H/H_0)=aH/H_0+b$ with $(a,b)=(12.4,1.27)$.

Similar plot for $\nu=2$ with same α is shown in Fig. 11. In this case, by contrast to Fig. 9, chiral edge mode crossing $k_y=0$ exists [see Fig. 7 (h-ii) and Fig. 11 (e)]. There are two kinds of branches of SABS: (1) chiral edge mode crossing $(k_x,k_y)=(0,0)$ and (2) SABS touching the ellipse given by $k_x^2/\cos^2(\pi/8)+k_y^2=k_{\rm F}^2$. The slope of chiral

edge mode becomes gradual (steep) for $\gamma = 0$ ($\gamma = \pi$) in the presence of the magnetic field. The contribution for zero bias conductance becomes suppressed (enhanced) for $\gamma = \pi$ ($\gamma = 0$). On the other hand, qualitative feature of SABS touching the ellipse is similar to that for $\nu = 1$ shown in Fig. 9. In the presence of the magnetic field for $\gamma = \pi$, ZESABS exists near $(k_x, k_y) = (\pm k_{\rm F}, 0)$ and around the ellipse [Fig. 11 (a)]. Since the contribution to zero bias conductance from SABS touching the ellipse is dominant as compared to that of chiral edge mode, the resulting σ has a ZBCP. On the other hand, if the direction of the magnetic field is opposite, ZBCP is absent [Fig. 11 (i)]. In Fig. 12 (a), we show how ZBCP developes with increasing magnetic field. Even for small magnitude of H ($H/H_0 = 0.01$), ZBCP appears similar to Fig. 10 (a). The magnitude of conductance at zero-bias as a function of H is shown in Fig. 12 (b) and it is approximately linear function of H. The slope a of fitting function $f(H/H_0) = aH/H_0 + b$ is smaller than that for $\Delta_{\rm 3d}^{\nu=1}$.

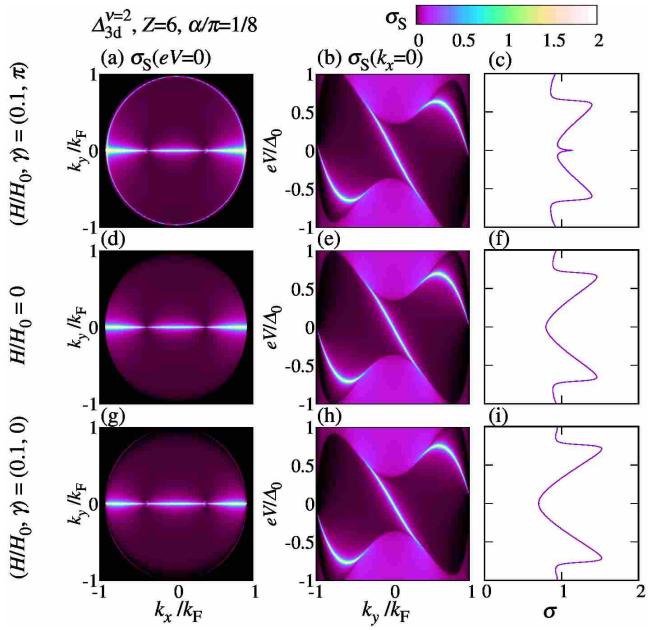

FIG. 11. Angle-resolved conductance of $\Delta_{\rm 3d}^{\nu=2}$ with $\alpha = \pi/8$. The model parameters used in this calculation is the same as in Fig. 9 except for pair potential Δ.

Next, let us discuss special case of $\Delta_{\rm 3d}^{\nu=1}$ for $\alpha = \pi/4$ at which there is no ZESABS without magnetic field [Fig. 7 (d-iii)]. The magnitude of the zero bias conductance for $H = 0$ is very small [Fig. 13 (f)] and it becomes larger for $\gamma = \pi$ [Fig. 13 (c)] due to the similar mechanism explained in Fig. 9. For $\gamma = 0$ [Fig. 13 (i)], although there is no SABS at zero-energy, the conductance becomes slightly larger than that for $H = 0$.

Whether the magnitude of ZBCP becomes larger or smaller by applying the infinitesimal small magnitude of magnetic field is summarized in Table IV. For 2D-like chiral superconductor with $\nu = 1$, since the energy dispersion of SABS is given by $E(\mathbf{k}_\parallel) = -k_y/k_{\rm F}$ [Eq. (76) and Eq. (77)], the magnitude of $\sigma(eV = 0)$ becomes larger for $\gamma = 0$ and smaller for $\gamma = \pi$. In other cases, there is no simple law due to the complicated energy dispersion of SABS. Using this table, we can classify five cases. If we make a junction for $\alpha = \pi/2$, we can distinguish between $\nu = 0$ (k_z'), $\nu = 1$ [$k_z'(k_x' + ik_y')$, $(k_x' + ik_y')$] and $\nu = 2$ [$k_z'(k_x' + ik_y')^2$, $(k_x' + ik_y')^2$]. Further, if we make a junction for $\alpha = 0$, we can distinguish between $k_z'(k_x' + ik_y')^\nu$ and $(k_x' + ik_y')^\nu$ with $(\nu = 1, 2)$.

To clarify γ dependence of conductance, we plot $\sigma(eV = 0)$ as a function of γ for $\alpha = \pi/4$, and $\pi/2$ in Fig. 14. For $\alpha = 0$, $\sigma(eV = 0)$ is constant as a function of γ due to the rotational symmetry of the pair potentials (not shown). Since $\Delta_{\rm 3d}^{\nu=0}$ conserves time reversal sym-

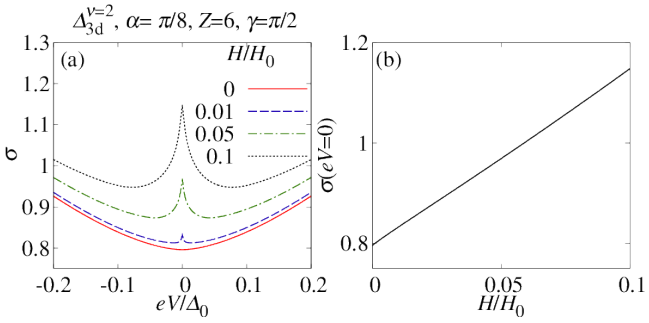

FIG. 12. (a) Conductance is plotted as a function of eV for $H/H_0 = 0$, 0.01, 0.05 and 0.1 with $\gamma = \pi/2$. (b) Conductance at $eV = 0$ is plotted as a function of H/H_0. This plot is fitted by the linear function $f(H/H_0) = aH/H_0 + b$ with $(a, b) = (3.49, 0.796)$.

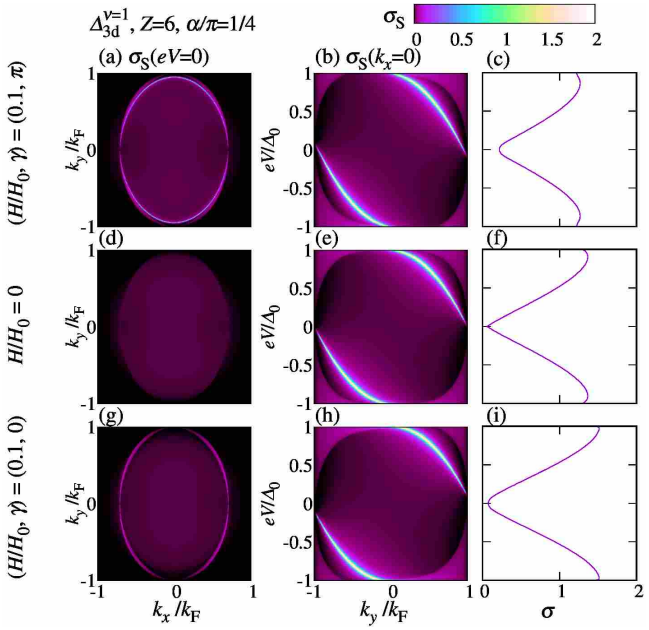

FIG. 13. Angle-resolved conductance of $\Delta_{\rm 3d}^{\nu=1}$ with $\alpha = \pi/4$. The parameters are the same as Fig. 9 except for α.

TABLE IV. Line shape of $\sigma(eV)$ near $eV = 0$ for $H = 0$. p: peak, d: dip. Whether the magnitude of $\sigma(eV = 0)$ is enhanced (suppressed) by magnetic field indicated by $\uparrow$ ($\downarrow$). We choose the infinitesimal applied magnetic field as $H/H_0 = 10^{-4}$. In the case $\Delta \propto k_z'$, the value of $\sigma(eV = 0)$ at $H > 0$ with $\gamma = 0$ and $\gamma = \pi$ are equivalent because σ is a π periodic function of γ.

			α				
$\Delta(\mathbf{k})$	H/H_0	γ	0	$\pi/8$	$\pi/4$	$3\pi/8$	$\pi/2$
k_z'	0	-	p	p	p	p	d
	10^{-4}	$0, \pi$	$\downarrow$	$\downarrow$	$\downarrow$	$\downarrow$	$\uparrow$
$k_z'(k_x' + ik_y')$	0	-	p	d	d	d	p
	10^{-4}	0	$\downarrow$	$\downarrow$	$\uparrow$	$\uparrow$	$\uparrow$
	10^{-4}	π	$\downarrow$	$\uparrow$	$\uparrow$	$\downarrow$	$\downarrow$
$(k_x' + ik_y')$	0	-	d	d	p	p	p
	10^{-4}	0	$\uparrow$	$\uparrow$	$\uparrow$	$\uparrow$	$\uparrow$
	10^{-4}	π	$\downarrow$	$\downarrow$	$\downarrow$	$\downarrow$	$\downarrow$
$k_z'(k_x' + ik_y')^2$	0	-	p	d	d	p	d
	10^{-4}	0	$\downarrow$	$\downarrow$	$\uparrow$	$\uparrow$	$\downarrow$
	10^{-4}	π	$\downarrow$	$\uparrow$	$\downarrow$	$\downarrow$	$\uparrow$
$(k_x' + ik_y')^2$	0	-	d	p	p	d	d
	10^{-4}	0	$\uparrow$	$\uparrow$	$\uparrow$	$\downarrow$	$\downarrow$
	10^{-4}	π	$\uparrow$	$\downarrow$	$\downarrow$	$\uparrow$	$\uparrow$

metry, *i.e.*, the energy dispersion of SABS has two-fold rotational symmetry [Fig. 6 (d-i)-(d-v)], σ has π periodicity [Fig. 14 (b), (c)]. In other cases, $\sigma(eV = 0)$ has 2π periodicity due to time reversal symmetry breaking.

γ which makes $\sigma(eV = 0)$ largest is summarized in Table V. In the case of $\Delta_{3d}^{\nu=0}$ with $\alpha = \pi/2$, $\sigma(eV = 0)$ becomes the smallest when the direction of the magnetic field is parallel to the direction of the projected line node. This result is consistent with that for the two-dimensional d-wave case[51,61]. But in the case of 3D chiral superconductor with $\Delta_{3d}^{\nu=1,2}$, this does not hold.

TABLE V. γ at which $\sigma(eV = 0)$ becomes maximum as a function of γ with $H/H_0 = 0.1$.

	α			
Δ	$\pi/8$	$\pi/4$	$3\pi/8$	$\pi/2$
k_z'	$\pi/2$,$3\pi/2$	$\pi/2$, $3\pi/2$	$\pi/2$, $3\pi/2$	0, π
$k_z'(k_x' + ik_y')$	π	π	0	0
$(k_x' + ik_y')$	π	0	π	0
$k_z'(k_x' + ik_y')^2$	π	0	0	π
$(k_x' + ik_y')^2$	~ 0	~ 0	π	π

C. Symmetry of pairing potential of UPt_3

Recently, the guide to determine the pairing symmetry of UPt_3 by using quasiparticle interference in slab model is theoretically proposed[62]. But the role of SABS on charge transport in junctions has not been revealed yet. We also propose a way to determine the pairing symmetry by using Doppler shift. In this subsection, we

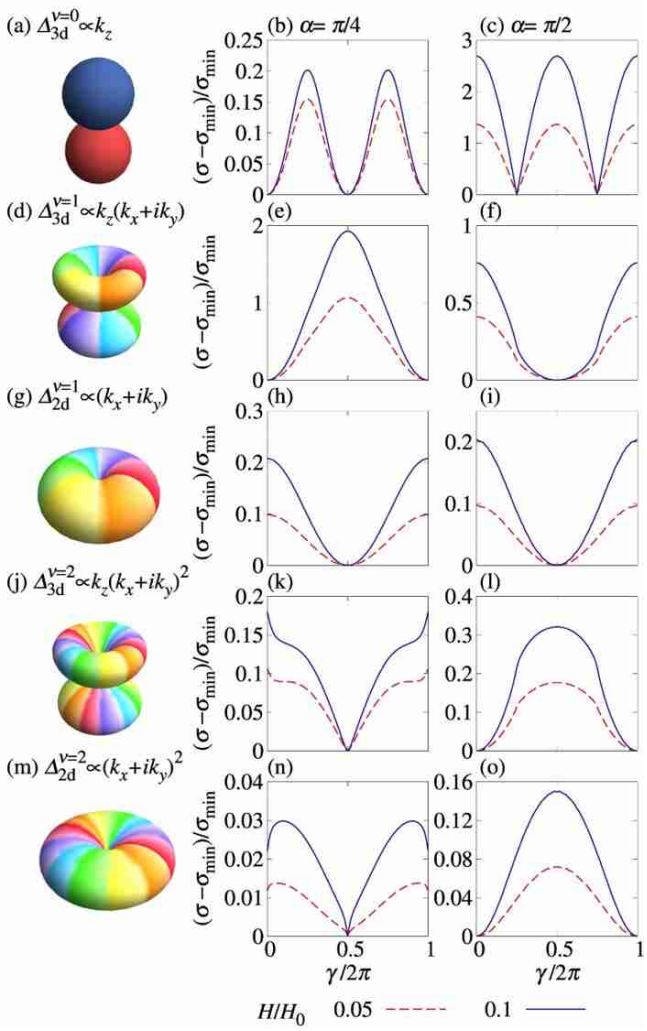

FIG. 14. Normalized conductance at $eV = 0$ is plotted as a function of γ for $\nu = 0, 1, 2$ with $Z = 6$. Schematic pictures of the pair potential are shown in (a), (d), (g), (j) and (m). $\alpha = \pi/4$ for (b), (e), (h), (k) and (n). $\alpha = \pi/2$ for (c), (f), (i), (l) and (o). $\sigma_{\rm min}$ is a minimum value of $\sigma(eV = 0)$ as a function of γ for $H/H_0 = 0.05$ and $H/H_0 = 0.1$.

consider $\Delta_{3d}^{\nu=2}$, $\Delta_{E_{1u}}^{\rm chiral}$ and $\Delta_{E_{1u}}^{\rm planar}$ as candidates of the pairing symmetry. $\Delta_{E_{1u}}^{\rm chiral}$ does not have time reversal symmetry and $\Delta_{E_{1u}}^{\rm planar}$ has time reversal symmetry. For $\Delta_{E_{1u}}^{\rm planar}$, conductance is given by Eq. (63).

Firstly, let us discuss SABS of $\Delta_{E_{1u}}^{\rm chiral}$ and $\Delta_{E_{1u}}^{\rm planar}$ (Fig. 15). The position of point and line nodes are shown on the Fermi surface for $\alpha = \pi/8$ [Fig. 15 (a-i)], $\alpha = \pi/4$ (a-ii), $\alpha = 3\pi/8$ (a-iii) and $\alpha = \pi/2$ (a-iv). Corresponding projected point and line nodes on the $k_x - k_y$ plane are replotted from Fig. 15 (b-i) to (b-iv). In the case of $\Delta_{E_{1u}}^{\rm planar}$, as explained in Sec. II B, the energy dispersion of SABS for $\Delta_{E_{1u}}^{\rm planar}$ is $\pm E^{\rm chiral}(\mathbf{k})$. For example, Fig. 15 (e-i) is the same as (h-i) and Fig. 15 (h-i) and (i-i) are the energy dispersion of SABS for $\Delta_{E_{1u}}^{\rm planar}$. Due to the pres-

ence of two line nodes, there is no SABS at $\alpha = 0$ for both $\Delta^{\rm chiral}_{E_{1u}}$ and $\Delta^{\rm planar}_{E_{1u}}$ (not shown). For $\alpha > 0$, ZESABS of $\Delta^{\rm chiral}_{E_{1u}}$ [Fig. 15 (d-i)-(d-iv)] and that of $\Delta^{\rm planar}_{E_{1u}}$ [Fig. 15 (g-i)-(g-iv)] are the same because $S_1 = S_2$ [Eq. (64) and Eq. (65)]. The number of ZESABSs is discussed in Appendix A 1.

The energy dispersion of SABS becomes very complicated as seen from Fig. 15 (e-i) to (e-iv) for $\Delta^{\rm chiral}_{E_{1u}}$ and from [(h-i) and (i-i)] to [(h-iv) and (i-iv)] for $\Delta^{\rm planar}_{E_{1u}}$. This is due to the presence of two line nodes and two point nodes. The energy dispersion of SABS at $\alpha = \pi/2$ is summarized in Table VI.

TABLE VI. The energy dispersion of SABS $E(\mathbf{k}_\parallel) r_{E_{1u}}/\Delta_0$ at $\alpha = \pi/2$ is shown for $\Delta^{\rm chiral}_{E_{1u}}(\mathbf{k})$ and $\Delta^{\rm planar}_{E_{1u}}(\mathbf{k})$. $\hat{k}_i = k_i/k_{\rm F} (i = x, y, z)$.

$\Delta(\mathbf{k})$	$E(\mathbf{k}_\parallel) r_{E_{1u}}/\Delta_0$
$\Delta^{\rm chiral}_{E_{1u}}(\mathbf{k})$	$-\hat{k}_y\lvert 5\hat{k}_x^2 - 1\rvert$
$\Delta^{\rm planar}_{E_{1u}}(\mathbf{k})$	$\pm\hat{k}_y\lvert 5\hat{k}_x^2 - 1\rvert$

In Fig. 16, conductance for $\Delta^{\nu=2}_{\rm 3d}$, $\Delta^{\rm chiral}_{E_{1u}}$ and $\Delta^{\rm planar}_{E_{1u}}$ are shown. Although the angle resolved conductance ($\sigma_{\rm S}$) of $\Delta^{\rm planar}_{E_{1u}}$ has a counter propagating mode in addition to the same chiral edge mode shown in $\Delta^{\rm chiral}_{E_{1u}}$, the angular averaged conductance (σ) is the same [Fig. 16 (b)]. Therefore, we can distinguish $\Delta^{\nu=2}_{\rm 3d}$ from ($\Delta^{\rm chiral}_{E_{1u}}$, $\Delta^{\rm planar}_{E_{1u}}$) by conductance but we cannot distinguish between $\Delta^{\rm chiral}_{E_{1u}}$ and $\Delta^{\rm planar}_{E_{1u}}$.

To distinguish $\Delta^{\rm chiral}_{E_{1u}}$ from $\Delta^{\rm planar}_{E_{1u}}$, we discuss the directional dependence of the magnetic field on conductance (Fig. 17). Because $\Delta^{\rm chiral}_{E_{1u}}$ ($\Delta^{\rm planar}_{E_{1u}}$) does not have (has) the time reversal symmetry, $\sigma(eV = 0)$ has 2π (π) periodicity. The difference of conductance as a function of eV with $H = 0$ and that of γ with the magnetic field between $\Delta^{\nu=2}_{\rm 3d}$, $\Delta^{\rm chiral}_{E_{1u}}$ and $\Delta^{\rm planar}_{E_{1u}}$ are summarized in Table VII.

TABLE VII. Position of conductance peak with $(\alpha, H) = (0, 0)$ (Fig. 16) and period of $\sigma(eV = 0)$ as a function of γ with $\alpha = \pi/2$ in the presence of the magnetic field (Fig. 17).

	$\Delta^{\nu=2}_{\rm 3d}$	$\Delta^{\rm chiral}_{E_{1u}}$	$\Delta^{\rm planar}_{E_{1u}}$
Conductance peak	$eV = 0$	$eV = \Delta_0$	$eV = \Delta_0$
Period of $\sigma(\gamma)$	2π	2π	π

Whether ZBCP becomes larger or smaller when infinitesimal magnitude of the magnetic field is applied is summarized in Table VIII and γ which makes conductance largest is summarized in Table IX.

Recently, Y. Yanase has proposed the extended version of E_{2u} symmetry[55] as a model of the pairing symmetry of UPt_3. It is a linear combination of spin-triplet p and f-wave pairings. It is interesting to clarify whether the obtained results in Table VII is changed by the disappearance of line node by the mixing of small magnitude of chiral p-wave pair potential and $\Delta^{\nu=2}_{\rm 3d}$. We consider non-unitary pair potential given by Eq. (38). For this purpose, we have used a general formula of tunneling conductance Eq. (58) derived in Appendix C. For $\eta = 1$, the obtained conductance is shown in Fig. 18. In this case there remain two point nodes and a line node [Fig. 3 (b-i)-(b-iii) and Fig. 4 (b-i)-(b-iii)]. When nonzero δ is introduced, ZBCP splits, but the shape of conductance is still distinct from that of E_{1u} symmetry [Fig. 16 (b)]. For fixed δ, the line shape of conductance σ does not change qualitatively with the change of η [Fig. 19 (a) and (b)]. Hence, it is expected that if spin-triplet p-wave pair potential is additionally introduced into $\Delta^{\nu=2}_{\rm 3d}$, E_{1u} and extended version of E_{2u} can be distinguished by tunneling conductance.

TABLE VIII. Line shape of $\sigma(eV)$ near $eV = 0$ with $H = 0$. p: peak, d: dip. Whether the magnitude of $\sigma(eV = 0)$ is enhanced (suppressed) by the magnetic field indicated by $\uparrow$ ($\downarrow$). We choose the infinitesimal magnitude of the magnetic field as $H/H_0 = 10^{-4}$. The value of $\sigma(eV)$ for $\Delta^{\rm planar}_{E_{1u}}$ at $\gamma = 0$ and $\gamma = \pi$ are equivalent because σ is a π periodic function of γ.

			α				
$\Delta(\mathbf{k})$	H/H_0	γ	0	$\pi/8$	$\pi/4$	$3\pi/8$	$\pi/2$
$\Delta^{\rm chiral}_{E_{1u}}$	0	-	d	d	d	d	p
	10^{-4}	0	$\uparrow$	$\downarrow$	$\uparrow$	$\uparrow$	$\uparrow$
	10^{-4}	π	$\uparrow$	$\uparrow$	$\uparrow$	$\downarrow$	$\downarrow$
$\Delta^{\rm planar}_{E_{1u}}$	0	-	d	d	d	d	p
	10^{-4}	$0, \pi$	$\uparrow$	$\uparrow$	$\uparrow$	$\uparrow$	$\uparrow$

TABLE IX. The position of γ at which $\sigma(eV = 0)$ becomes maximum as a function of γ.

	α			
Δ	$\pi/8$	$\pi/4$	$3\pi/8$	$\pi/2$
$\Delta^{\rm chiral}_{E_{1u}}$	π	0	0	0
$\Delta^{\rm planar}_{E_{1u}}$	0,π	0,π	0,π	0,π

IV. DISCUSSION AND CONCLUSION

In this paper, we have studied the surface Andreev bound state (SABS) and quasiparticle tunneling spectroscopy of three-dimensional (3D) chiral superconductors by changing the misorientation angle of superconductors. We have analytically derived a formula of the energy dispersion of SABS available for general pair potential when original 4×4 matrix of BdG Hamiltonian can be decomposed into two blocks of 2×2 matrix. We apply this formula to calculate SABS for 3D chiral superconductors where pair potential is given by $\Delta_0 k_z (k_x + ik_y)^\nu / k_{\rm F}^{\nu+1}$ ($\nu = 1, 2$). SABS has a complex momentum dependence due to the coexistence of point and line nodes. The number of branches of the energy

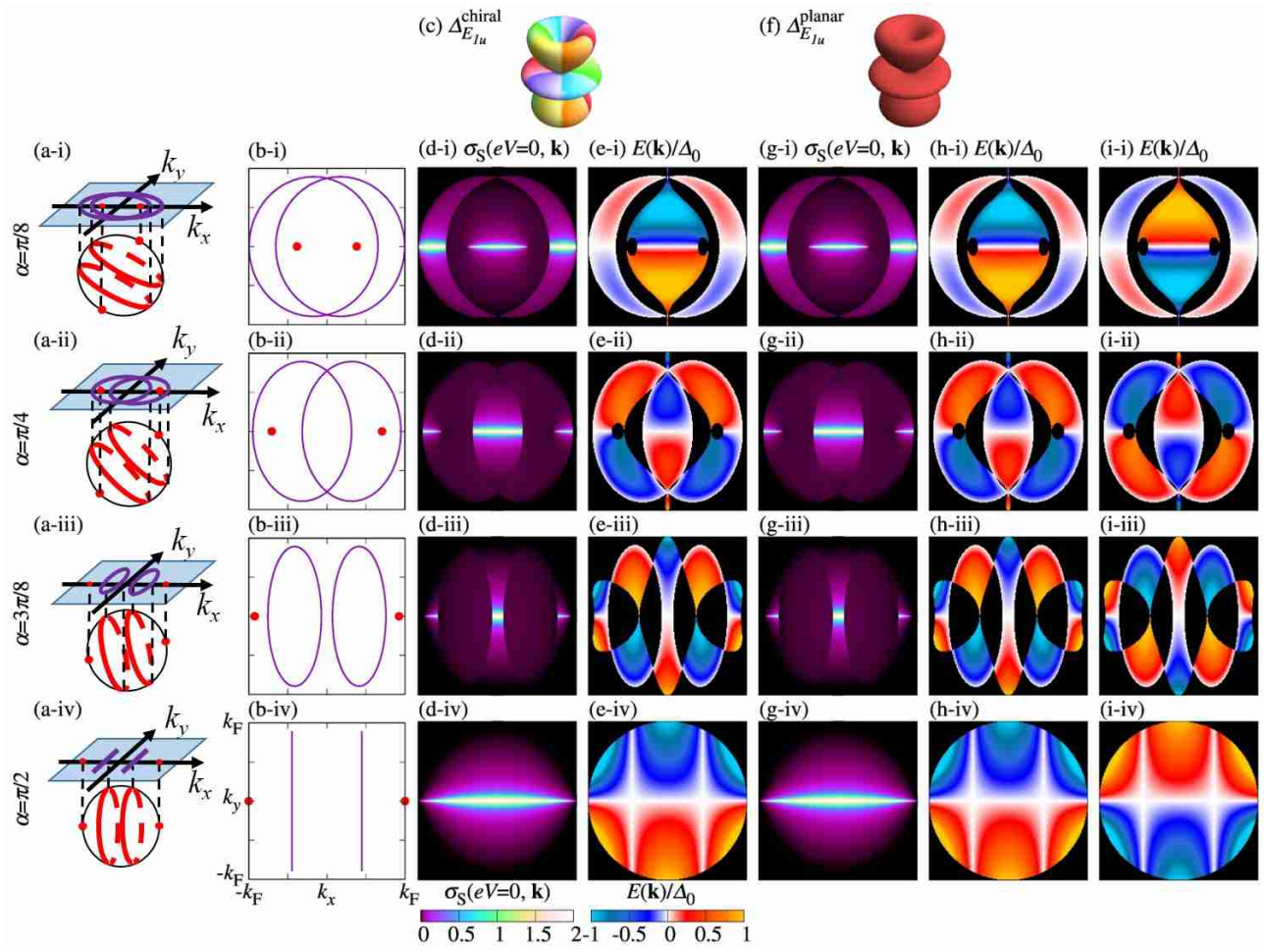

FIG. 15. Schematic illustration of point nodes (red dots) and line nodes (red lines) for (a-i) $\alpha = \pi/8$, (a-ii) $\alpha = \pi/4$, (a-iii) $\alpha = 3\pi/8$ and (a-iv) $\alpha = \pi/2$. Point nodes and line nodes on $k_x - k_y$ plane corresponding to (a-i)-(a-iv) are shown in (b-i)-(b-iv). Schematic picture of the pair potential for (c) $\Delta_{E_{1u}}^{\rm chiral}$ and (f) $\Delta_{E_{1u}}^{\rm planar}$. Angle resolved zero bias conductance $\sigma_{\rm S}(eV = 0, \mathbf{k})$ with $Z = 6$ is plotted as a function of k_x and k_y for $\Delta_{E_{1u}}^{\rm chiral}$ [(d-i)-(d-iv)] and for $\Delta_{E_{1u}}^{\rm planar}$ [(g-i)-(g-iv)]. The energy dispersion of SABS $E(\mathbf{k}_\parallel)$ for given α are plotted as a function of k_x and k_y for $\Delta_{E_{1u}}^{\rm chiral}$ [(e-i)-(e-iv)] and for $\Delta_{E_{1u}}^{\rm planar}$ [(h-i) and (i-i)]-[(h-iv) and (i-iv)].

dispersion of SABS with topological origin can be understood by the winding and Chern numbers. We have calculated the tunneling conductance of normal metal / insulator / chiral superconductor junctions in the presence of the applied magnetic field which induces Doppler shift. Differently from previous studies of Doppler effect on tunneling conductance, zero bias conductance dip can change into zero bias conductance peak by applying the magnetic field. This unique feature originates from the complicated energy dispersion of SABS. We have also studied SABS and tunneling conductance of UPt_3 focusing on four possible candidates of the pairing symmetry: E_{2u}, E_{1u}-planar, E_{1u}-chiral, and extended version of E_{2u} pairings. Since the last pairing is non-unitary, we have developed a conductance formula which is available for general pair potential. By using this formula, we have shown that these four parings can be identified by tunneling spectroscopy both with and without magnetic field. Thus, our theory serves as a guide to determine the pairing symmetry of UPt_3.

In this paper, we are focusing on SABS and quasiparticle tunneling spectroscopy. As a next step, it is interesting to calculate Josephson effect in chiral superconductor including spin-triplet non-unitary pairings[63], where both point and line node exists. Especially, it is known from the studies of d-wave superconductor, the role of α induces non-monotonic temperature dependence of maximum Josephson current[64–67]. To pursue such a kind of exotic temperature dependence of Josephson current is really interesting.

In this paper, we have studied the case where normal metal is ballistic. It is an challenging issue to extend our theory to diffusive normal metal (DN) / superconductor junctions where penetration of the Cooper pair by proximity effect modifies the total resistance of the junctions[68,69]. Especially, it is known that anomalous

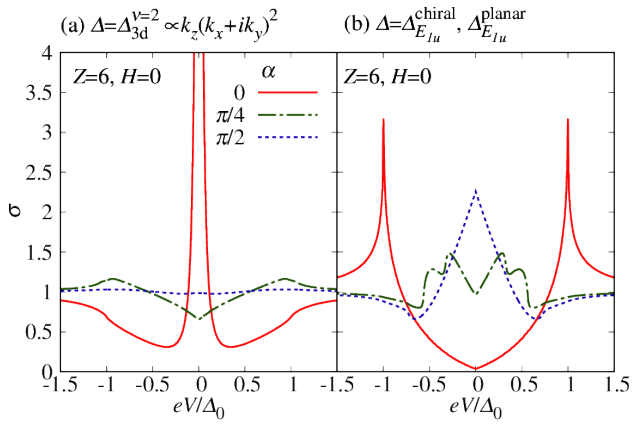

FIG. 16. Normalized conductance for spin-triplet f-wave symmetry as a function of eV for $\alpha = 0$ (solid line), $\alpha = \pi/4$ (dash-dotted line), and $\alpha = \pi/2$ (dotted line). (a) $\Delta_{3d}^{\nu=2}$, (b) $\Delta_{E_{1u}}^{\rm chiral}$, σ of $\Delta_{E_{1u}}^{\rm planar}$ coincides with that for $\Delta_{E_{1u}}^{\rm chiral}$.

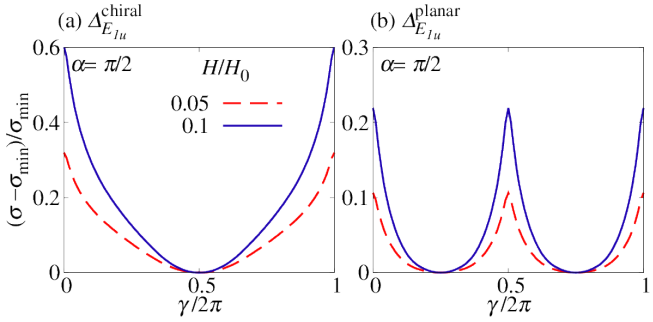

FIG. 17. Normalized conductance at $Z = 6$ as a function of γ for $\alpha = \pi/2$. $H/H_0 = 0.1$(solid line) and 0.05(dashed line).

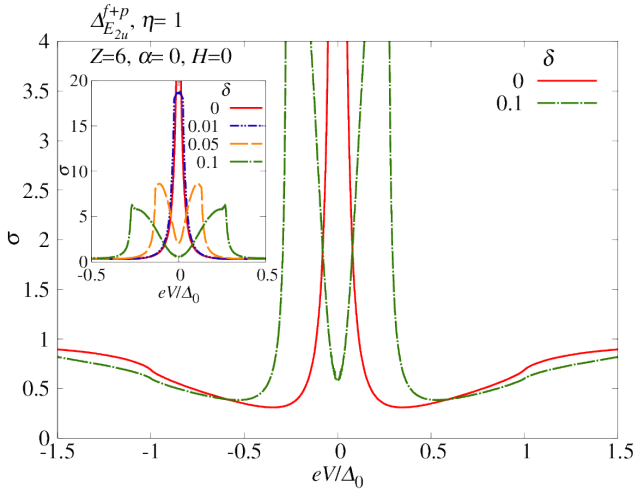

FIG. 18. Normalized conductance σ by its value in normal state for $\Delta_{E_{2u}}^{f+p}$ is plotted as a function of eV for several δ with $\eta = 1$ and $Z = 6$. Inset is the magnification near $eV = 0$.

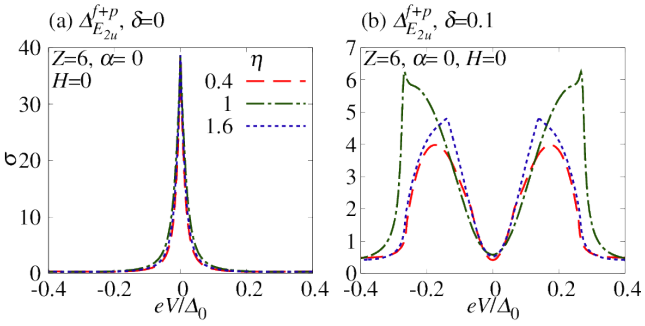

FIG. 19. Normalized conductance σ by its value in normal state for $\Delta_{E_{2u}}^{f+p}$ is plotted as a function of eV for several η with $Z = 6$. (a)$\delta = 0$ and (b) $\delta = 0.1$.

proximity effect having zero energy peak of local density of states in DN via odd-frequency pairing occurs in spin-triplet superconductor junctions[70–76]. Extension of previous two dimensional studies to three-dimensional one is also promising.

ACKNOWLEDGMENTS

The authors are grateful to M. Sato for discussions. This work was supported by a Grant-in-Aid for Scientific Research on Innovative Areas Topological Material Science JPSJ KAKENHI (Grants No. JP15H05851, and No. JP15H05853), a Grant-in-Aid for Scientific Research B (Grant No. JP15H03686), a Grant-in-Aid for Challenging Exploratory Research (Grant No. JP15K13498) from the Ministry of Education, Culture, Sports, Science, and Technology, Japan (MEXT). The work of S.K. was supported by Building of Consortia for the Development of Human Resources in Science and Technology and Grant-in-Aid for Research Activity Start-up (Grand No. JP16H06861).

[1] S. Kashiwaya and Y. Tanaka, Rep. Prog. Phys. **63**, 1641 (2000).
[2] Y. Tanaka, M. Sato, and N. Nagaosa, J. Phys. Soc. Jpn. **81**, 011013 (2012).
[3] X.-L. Qi and S.-C. Zhang, Rev. Mod. Phys. **83**, 1057 (2011).
[4] C. R. Hu, Phys. Rev. Lett. **72**, 1526 (1994).
[5] M.Sato, Y.Tanaka, K.Yada, and T.Yokoyama, Phys. Rev. B **83**, 224511 (2011).
[6] Y. Tanaka and S. Kashiwaya, Phys. Rev. Lett. **74**, 3451 (1995).
[7] S. Kashiwaya, Y. Tanaka, M. Koyanagi, H. Takashima, and K. Kajimura, Phys. Rev. B **51**, 1350 (1995).
[8] S. Kashiwaya, Y. Tanaka, N. Terada, M. Koyanagi, S. Ueno, L. Alff, H. Takashima, Y. Tanuma, and K. Kajimura, J. Phys. Chem. Solid **59**, 2034 (1998).
[9] M. Covington, M. Aprili, E. Paraoanu, L. H. Greene, F. Xu, J. Zhu, and C. A. Mirkin, Phys. Rev. Lett. **79**, 277 (1997).
[10] L. Alff, H. Takashima, S. Kashiwaya, N. Terada, H. Ihara, Y. Tanaka, M. Koyanagi, and K. Kajimura, Phys. Rev. B **55**, R14757 (1997).
[11] J. Y. T. Wei, N.-C. Yeh, D. F. Garrigus, and M. Strasik, Phys. Rev. Lett. **81**, 2542 (1998).
[12] A. Biswas, P. Fournier, M. M. Qazilbash, V. N. Smolyaninova, H. Balci, and R. L. Greene, Phys. Rev. Lett. **88**, 207004 (2002).
[13] L. J. Buchholtz and G. Zwicknagl, Phys. Rev. B **23**, 5788 (1981).
[14] J. Hara and K. Nagai, Prog. Theor. Phys. **76**, 1237 (1986).
[15] M. Yamashiro, Y. Tanaka, Y. Tanuma, and S. Kashiwaya, J. Phys. Soc. Jpn. **67**, 3224 (1998).
[16] Y. Tanaka, Y. Tanuma, K. Kuroki, and S. Kashiwaya, Journal of the Physical Society of Japan **71**, 2102 (2002).
[17] H. Kwon, K. Sengupta, and V. Yakovenko, Eur. Phys. J. B **37**, 349 (2004).
[18] M. Yamashiro, Y. Tanaka, and S. Kashiwaya, Phys. Rev. B **56**, 7847 (1997).
[19] C. Honerkamp and M. Sigrist, Journal of Low Temperature Physics **111**, 895 (1998).
[20] S. Kashiwaya, H. Kashiwaya, H. Kambara, T. Furuta, H. Yaguchi, Y. Tanaka, and Y. Maeno, Phys. Rev. Lett. **107**, 077003 (2011).
[21] S. Wu and K. V. Samokhin, Phys. Rev. B **81**, 214506 (2010).
[22] M. Fogelström, D. Rainer, and J. A. Sauls, Phys. Rev. Lett. **79**, 281 (1997).
[23] Y. Tanuma, K. Kuroki, Y. Tanaka, R. Arita, S. Kashiwaya, and H. Aoki, Phys. Rev. B **66**, 094507 (2002).
[24] Y. Tanaka, T. Yokoyama, A. V. Balatsky, and N. Nagaosa, Phys. Rev. B **79**, 060505 (2009).
[25] X.-L. Qi, T. L. Hughes, S. Raghu, and S.-C. Zhang, Phys. Rev. Lett. **102**, 187001 (2009).
[26] S. B. Chung and S.-C. Zhang, Phys. Rev. Lett. **103**, 235301 (2009).
[27] S. Murakawa, Y. Tamura, Y. Wada, M. Wasai, M. Saitoh, Y. Aoki, R. Nomura, Y. Okuda, Y. Nagato, M. Yamamoto, S. Higashitani, and K. Nagai, Phys. Rev. Lett. **103**, 155301 (2009).
[28] Y. Asano, Y. Tanaka, Y. Matsuda, and S. Kashiwaya, Phys. Rev. B **68**, 184506 (2003).
[29] L. Fu and E. Berg, Phys. Rev. Lett. **105**, 097001 (2010).
[30] S. Sasaki, M. Kriener, K. Segawa, K. Yada, Y. Tanaka, M. Sato, and Y. Ando, Phys. Rev. Lett. **107**, 217001 (2011).
[31] L. Hao and T. K. Lee, Phys. Rev. B **83**, 134516 (2011).
[32] T. H. Hsieh and L. Fu, Phys. Rev. Lett. **108**, 107005 (2012).
[33] A. Yamakage, K. Yada, M. Sato, and Y. Tanaka, Phys. Rev. B **85**, 180509 (2012).
[34] T. Hashimoto, K. Yada, M. Sato, and Y. Tanaka, Phys. Rev. B **92**, 174527 (2015).
[35] B. Lu, K. Yada, M. Sato, and Y. Tanaka, Phys. Rev. Lett. **114**, 096804 (2015).
[36] T. Hashimoto, S. Kobayashi, Y. Tanaka, and M. Sato, Phys. Rev. B **94**, 014510 (2016).
[37] S. Kobayashi, Y. Tanaka, and M. Sato, Phys. Rev. B **92**, 214514 (2015).
[38] E. R. Schemm, R. E. Baumbach, P. H. Tobash, F. Ronning, E. D. Bauer, and A. Kapitulnik, Phys. Rev. B **91**, 140506 (2015).
[39] Y. Kasahara, T. Iwasawa, H. Shishido, T. Shibauchi, K. Behnia, Y. Haga, T. D. Matsuda, Y. Onuki, M. Sigrist, and Y. Matsuda, Phys. Rev. Lett. **99**, 116402 (2007).
[40] T. Shibauchi, H. Ikeda, and Y. Matsuda, Philosophical Magazine **94**, 3747 (2014).
[41] E. R. Schemm, R. E. Baumbach, P. H. Tobash, F. Ronning, E. D. Bauer, and A. Kapitulnik, Phys. Rev. B **91**, 140506 (2015).
[42] J. Sauls, Advances in Physics **43**, 113 (1994).
[43] R. Joynt and L. Taillefer, Rev. Mod. Phys. **74**, 235 (2002).
[44] E. R. Schemm, W. J. Gannon, C. M. Wishne, W. P. Halperin, and A. Kapitulnik, Science **345**, 190 (2014), http://science.sciencemag.org/content/345/6193/190.full.pdf.
[45] P. Goswami and A. H. Nevidomskyy, Phys. Rev. B **92**, 214504 (2015).
[46] Y. Tsutsumi, K. Machida, T. Ohmi, and M. aki Ozaki, Journal of the Physical Society of Japan **81**, 074717 (2012).
[47] Y. Tsutsumi, M. Ishikawa, T. Kawakami, T. Mizushima, M. Sato, M. Ichioka, and K. Machida, Journal of the Physical Society of Japan **82**, 113707 (2013).
[48] S. Kashiwaya, Y. Tanaka, M. Koyanagi, and K. Kajimura, Phys. Rev. B **53**, 2667 (1996).
[49] G. E. Blonder, M. Tinkham, and T. M. Klapwijk, Phys. Rev. B **25**, 4515 (1982).
[50] C. Bruder, Phys. Rev. B **41**, 4017 (1990).
[51] Y. Tanuma, Y. Tanaka, K. Kuroki, and S. Kashiwaya, Phys. Rev. B **66**, 174502 (2002).
[52] M. Matsumoto and H. Shiba, Journal of the Physical Society of Japan **64**, 4867 (1995).
[53] S. Kashiwaya, Y. Tanaka, M. Koyanagi, H. Takashima, and K. Kajimura, Journal of Physics and Chemistry of Solids **56**, 1721 (1995).
[54] A. Furusaki, M. Matsumoto, and M. Sigrist, Phys. Rev. B **64**, 054514 (2001).
[55] Y. Yanase, ArXiv e-prints (2016), arXiv:1606.08563 [cond-mat.supr-con].
[56] S. Takami, K. Yada, A. Yamakage, M. Sato, and Y. Tanaka, J. Phys. Soc. Jpn. **83**, 064705 (2014).
[57] M. Sato, Y. Tanaka, K. Yada, and T. Yokoyama, Phys. Rev. B **83**, 224511 (2011).
[58] A. P. Schnyder and S. Ryu, Phys. Rev. B **84**, 060504

(2011).
[59] D. J. Thouless, M. Kohmoto, M. P. Nightingale, and M. den Nijs, Phys. Rev. Lett. **49**, 405 (1982).
[60] Y. Tanaka, H. Tsuchiura, Y. Tanuma, and S. Kashiwaya, Journal of the Physical Society of Japan **71**, 271 (2002).
[61] I. Vekhter, P. J. Hirschfeld, J. P. Carbotte, and E. J. Nicol, Phys. Rev. B **59**, R9023 (1999).
[62] F. Lambert, A. Akbari, P. Thalmeier, and I. Eremin, ArXiv e-prints (2016), arXiv:1608.07946 [cond-mat.supr-con].
[63] Y. Asano, Phys. Rev. B **64**, 224515 (2001).
[64] Y. Tanaka and S. Kashiwaya, Phys. Rev. B **53**, R11957 (1996).
[65] Y. S. Barash, H. Burkhardt, and D. Rainer, Phys. Rev. Lett. **77**, 4070 (1996).
[66] Y. Tanaka and S. Kashiwaya, Phys. Rev. B **56**, 892 (1997).
[67] Y. S. Barash, H. Burkhardt, and D. Rainer, Phys. Rev. Lett. **77**, 4070 (1996).
[68] Y. Tanaka, Y. Nazarov, and S. Kashiwaya, Phys. Rev. Lett. **90**, 167003 (2003).
[69] Y. Tanaka, Y. Nazarov, A. Golubov, and S. Kashiwaya, Phys. Rev. B **69**, 144519 (2004).
[70] Y. Tanaka and S. Kashiwaya, Phys. Rev. B **70**, 012507 (2004).
[71] Y. Tanaka, S. Kashiwaya, and T. Yokoyama, Phys. Rev. B **71**, 094513 (2005).
[72] Y. Asano, Y. Tanaka, and S. Kashiwaya, Phys. Rev. Lett. **96**, 097007 (2006).
[73] Y. Tanaka, Y. Asano, A. Golubov, and S. Kashiwaya, Phys. Rev. B **72**, 140503(R) (2005).
[74] Y. Tanaka and A. A. Golubov, Phys. Rev. Lett. **98**, 037003 (2007).
[75] Y. Tanaka, A. A. Golubov, S. Kashiwaya, and M. Ueda, Phys. Rev. Lett. **99**, 037005 (2007).
[76] Y. Tanaka, Y. Tanuma, and A. A. Golubov, Phys. Rev. B **76**, 054522 (2007).
[77] M. Sigrist and K. Ueda, Rev. Mod. Phys. **63**, 239 (1991).

Appendix A: Topological numbers

The 3D chiral superconductors host both a winding number and a Chern number relevant to ZESABSs. In the previous study, two of the present authors have discussed relevant topological numbers in 3D chiral superconductors with $\Delta_{3\mathrm{d}}^{\nu=1}$ and $\Delta_{3\mathrm{d}}^{\nu=2}$ by taking into account an additional symmetry[37]. At this point, we explain topological numbers in 3D chiral superconductors with $\Delta_{E_{1u}}^{\mathrm{chiral}}$ and $\Delta_{3\mathrm{d}}^{\nu>2}$.

1. Winding number in the case $\Delta_{E_{1u}}^{\mathrm{chiral}}$

Following the discussion in Ref. [37], a winding number is defined in a similar way to the case $\Delta_{3\mathrm{d}}^{\nu=2}$. However, $\Delta_{E_{1u}}^{\mathrm{chiral}}$ has two line nodes and is an even function of k_z, leading to a vanishing of zero-energy flat band for $\alpha = 0$. Thus, in the following, we consider winding number for $\alpha \neq 0$ and $k_y = 0$. In the $k_x - k_z$ plane, $\Delta_{E_{1u}}^{\mathrm{chiral}}$ is real, so we can define the winding number using time-reversal symmetry and spin-rotation symmetry:

$$W(k_x) \equiv \frac{-1}{4\pi i}\int_{-\infty}^{\infty} dk_z \mathrm{Tr}[\Gamma H^{-1}(\mathbf{k})\partial_{k_z} H(\mathbf{k})]\Big|_{k_y=0}, \tag{A1}$$

where $H(\mathbf{k})$ is the BdG Hamiltonian with $\epsilon(\mathbf{k}) = \frac{\hbar^2}{2m}(\mathbf{k}^2 - k_F^2)$ and $\Delta_{E_{1u}}^{\mathrm{chiral}}$. The chiral operator, which anti-commutes with $H(\mathbf{k})$, is given by $\Gamma = -\sigma_1\tau_2$, where σ_μ and τ_μ ($\mu = 0, 1, 2, 3$) are the identity matrix and the Pauli matrices in the spin and Nambu spaces, respectively. Furthermore, using the weak pairing assumption, Eq. (A1) is reduced into

$$W(k_x) = \sum_{\epsilon(\mathbf{k})=0} \mathrm{sgn}[\partial_{k_z}\epsilon(\mathbf{k})] \cdot \mathrm{sgn}[(5{k'}_z^2 - k_F^2){k'}_x], \tag{A2}$$

where $k'_x = k_x\cos\alpha - k_z\sin\alpha$ and $k'_z = k_x\sin\alpha + k_z\cos\alpha$ and the summation is taken for k_z satisfying $\epsilon(\mathbf{k}) = 0$.

To evaluate the winding number (A2), we define the characteristic angles: $\alpha_1 = \tan^{-1}\left(\frac{2}{\sqrt{5}+1}\right)$, $\alpha_2 = \tan^{-1}\left(\frac{2}{\sqrt{5}-1}\right)$, and $\alpha_3 = \tan^{-1}(2)$ and the positions of point and line nodes projected onto the k_x line in the (001) plane: $k_1^{\mathrm{line}} = \frac{k_F}{\sqrt{5}}(\sin\alpha + 2\cos\alpha)$ and $k_2^{\mathrm{line}} = \frac{k_F}{\sqrt{5}}(-\sin\alpha + 2\cos\alpha)$ for the line nodes and $k^{\mathrm{point}} = k_F\sin\alpha$ for the point nodes (see Fig. 20). These angles satisfy $0 < \frac{\pi}{8} < \alpha_1 < \frac{\pi}{4} < \alpha_2 < \alpha_3 < \frac{3\pi}{8} < \frac{\pi}{2}$. Calculating Eq. (A2), we obtain the winding number as follows:

- $0 < \alpha \leq \alpha_1$

$$W(k_x) = \begin{cases} 2 & -k_1^{\rm line} < k_x < -k_2^{\rm line} \\ -2 & -k^{\rm point} < k_x < k^{\rm point} \\ 2 & k_2^{\rm line} < k_x < k_1^{\rm line} \\ 0 & \text{otherwise} \end{cases} \tag{A3}$$

- $\alpha_1 < \alpha \leq \alpha_2$

$$W(k_x) = \begin{cases} 2 & -k_1^{\rm line} < k_x < -k^{\rm point} \\ -2 & -k_2^{\rm line} < k_x < k_2^{\rm line} \\ 2 & k^{\rm point} < k_x < k_1^{\rm line} \\ 0 & \text{otherwise} \end{cases} \tag{A4}$$

- $\alpha_2 < \alpha \leq \alpha_3$

$$W(k_x) = \begin{cases} -2 & -k^{\rm point} < k_x < -k_1^{\rm line} \\ -2 & -k_2^{\rm line} < k_x < k_2^{\rm line} \\ -2 & k_1^{\rm line} < k_x < k^{\rm point} \\ 0 & \text{otherwise} \end{cases} \tag{A5}$$

- $\alpha_3 < \alpha \leq \frac{\pi}{2}$

$$W(k_x) = \begin{cases} -2 & -k^{\rm point} < k_x < -k_1^{\rm line} \\ 2 & k_2^{\rm line} < k_x < -k_2^{\rm line} \\ -2 & k_1^{\rm line} < k_x < k^{\rm point} \\ 0 & \text{otherwise} \end{cases} \tag{A6}$$

The factor 2 comes from the spin degrees of freedom. The obtained results are consistent with the ZESABSs in Fig. 15.

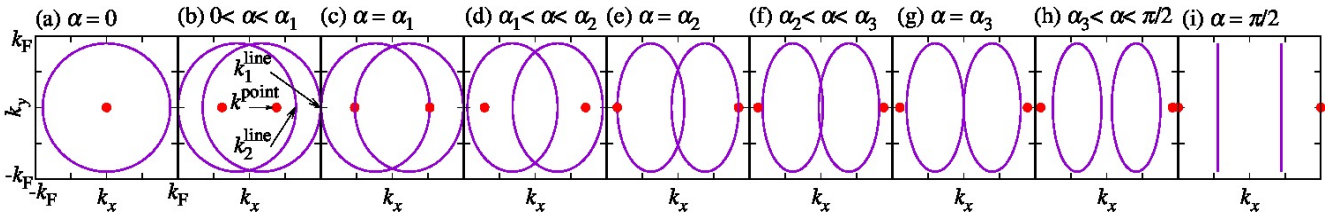

FIG. 20. The position of point nodes and line nodes for $\Delta_{E_{1u}}^{\rm chiral}$ projected on $k_x - k_y$ plane are shown for (a) $\alpha = 0$, (b) $0 < \alpha < \alpha_1$, (c) $\alpha = \alpha_1$, (d) $\alpha_1 < \alpha < \alpha_2$, (e) $\alpha = \alpha_2$, (f) $\alpha_2 < \alpha < \alpha_3$, (f) $\alpha = \alpha_3$, (h) $\alpha_3 < \alpha < \pi/2$ and (i) $\alpha = \pi/2$. (b), (d), (h) and (i) are the same as Fig. 15 (b-i), (b-ii) (b-iii) and (b-iv), respectively. $k_1^{\rm line}$, $k_2^{\rm line}$ and $k^{\rm point}$ for $0 < \alpha < \alpha_1$ are shown in (b).

2. Chern number in the case $\Delta_{\rm 3d}^{\nu>2}$

In 3D chiral superconductors with $\Delta_{\rm 3d}^{\nu=1}$ and $\Delta_{\rm 3d}^{\nu=2}$, ZESABSs are understood from both the winding number and the Chern number. On the other hand, 3D chiral superconductors with $\Delta_{\rm 3d}^{\nu>2}$ has the redundant ZESABSs for $0 < \alpha \leq \frac{\pi}{4}$. To understand this type of ZESABSs, we introduce the Chern number defined on a cylinder:

$$N = \frac{i}{2\pi} \sum_{n \in {\rm occ}} \int_{-\infty}^{\infty} dk_z \int_0^{2\pi} \rho d\theta \, \epsilon^{ab} \partial_{k_a} \langle u_n(\mathbf{k}) | \partial_{k_b} | u_n(\mathbf{k}) \rangle, \tag{A7}$$

where the cylindrical coordinate is defined by $(\rho\cos\theta \pm k_F \sin\alpha, \rho\sin\theta, k_z)$, $|u_n(\mathbf{k})\rangle$ is an eigenstate of $H(\mathbf{k})$, and the summation is taken over all of occupied stats. We choose ρ such a way that the cylinder includes a single point node and does not touch the line node. Then, Eq. (A7) gives $\pm 2\nu$ in analogy with the Chern number on the $k_y - k_z$ plane[37], where 2 comes from the spin degrees of freedom. The nontrivial Chern number predicts 2ν ZESABSs terminated at the point nodes. As shown in Fig. 7 (d-ii) and (g-ii), single and double ZESABSs terminated at the point nodes appear on the k_x line, respectively. For $\nu > 2$, we find 2ν ZESABSs terminated at the point nodes [Fig. 21 (d) and (g)]. Note that the winding number also exists and explain ZESABSs in the k_x line.

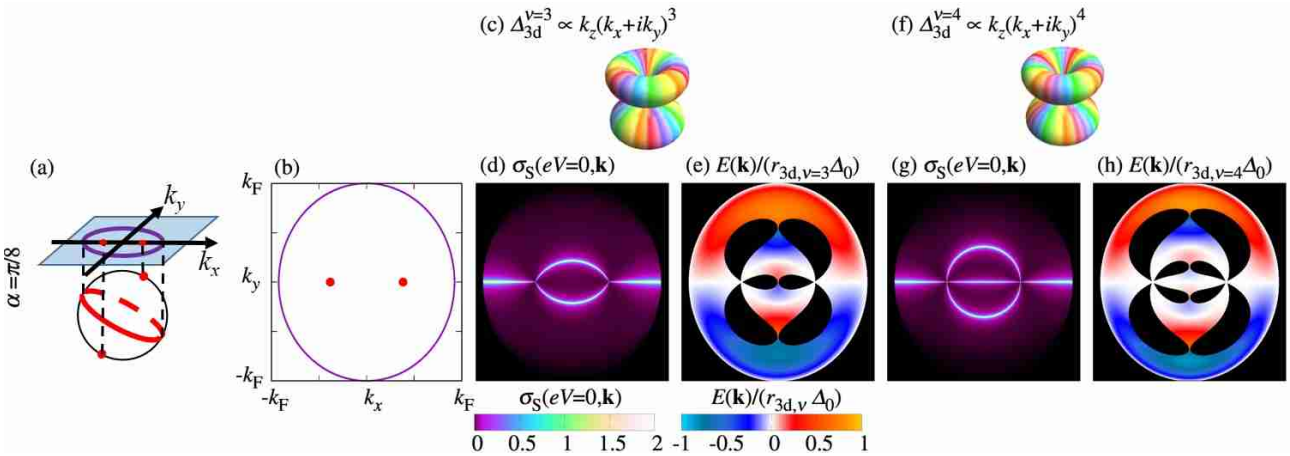

FIG. 21. (a) Schematic illustration of point nodes (red dots) and a line node (red line) for $\alpha = \pi/8$. Point nodes and a line node on $k_x - k_y$ plane corresponding to (a) are shown in (b). Schematic picture of pair potential for (c) $\Delta_{3d}^{\nu=3}$ and (f) $\Delta_{3d}^{\nu=4}$. (d) The angle resolved zero-bias conductance $\sigma_S(eV = 0, \mathbf{k})$ at $Z = 6$ are plotted as a function of k_x and k_y for (d) $\Delta_{3d}^{\nu=3}$ and (g) $\Delta_{3d}^{\nu=4}$. The energy dispersions of SABS $E(\mathbf{k})$ are plotted as a function of k_x and k_y for $\Delta_{3d}^{\nu=3}$ (e) and for $\Delta_{3d}^{\nu=4}$ (h).

Appendix B: SABS

In Appendix B, we show how to derive the SABS. Since $|\Gamma_\pm| = 1$ [$\Gamma_\pm$ is given by Eqs. (23) and (24)] is satisfied in in-gap state, we introduce $\theta_\pm$ as follows,

$$E = |\Delta_+| \cos\theta_+, \tag{B1}$$
$$= |\Delta_-| \cos\theta_-. \tag{B2}$$

with $\Delta_+ = \Delta(\mathbf{k})$, $\Delta_- = \Delta(\tilde{\mathbf{k}})$. Since θ_+ and θ_- are not independent, we obtain

$$\kappa \frac{\cos\theta_+}{\cos\theta_-} = 1, \tag{B3}$$

with

$$\kappa = \frac{|\Delta_+|}{|\Delta_-|}. \tag{B4}$$

θ_+ (θ_-) is used for the definition of Γ_+ (Γ_-) and is confined in the domain $0 \le \theta_\pm \le \pi$. Then, $\Gamma_\pm$ is given by

$$\begin{aligned}\Gamma_+ &= \frac{\Delta_+^*}{E + i\sqrt{|\Delta_+|^2 - E^2}} \\ &= \frac{\Delta_+^*}{|\Delta_+|\cos\theta_+ + i\sqrt{|\Delta_+|^2 - |\Delta_+|^2\cos^2\theta_+}} \\ &= \frac{e^{-i\phi_+}}{e^{i\theta_+}} \\ &= \exp\left[i(-\phi_+ - \theta_+)\right], \end{aligned} \tag{B5}$$
$$\Gamma_- = \exp\left[i(\phi_- - \theta_-)\right], \tag{B6}$$

where $\phi_\pm$ is defined by $\Delta_\pm = |\Delta_\pm| \exp(i\phi_\pm)$. Then, the SABS satisfies following conditions,

$$0 = \mathrm{Im}\Gamma_+\Gamma_- = \sin\left(\phi - \theta_+ - \theta_-\right), \tag{B7}$$
$$1 = \mathrm{Re}\Gamma_+\Gamma_- = \cos\left(\phi - \theta_+ - \theta_-\right), \tag{B8}$$

with

$$\phi = -\phi_+ + \phi_-. \tag{B9}$$

From Eqs. (B7) and (B8), the relation between ϕ and $\theta_\pm$ is obtained,

$$\begin{aligned} \phi - \theta_+ - \theta_- =& -2n\pi, \\ \Leftrightarrow \theta_+ + \theta_- =& 2n\pi + \phi, \end{aligned} \tag{B10}$$

where n is an integer. The dispersion relation is given by Eq. (B1) and Eq. (B10) or Eq. (B2) and Eq. (B10).

In order to eliminate θ_-, substitute Eq. (B10) for Eq. (B3). Then, we get

$$\begin{aligned} &\cos\theta_+(\kappa - \cos\phi) = \sin\theta_+ \sin\phi, \\ \Rightarrow &\cos^2\theta_+ \left[(\kappa - \cos\phi)^2 + \sin^2\phi\right] = \sin^2\phi. \end{aligned} \tag{B11}$$

I)$\phi = 2m\pi$ (m: integer) with $\kappa = 1$
$(\theta_+,\ \theta_-) \neq (\pi/2,\ \pi/2)$ is satisfied by Eq. (B10). From Eq. (B3), we obtain

$$\cos\theta_+ = \cos\theta_-. \tag{B12}$$

This condition is held with $(\theta_+, \theta_-) = (0,\ 0)$ or $(\pi,\ \pi)$. However, from Eq. (B1) or Eq. (B2), $E = \pm|\Delta_+| = \pm|\Delta_-|$ is satisfied. This means that the obtained energy dispersion is not inside the energy gap and is not SABS (in-gap state).

II) $\phi \neq 2m\pi$ or $\kappa \neq 1$
From Eq. (B11), we obtain $\cos\theta_\pm$ and $\sin\theta_\pm$ as follows

$$\cos\theta_+ = \pm\frac{\sin\phi}{\sqrt{(\kappa - \cos\phi)^2 + \sin^2\phi}}, \tag{B13}$$
$$\sin\theta_+ = \frac{|\kappa - \cos\phi|}{\sqrt{(\kappa - \cos\phi)^2 + \sin^2\phi}}, \tag{B14}$$
$$\cos\theta_- = \pm\frac{\sin\phi}{\sqrt{(\kappa^{-1} - \cos\phi)^2 + \sin^2\phi}}, \tag{B15}$$
$$\sin\theta_- = \frac{|\kappa^{-1} - \cos\phi|}{\sqrt{(\kappa^{-1} - \cos\phi)^2 + \sin^2\phi}}, \tag{B16}$$

where the sign of $\cos\theta_+$ and $\cos\theta_-$ are the same. We must check whether four equations from Eq. (B13) to Eq. (B16) are consistent with Eq. (B10) or not. From Eq. (B10), we obtain following relations,

$$\begin{aligned} &\sin(\theta_+ + \theta_-) = \sin\phi, \\ \Leftrightarrow &\pm\sin\phi\left(|\kappa - \cos\phi| + |\kappa^{-1} - \cos\phi|\right) \\ =&\sin\phi\sqrt{(\kappa - \cos\phi)^2 + \sin^2\phi}\sqrt{(\kappa^{-1} - \cos\phi)^2 + \sin^2\phi}, \end{aligned} \tag{B17}$$

$$\begin{aligned} &\cos(\theta_+ + \theta_-) = \cos\phi, \\ \Leftrightarrow &\sin^2\phi - |\kappa - \cos\phi||\kappa^{-1} - \cos\phi| \\ =&\cos\phi\sqrt{(\kappa - \cos\phi)^2 + \sin^2\phi}\sqrt{(\kappa^{-1} - \cos\phi)^2 + \sin^2\phi}. \end{aligned} \tag{B18}$$

From Eq. (B17), we must consider following four cases.
II-1) $\sin\phi = 0$
i)$\phi = 2l\pi$ (l: integer)

Substitute $\phi = 2l\pi$ for Eq. (B18), lefthand side of Eq. (B17) is negative but righthand side of it is positive. Therefore, there is no SABS.

ii)$\underline{\phi = (2l-1)\pi \ (l\text{: integer})}$

$\phi = (2l-1)\pi$ satisfies Eq. (B18). From Eq. (B10),we obtain

$$\theta_+ + \theta_- = \pi. \tag{B19}$$

This equation contradicts the fact that the sign of $\cos\theta_+$ equals to that of $\cos\theta_-$ except for $\theta_\pm = \pi/2$. Only for $\theta_+ = \theta_- = \pi/2$, we obtain

$$\frac{\Delta_+}{|\Delta_+|} = -\frac{\Delta_-}{|\Delta_-|}. \tag{B20}$$

This is the condition known for zero-energy SABS in unconventional superconductors[1,6].

II-2) $\sin\phi \neq 0$

Hereafter, we suppose $\kappa \leq 1$. In the case of $\kappa > 1$, the same discussion can be held with replacing κ by κ^{-1}.

i)$\underline{\kappa - \cos\phi \geq 0}$

In this case, Eq. (B17) becomes

$$\pm(\kappa + \kappa^{-1} - 2\cos\phi) = \sqrt{(\kappa - \cos\phi)^2 + \sin^2\phi}\sqrt{(\kappa^{-1} - \cos\phi)^2 + \sin^2\phi}. \tag{B21}$$

The case of negative sign of lefthand side does not satisfy above equation. If we choose positive sign, it is not difficult to confirm that the above equation is always satisfied.

On the other hand, Eq. (B18) becomes

$$\begin{aligned}\sin^2\phi - 1 + \cos\phi(\kappa + \kappa^{-1}) - \cos^2\phi &= \cos\phi\left[(\kappa + \kappa^{-1}) - 2\cos\phi\right] \\ &= \cos\phi\sqrt{(\kappa - \cos\phi)^2 + \sin^2\phi}\sqrt{(\kappa^{-1} - \cos\phi)^2 + \sin^2\phi}.\end{aligned} \tag{B22}$$

For $\cos\phi = 0$, Eq. (B22) is satisfied and and it means that it is a solution of SABS. In the case of $\cos\phi \neq 0$, Eq. (B18) becomes the same as Eq. (B17) when we choose plus sign in Eq. (B18). For $\kappa - \cos\phi \geq 0$, there always exists solution of SABS for arbitrary ϕ.

ii)$\underline{\kappa - \cos\phi < 0}$

Eq. (B17) becomes

$$\pm(-\kappa + \kappa^{-1}) = \sqrt{(\kappa - \cos\phi)^2 + \sin^2\phi}\sqrt{(\kappa^{-1} - \cos\phi)^2 + \sin^2\phi}.$$

The negative sign of lefthand side does not satisfy this equation. By taking square of this equation, we obtain

$$\begin{aligned}(\kappa - \kappa^{-1})^2 =& 2 + (\kappa^2 + \kappa^{-2}) + 4\cos^2\phi - 4\cos\phi(\kappa + \kappa^{-1}), \\ \Leftrightarrow \cos\phi =& \frac{1}{2}\left[\kappa + \kappa^{-1} \pm \sqrt{(\kappa - \kappa^{-1})^2}\right] \\ =& \kappa,\ \kappa^{-1}.\end{aligned}$$

The relation $\cos\phi = \kappa$ contradicts $\kappa - \cos\phi < 0$ and $\cos\phi = \kappa^{-1}$ contradicts $\kappa^{-1} \geq 1$. Then, there is no solution of SABS.

To summarize, if $\sin\phi = \sin(-\phi_+ + \phi_-) \neq 0$ is satisfied, the energy dispersion of SABS is given by

$$\begin{aligned}E(\mathbf{k}_\parallel) =& \frac{|\Delta_+||\Delta_-|\sin\phi}{\sqrt{|\Delta_+|^2 + |\Delta_-|^2 - 2|\Delta_+||\Delta_-|\cos\phi}} \\ =& \frac{|\Delta_+||\Delta_-|\sin\phi}{\sqrt{(\Delta_+ - \Delta_-)(\Delta_+^* - \Delta_-^*)}} \\ =& \frac{|\Delta_+||\Delta_-|\sin\phi}{|\Delta_+ - \Delta_-|},\end{aligned} \tag{B23}$$

$$\text{with} \quad \left(\frac{|\Delta_+|}{|\Delta_-|} - \cos\phi\right)\left(\frac{|\Delta_-|}{|\Delta_+|} - \cos\phi\right) \geq 0. \tag{B24}$$

For $\sin\phi = 0$,

$$E(\mathbf{k}_\parallel) = 0, \tag{B25}$$

$$\text{with } \frac{\Delta_+}{|\Delta_+|} = -\frac{\Delta_-}{|\Delta_-|}. \tag{B26}$$

Hereafter, we give some examples of two-dimensional superconductors. Since we consider the case that the interface is located at $x = 0$, k_y is a good quantum number.

1)Two-dimensional spin-triplet p-wave case

Pair potentials $\Delta_\pm$ are given by

$$\Delta_+ = \frac{\Delta_0}{k_\mathrm{F}} \left(k_x \cos\alpha + k_y \sin\alpha\right), \tag{B27}$$

$$\Delta_- = \frac{\Delta_0}{k_\mathrm{F}} \left(-k_x \cos\alpha + k_y \sin\alpha\right), \tag{B28}$$

with $0 \le \alpha \le \pi/2$. Because these pair potentials do not have the imaginary part, the energy dispersion of SABS is $E(\mathbf{k}_\parallel) = 0$ when Eq. (B26) is satisfied. We obtain the domain of $\mathbf{k}$ on the Fermi surface which satisfies Eq. (B26). We firstly calculate the ratios $\Delta_+/\mid\Delta_+\mid$ and $\Delta_-/\mid\Delta_-\mid$. They are given by

$$\frac{\Delta_+}{|\Delta_+|} = \mathrm{sgn}(k_x \cos\alpha + k_y \sin\alpha),$$

$$\frac{\Delta_-}{|\Delta_-|} = \mathrm{sgn}(-k_x \cos\alpha + k_y \sin\alpha).$$

Then, we obtain

$$\begin{aligned}(k_x \cos\alpha + k_y \sin\alpha)(-k_x \cos\alpha + k_y \sin\alpha) &= -k_x^2 \cos^2\alpha + k_y^2 \sin^2\alpha < 0,\\ \Leftrightarrow \tan^2\alpha &< \frac{k_x^2}{k_y^2} = \frac{k_\mathrm{F}^2 - k_y^2}{k_y^2},\\ \Leftrightarrow k_y^2 &< k_\mathrm{F}^2 \cos^2\alpha.\end{aligned} \tag{B29}$$

If we define $k_y/k_\mathrm{F} = \sin\theta$ $(-\pi/2 \le \theta \le \pi/2)$, above inequality can be given by

$$\begin{aligned}|\sin\theta| &= |\cos(\theta + \pi/2)| < \cos\alpha,\\ \Leftrightarrow \alpha - \pi/2 &< \theta < \pi/2 - \alpha.\end{aligned} \tag{B30}$$

To summarize, for spin-triple p-wave pairing, the SABS is given by

$$E(k_y) = 0, \tag{B31}$$

$$\text{with } \alpha - \pi/2 < \theta < \pi/2 - \alpha. \tag{B32}$$

ii)Two-dimensional spin-singlet d-wave case[1,4]

The corresponding pair potentials $\Delta_\pm$ are given by

$$\Delta_+ = \frac{\Delta_0}{k_\mathrm{F}^2} \left[(k_x^2 - k_y^2)\cos 2\alpha + 2k_x k_y \sin 2\alpha\right], \tag{B33}$$

$$\Delta_- = \frac{\Delta_0}{k_\mathrm{F}^2} \left[(k_x^2 - k_y^2)\cos 2\alpha - 2k_x k_y \sin 2\alpha\right], \tag{B34}$$

with $0 \le \alpha \le \pi/4$. Because these pair potentials do not have the imaginary part, the energy dispersion of SABS is $E(\mathrm{k}_\parallel) = 0$ when Eq. (B26) is satisfied. We obtain the domain of $\mathbf{k}$ on the Fermi surface which satisfies Eq. (B26).

$$\begin{aligned}&\left[(k_x^2 - k_y^2)\cos 2\alpha + 2k_x k_y \sin 2\alpha\right]\left[(k_x^2 - k_y^2)\cos 2\alpha - 2k_x k_y \sin 2\alpha\right]\\ =&(k_x^2 - k_y^2)^2 \cos^2 2\alpha - 4k_x^2 k_y^2 \sin^2 2\alpha < 0,\\ \Leftrightarrow \frac{(k_x^2 - k_y^2)^2}{4k_x^2 k_y^2} =& \frac{(k_\mathrm{F}^2 - 2k_y^2)^2}{4(k_\mathrm{F}^2 - k_y^2)k_y^2} < \tan^2 2\alpha,\\ \Leftrightarrow \left(2\frac{k_y^2}{k_\mathrm{F}^2} - 1\right)^2 <& \sin^2 2\alpha\end{aligned} \tag{B35}$$

If we define $k_y/k_{\rm F}=\sin\theta$ $(-\pi/2\le\theta\le\pi/2)$, above inequality can be written by

$$\begin{aligned}|\cos 2\theta| =&|\sin(2\theta-\pi/2)|<\sin 2\alpha,\\ \Leftrightarrow -\alpha-\pi/4<&\theta<\alpha-\pi/4 \text{ or } -\alpha+\pi/4<\theta<\alpha+\pi/4.\end{aligned} \tag{B36}$$

We can summarize that in the d-wave case, the SABS is given by

$$E(k_y)=0, \tag{B37}$$

$$\text{with } -\alpha-\pi/4<\theta<\alpha-\pi/4 \text{ or } -\alpha+\pi/4<\theta<\alpha+\pi/4. \tag{B38}$$

iii)Two-dimensional spin-triplet chiral p-wave case
The pair potentials $\Delta_\pm$ are given by

$$\Delta_+=\frac{\Delta_0}{k_{\rm F}}\left(k_x+ik_y\right), \tag{B39}$$

$$\Delta_-=\frac{\Delta_0}{k_{\rm F}}\left(-k_x+ik_y\right). \tag{B40}$$

The absolute value of the pair potentials are $|\Delta_+|^2=|\Delta_-|^2=\Delta_0^2$. Then Eq. (B24) becomes

$$(1-\cos\alpha)\ge 0.$$

This inequality is always satisfied and the energy dispersion of SABS is given by

$$E(k_y)=\frac{\Delta_0}{k_{\rm F}}\frac{2k_xk_y}{|2k_x|}=\Delta_0\frac{k_y}{k_{\rm F}}, \tag{B41}$$

for any k_y.
iv)Two-dimensional spin-singlet chiral d-wave case
The pair potentials $\Delta_\pm$ are given by

$$\Delta_+=\frac{\Delta_0}{k_{\rm F}^2}(k_x+ik_y)^2, \tag{B42}$$

$$\Delta_-=\frac{\Delta_0}{k_{\rm F}^2}(-k_x+ik_y)^2. \tag{B43}$$

The absolute value of the pair potentials are

$$|\Delta_+|^2=|\Delta_-|^2=\frac{\Delta_0^2}{k_{\rm F}^4}\left[(k_x^2+k_y^2)^2+4k_x^2k_y^2\right]=\frac{\Delta_0^2}{k_{\rm F}^4}\left[k_{\rm F}^4+4(k_{\rm F}^2-k_y^2)k_y^2\right].$$

Then Eq. (B24) becomes

$$(1-\cos\alpha)\ge 0.$$

This inequality is always satisfied and the energy dispersion of SABS is

$$E(k_y)=\frac{\Delta_0}{k_{\rm F}^2}\frac{-4k_xk_y(k_x^2-k_y^2)}{|4k_xk_y|}=-\Delta_0\left(1-2\frac{k_y^2}{k_{\rm F}^2}\right)\mathrm{sgn}(k_y), \tag{B44}$$

for any k_y.
v)Two-dimensional spin-triplet chiral f-wave case
The pair potentials $\Delta_\pm$ are given by

$$\Delta_+=\frac{\Delta_0}{k_{\rm F}^3}(k_x+ik_y)^3, \tag{B45}$$

$$\Delta_-=\frac{\Delta_0}{k_{\rm F}^3}(-k_x+ik_y)^3. \tag{B46}$$

The absolute value of the pair potentials are

$$|\Delta_+|^2 = |\Delta_-|^2 = \frac{\Delta_0^2}{k_{\rm F}^6}\left[(k_x^3 - 3k_x k_y^2)^2 + (3k_x^2 k_y - k_y^3)^2\right].$$

Then Eq. (B24) becomes

$$(1 - \cos\alpha) \geq 0.$$

This inequality is always satisfied and the energy dispersion of SABS is

$$E(k_y) = \frac{\Delta_0}{k_{\rm F}^3} k_y (3k_{\rm F}^2 - 4k_y^2)\mathrm{sgn}(k_{\rm F}^2 - 4k_y^2) = \Delta_0 \frac{k_y}{k_{\rm F}}\left(3 - 4\frac{k_y^2}{k_{\rm F}^2}\right)\mathrm{sgn}(k_{\rm F}^2 - 4k_y^2), \tag{B47}$$

for any k_y.

Appendix C: Conductance for general pair potential

In this Appendix, we derive a conductance formula for any pair potential with single band superconductor where $\hat{\varepsilon}(\mathbf{k})$ in Eq. 2 does not have an off-diagonal element. In Sec. C 1, we introduce eigen vectors used for the wave function of superconducting side. In Sec. C 2, we check orthogonal relation of these vectors. The intermediate expression of Eq. C36 in Sec. C 2 is used in Sec. C 3. In Sec. C 3, we solve boundary conditions and derive conductance. In Sec. C 4, we explain that conductance is invariant under the spin rotation.

1. Derivation of eigen vectors

In this subsection, we derive the eigen vectors of the BdG Hamiltonian. In Eq. (18), we define $\psi^{\rm S}_{e,\sigma}$ and $\psi^{\rm S}_{h,\sigma}$ as

$$\psi^{\rm S}_{e,\uparrow} = \begin{pmatrix} u_{+,p} \\ v_{+,p} \end{pmatrix},\ \psi^{\rm S}_{e,\downarrow} = \begin{pmatrix} u_{+,m} \\ v_{+,m} \end{pmatrix}, \tag{C1}$$

$$\psi^{\rm S}_{h,\uparrow} = \begin{pmatrix} v_{-,p} \\ u_{-,p} \end{pmatrix},\ \psi^{\rm S}_{h,\downarrow} = \begin{pmatrix} v_{-,m} \\ u_{-,m} \end{pmatrix}. \tag{C2}$$

$u_{\pm,p(m)}$ and $v_{\pm,p(m)}$ satisfy

$$\begin{pmatrix} \tilde{\omega}_{+,p(m)}\sigma_0 & \Delta_+ \\ \Delta_+^\dagger & -\tilde{\omega}_{+,p(m)}\sigma_0 \end{pmatrix}\begin{pmatrix} u_{+,p(m)} \\ v_{+,p(m)} \end{pmatrix} = E\begin{pmatrix} u_{+,p(m)} \\ v_{+,p(m)} \end{pmatrix}, \tag{C3}$$

$$\begin{pmatrix} -\tilde{\omega}_{-,p(m)}\sigma_0 & \Delta_- \\ \Delta_-^\dagger & \tilde{\omega}_{-,p(m)}\sigma_0 \end{pmatrix}\begin{pmatrix} v_{-,p(m)} \\ u_{-,p(m)} \end{pmatrix} = E\begin{pmatrix} v_{-,p(m)} \\ u_{-,p(m)} \end{pmatrix}, \tag{C4}$$

where σ_0 is the 2×2 identity matrix and

$$\Delta_\pm = [D_\pm + \mathbf{d}_\pm \cdot \boldsymbol{\sigma}] i\sigma_2 \tag{C5}$$

$$\tilde{\omega}_{\pm,p} = \sqrt{E^2 - (|\mathbf{d}_\pm|^2 + |D_\pm|^2 + |\mathbf{J}_\pm|)}, \tag{C6}$$

$$\tilde{\omega}_{\pm,m} = \sqrt{E^2 - (|\mathbf{d}_\pm|^2 + |D_\pm|^2 - |\mathbf{J}_\pm|)}, \tag{C7}$$

$$\mathbf{J}_\pm = \pm\mathbf{F}_\pm + \mathbf{q}_\pm \tag{C8}$$

$$\mathbf{F}_\pm = D_\pm \mathbf{d}_\pm^* + D_\pm^* \mathbf{d}_\pm, \tag{C9}$$

$$\mathbf{q}_\pm = i\mathbf{d}_\pm \times \mathbf{d}_\pm^*, \tag{C10}$$

with $D_+ = D(\mathbf{k})$, $D_- = D(\tilde{\mathbf{k}})$, $\mathbf{d}_+ = \mathbf{d}(\mathbf{k})$, $\mathbf{d}_- = \mathbf{d}(\tilde{\mathbf{k}})$ and $\tilde{\mathbf{k}} = (k_x, k_y, -k_z)$. $\mathbf{F}_\pm$ and $\mathbf{q}_\pm$ are real valued functions and perpendicular to each other. D is a spin-singlet pair amplitude and $\mathbf{d}$ is a triplet one. $\tilde{\omega}_{\pm,p(m)}$ is derived by diagonalizing following matrix with the eigen value E^2.

$$\begin{pmatrix} \pm\omega\sigma_0 & \Delta_\pm \\ \Delta_\pm^\dagger & \mp\omega\sigma_0 \end{pmatrix}^2 = \begin{pmatrix} \omega^2\sigma_0 + \Delta_\pm\Delta_\pm^\dagger & 0 \\ 0 & \omega^2\sigma_0 + \Delta_\pm^\dagger\Delta_\pm \end{pmatrix} \tag{C11}$$

with

$$\Delta_\pm\Delta_\pm^\dagger = |D_\pm|^2 + |\mathbf{d}_\pm|^2 + (\mathbf{F}_\pm + \mathbf{q}_\pm)\cdot\boldsymbol{\sigma}, \tag{C12}$$

$$\Delta_\pm^\dagger\Delta_\pm = |D_\pm|^2 + |\mathbf{d}_\pm|^2 + (-\mathbf{F}_\pm + \mathbf{q}_\pm)\cdot\boldsymbol{\sigma}^*, \tag{C13}$$

where the relation $\sigma_2\boldsymbol{\sigma}\sigma_2 = -\boldsymbol{\sigma}^*$ is used.

From Eqs. (C3) and (C4),

$$\begin{aligned}
\tilde{\omega}_{+,p(m)}u_{+,p(m)} + \Delta_+ v_{+,p(m)} &= Eu_{+,p(m)},\\
\Delta_+^\dagger u_{+,p(m)} - \tilde{\omega}_{+,p(m)}v_{+,p(m)} &= Ev_{+,p(m)},\\
\Rightarrow u_{+,p(m)}(E-\tilde{\omega}_{+,p(m)})(E+\tilde{\omega}_{+,p(m)}) &= \Delta_+\Delta_+^\dagger u_{+,p(m)}, \qquad \text{(C14)}\\
-\tilde{\omega}_{-,p(m)}v_{-,p(m)} + \Delta_- u_{-,p(m)} &= Ev_{-,p(m)},\\
\Delta_-^\dagger v_{-,p(m)} + \tilde{\omega}_{-,p(m)}u_{-,p(m)} &= Eu_{-,p(m)},\\
\Rightarrow u_{-,p(m)}(E-\tilde{\omega}_{-,p(m)})(E+\tilde{\omega}_{-,p(m)}) &= \Delta_-^\dagger\Delta_- u_{-,p(m)}. \qquad \text{(C15)}
\end{aligned}$$

To simplify above equations, we define 2×2 matrices as

$$\check{\omega}_{\pm,pm} = \begin{pmatrix} \tilde{\omega}_{\pm,p} & 0 \\ 0 & \tilde{\omega}_{\pm,m}\end{pmatrix}, \tag{C16}$$

$$u_\pm = \begin{pmatrix} u_{\pm,p} & u_{\pm,m}\end{pmatrix}, \tag{C17}$$

$$v_\pm = \begin{pmatrix} v_{\pm,p} & v_{\pm,m}\end{pmatrix}. \tag{C18}$$

Eqs. (C14) and (C15) become

$$u_+(E\sigma_0 - \check{\omega}_{+,pm})(E\sigma_0 + \check{\omega}_{+,pm}) = \Delta_+\Delta_+^\dagger u_+, \tag{C19}$$

$$u_-(E\sigma_0 - \check{\omega}_{-,pm})(E\sigma_0 + \check{\omega}_{-,pm}) = \Delta_-^\dagger\Delta_- u_-. \tag{C20}$$

u_+ and u_- are given by[77]

$$u_+ = \tilde{a}_+\left(|\mathbf{J}_+|\sigma_0 + \mathbf{J}_+\cdot\boldsymbol{\sigma}\right)(\sigma_0+\sigma_3) + \tilde{b}_+\left(|\mathbf{J}_+|\sigma_0 - \mathbf{J}_+\cdot\boldsymbol{\sigma}\right)(\sigma_0-\sigma_3), \tag{C21}$$

$$u_- = \tilde{a}_-\left(|\mathbf{J}_-|\sigma_0 + \mathbf{J}_-\cdot\boldsymbol{\sigma}^*\right)(\sigma_0+\sigma_3) + \tilde{b}_-\left(|\mathbf{J}_-|\sigma_0 - \mathbf{J}_-\cdot\boldsymbol{\sigma}^*\right)(\sigma_0-\sigma_3), \tag{C22}$$

with

$$\tilde{a}_\pm(\tilde{b}_\pm) = \sqrt{\frac{1}{16|\mathbf{J}_\pm|[|\mathbf{J}_\pm| + (\mathbf{J}_\pm)_3]}\frac{E+\tilde{\omega}_{\pm,p(m)}}{E}}. \tag{C23}$$

By using $u_\pm$, $v_\pm$ can be expressed as

$$v_+ = \Delta_+^\dagger u_+(E\sigma_0 + \check{\omega}_{+,pm})^{-1}, \tag{C24}$$

$$v_- = \Delta_- u_-(E\sigma_0 + \check{\omega}_{-,pm})^{-1}. \tag{C25}$$

2. Orthogonal relation of $u_\pm$ and $v_\pm$

In this subsection, we check that a matrix composed of $u_\pm$ and $v_\pm$ is an unitary matrix. $u_\pm$ and $v_\pm$ satisfy the following equation.

$$\begin{aligned}
\sigma_0 &= u_\pm^\dagger(\mathbf{k})u_\pm(\mathbf{k}) + v_\pm^\dagger(\mathbf{k})v_\pm(\mathbf{k})\\
&= u_\pm(\mathbf{k})u_\pm^\dagger(\mathbf{k}) + v_\pm^*(-\mathbf{k})v_\pm^{\mathrm{T}}(-\mathbf{k}),
\end{aligned} \tag{C26}$$

because

$$U_\pm = \begin{pmatrix} u_\pm(\mathbf{k}) & v_\pm^*(-\mathbf{k}) \\ v_\pm(\mathbf{k}) & u_\pm^*(-\mathbf{k})\end{pmatrix} \tag{C27}$$

is an unitary matrix. Here, we check Eq. (C26).

Firstly, we check $u_+^\dagger u_+ + v_+^\dagger v_+ = \sigma_0$. It is noted that $\mathbf{J}_\pm$ is a real-valued vector.

$$\begin{aligned}
u_+^\dagger u_+ =&\tilde{a}_+^2(\sigma_0+\sigma_3)\left[|\mathbf{J}_+|\sigma_0+\mathbf{J}_+\cdot\boldsymbol{\sigma}\right]^2(\sigma_0+\sigma_3)\\
&+\tilde{a}_+\tilde{b}_+(\sigma_0+\sigma_3)\left[|\mathbf{J}_+|^2\sigma_0-|\mathbf{J}_+|^2\sigma_0\right](\sigma_0-\sigma_3)\\
&+\tilde{a}_+\tilde{b}_+(\sigma_0-\sigma_3)\left[|\mathbf{J}_+|^2\sigma_0-|\mathbf{J}_+|^2\sigma_0\right](\sigma_0+\sigma_3)\\
&+\tilde{b}_+^2(\sigma_0-\sigma_3)\left[|\mathbf{J}_+|\sigma_0-\mathbf{J}_+\cdot\boldsymbol{\sigma}\right]^2(\sigma_0-\sigma_3)\\
=&2\tilde{a}_+^2|\mathbf{J}_+|(\sigma_0+\sigma_3)\left[|\mathbf{J}_+|\sigma_0+\mathbf{J}_+\cdot\boldsymbol{\sigma}\right](\sigma_0+\sigma_3)+2\tilde{b}_+^2|\mathbf{J}_+|(\sigma_0-\sigma_3)\left[|\mathbf{J}_+|\sigma_0-\mathbf{J}_+\cdot\boldsymbol{\sigma}\right](\sigma_0-\sigma_3),
\end{aligned}\tag{C28}$$

Here we used the following relations.

$$\begin{aligned}
\mathbf{J}_+\cdot\boldsymbol{\sigma}\sigma_3 =&(\mathbf{J}_+)_1(-i\sigma_2)+(\mathbf{J}_+)_2(i\sigma_1)+(\mathbf{J}_+)_3\sigma_0, &\text{(C29)}\\
\sigma_3\mathbf{J}_+\cdot\boldsymbol{\sigma} =&(\mathbf{J}_+)_1(i\sigma_2)+(\mathbf{J}_+)_2(-i\sigma_1)+(\mathbf{J}_+)_3\sigma_0, &\text{(C30)}\\
\sigma_3\mathbf{J}_+\cdot\boldsymbol{\sigma}\sigma_3 =&-(\mathbf{J}_+)_1\sigma_1-(\mathbf{J}_+)_2\sigma_2+(\mathbf{J}_+)_3\sigma_3, &\text{(C31)}\\
(\sigma_0\pm\sigma_3)\sigma_0(\sigma_0\pm\sigma_3) =&2(\sigma_0\pm\sigma_3), &\text{(C32)}\\
(\sigma_0\pm\sigma_3)\mathbf{J}_+\cdot\boldsymbol{\sigma}(\sigma_0\pm\sigma_3) =&\pm 2(\mathbf{J}_+)_3(\sigma_0\pm\sigma_3). &\text{(C33)}
\end{aligned}$$

Then

$$\begin{aligned}
u_+^\dagger u_+ =&4|\mathbf{J}_+|\left[|\mathbf{J}_+|+(\mathbf{J}_+)_3\right]\left[\tilde{a}_+^2(\sigma_0+\sigma_3)+\tilde{b}_+^2(\sigma_0-\sigma_3)\right]\\
=&8|\mathbf{J}_+|\left[|\mathbf{J}_+|+(\mathbf{J}_+)_3\right]\begin{pmatrix}\tilde{a}_+^2 & 0\\ 0 & \tilde{b}_+^2\end{pmatrix}.
\end{aligned}\tag{C34}$$

From Eqs. (C12), (C19) and (C24), $v_+^\dagger v_+$ can be caluclated as

$$\begin{aligned}
v_+^\dagger v_+ =&(E\sigma_0+\breve{\omega}_{+,pm})^{-1}u_+^\dagger\Delta_+\Delta_+^\dagger u_+(E\sigma_0+\breve{\omega}_{+,pm})^{-1}\\
=&(E\sigma_0+\breve{\omega}_{+,pm})^{-1}u_+^\dagger u_+(E\sigma_0-\breve{\omega}_{+,pm})(E\sigma_0+\breve{\omega}_{+,pm})(E\sigma_0+\breve{\omega}_{+,pm})^{-1}\\
=&4|\mathbf{J}_+|\left[|\mathbf{J}_+|+(\mathbf{J}_+)_3\right]\left[\tilde{a}_+^2(\sigma_0+\sigma_3)+\tilde{b}_+^2(\sigma_0-\sigma_3)\right](E\sigma_0+\breve{\omega}_{+,pm})^{-1}(E\sigma_0-\breve{\omega}_{+,pm})\\
=&8|\mathbf{J}_+|\left[|\mathbf{J}_+|+(\mathbf{J}_+)_3\right]\begin{pmatrix}\tilde{a}_+^2\frac{E-\tilde{\omega}_{+,p}}{E+\tilde{\omega}_{+,p}} & 0\\ 0 & \tilde{b}_+^2\frac{E-\tilde{\omega}_{+,m}}{E+\tilde{\omega}_{+,m}}\end{pmatrix}.
\end{aligned}\tag{C35}$$

Combined with Eqs. (C23), (C34) and (C35), $u_+^\dagger u_+ + v_+^\dagger v_+ = \sigma_0$ is derived. $u_-^\dagger u_- + v_-^\dagger v_- = \sigma_0$ is derived similarly.

Next confirm the relation $u_+u_+^\dagger + (v_+v_+^\dagger)^* = \sigma_0$ [second row of Eq. (C26)].

$$\begin{aligned}
u_+u_+^\dagger =&2\tilde{a}_+^2\left(|\mathbf{J}_+|\sigma_0+\mathbf{J}_+\cdot\boldsymbol{\sigma}\right)(\sigma_0+\sigma_3)\left(|\mathbf{J}_+|\sigma_0+\mathbf{J}_+\cdot\boldsymbol{\sigma}\right)+2\tilde{b}_+^2\left(|\mathbf{J}_+|\sigma_0-\mathbf{J}_+\cdot\boldsymbol{\sigma}\right)(\sigma_0-\sigma_3)\left(|\mathbf{J}_+|\sigma_0-\mathbf{J}_+\cdot\boldsymbol{\sigma}\right)\\
=&4\left[|\mathbf{J}_+|+(\mathbf{J}_+)_3\right]\left[\tilde{a}_+^2(|\mathbf{J}_+|\sigma_0+\mathbf{J}_+\cdot\boldsymbol{\sigma})+\tilde{b}_+^2(|\mathbf{J}_+|\sigma_0-\mathbf{J}_+\cdot\boldsymbol{\sigma})\right]\\
=&\frac{1}{4|\mathbf{J}_+|}\left[\frac{E+\tilde{\omega}_{+,p}}{E}(|\mathbf{J}_+|\sigma_0+\mathbf{J}_+\cdot\boldsymbol{\sigma})+\frac{E+\tilde{\omega}_{-,p}}{E}(|\mathbf{J}_+|\sigma_0-\mathbf{J}_+\cdot\boldsymbol{\sigma})\right]
\end{aligned}\tag{C36}$$

where we have used the following five relations

$$(|\mathbf{J}_+|\sigma_0 \pm \mathbf{J}_+\cdot\boldsymbol{\sigma})\,(\sigma_0\pm\sigma_3)\,(|\mathbf{J}_+|\sigma_0 \pm \mathbf{J}_+\cdot\boldsymbol{\sigma}) = 2|\mathbf{J}_+|(|\mathbf{J}_+|\sigma_0 \pm \mathbf{J}_+\cdot\boldsymbol{\sigma}) \pm (|\mathbf{J}_+|\sigma_0 \pm \mathbf{J}_+\cdot\boldsymbol{\sigma})\,\sigma_3\,(|\mathbf{J}_+|\sigma_0 \pm \mathbf{J}_+\cdot\boldsymbol{\sigma}), \tag{C37}$$

$$\begin{aligned}(|\mathbf{J}_+|\sigma_0 \pm \mathbf{J}_+\cdot\boldsymbol{\sigma})\,\sigma_3\,(|\mathbf{J}_+|\sigma_0 \pm \mathbf{J}_+\cdot\boldsymbol{\sigma}) &= (|\mathbf{J}_+|\sigma_0 \pm \mathbf{J}_+\cdot\boldsymbol{\sigma})\,\{|\mathbf{J}_+|\sigma_3 \pm [i\,(\mathbf{J}_+\times\boldsymbol{\sigma})_3 + (\mathbf{J}_+)_3\sigma_0]\}\\ &= |\mathbf{J}_+|\,\{|\mathbf{J}_+|\sigma_3 \pm [i(\mathbf{J}_+\times\boldsymbol{\sigma})_3 + (\mathbf{J}_+)_3\sigma_0]\}\\ &\quad + \left\{\pm[-i|\mathbf{J}_+|(\mathbf{J}_+\times\boldsymbol{\sigma})_3 + |\mathbf{J}_+|(\mathbf{J}_+)_3\sigma_0] - |\mathbf{J}_+|^2\sigma_3 + 2(\mathbf{J}_+)_3\mathbf{J}_+\cdot\boldsymbol{\sigma}\right\}\\ &= \pm\,2(\mathbf{J}_+)_3(|\mathbf{J}_+|\sigma_0 \pm \mathbf{J}_+\cdot\boldsymbol{\sigma}),\end{aligned} \tag{C38}$$

$$\begin{aligned}\mathbf{J}_+\cdot\boldsymbol{\sigma}\sigma_3 &= (\mathbf{J}_+)_1(-i\sigma_2) + (\mathbf{J}_+)_2(i\sigma_1) + (\mathbf{J}_+)_3\sigma_0\\ &= -\,i(\mathbf{J}_+\times\boldsymbol{\sigma})_3 + (\mathbf{J}_+)_3\sigma_0,\end{aligned} \tag{C39}$$

$$\sigma_3\mathbf{J}_+\cdot\boldsymbol{\sigma} = i(\mathbf{J}_+\times\boldsymbol{\sigma})_3 + (\mathbf{J}_+)_3\sigma_0, \tag{C40}$$

$$\begin{aligned}\mathbf{J}_+\cdot\boldsymbol{\sigma}i(\mathbf{J}_+\times\boldsymbol{\sigma})_3 &= i\mathbf{J}_+\cdot\boldsymbol{\sigma}\,[(\mathbf{J}_+)_1\sigma_2 - (\mathbf{J}_+)_2\sigma_1]\\ &= i(\mathbf{J}_+)_1\,[(\mathbf{J}_+)_1 i\sigma_3 - (\mathbf{J}_+)_2\sigma_0] + i(\mathbf{J}_+)_2[(\mathbf{J}_+)_1\sigma_0 - (\mathbf{J}_+)_2(-i\sigma_3)]\\ &\quad + i(\mathbf{J}_+)_3[(\mathbf{J}_+)_1(-i\sigma_1) - (\mathbf{J}_+)_2 i\sigma_2]\\ &= (\mathbf{J}_+)_3\mathbf{J}_+\cdot\boldsymbol{\sigma} - |\mathbf{J}_+|^2\sigma_3.\end{aligned} \tag{C41}$$

Then we calculate $v_+^*(-\mathbf{k})v_+^{\mathrm{T}}(-\mathbf{k}) = [v_+(-\mathbf{k})v_+^\dagger(-\mathbf{k})]^*$. First, we define

$$\mathbf{J}' = -\mathbf{F}_+ + \mathbf{q}_+. \tag{C42}$$

It is noted that $|\mathbf{J}_+| = |\mathbf{J}'|$ since $\mathbf{F}_+$ and $\mathbf{q}_+$ are perpendicular to each other. Then, from $D_\pm(-\mathbf{k}) = D_\pm(\mathbf{k})$ and $\mathbf{d}_\pm(-\mathbf{k}) = -\mathbf{d}_\pm(\mathbf{k})$, we obtain the relations,

$$v_+(-\mathbf{k}) = \{[D_+(\mathbf{k}) - \mathbf{d}_+(\mathbf{k})\cdot\boldsymbol{\sigma}]i\sigma_2\}^\dagger\,u_+(-\mathbf{k})(E\sigma_0 + \breve{\omega}_{+,pm})^{-1}, \tag{C43}$$

$$u_+(-\mathbf{k}) = \tilde{a}_+(-\mathbf{k})\,(|\mathbf{J}'|\sigma_0 + \mathbf{J}'\cdot\boldsymbol{\sigma})\,(\sigma_0+\sigma_3) + \tilde{b}_+(-\mathbf{k})\,(|\mathbf{J}'|\sigma_0 - \mathbf{J}'\cdot\boldsymbol{\sigma})\,(\sigma_0-\sigma_3). \tag{C44}$$

Because $\breve{\omega}_{+,pm}(-\mathbf{k}) = \breve{\omega}_{+,pm}(\mathbf{k})$,

$$\begin{aligned}v_+(-\mathbf{k})v_+^\dagger(-\mathbf{k}) &= 2[\tilde{a}_+(-\mathbf{k})]^2\frac{1}{(E+\tilde{\omega}_{+,p})^2}\Delta^\dagger(-\mathbf{k})\,(|\mathbf{J}'|\sigma_0 + \mathbf{J}'\cdot\boldsymbol{\sigma})\,(\sigma_0+\sigma_3)\,(|\mathbf{J}'|\sigma_0 + \mathbf{J}'\cdot\boldsymbol{\sigma})\,\Delta(-\mathbf{k})\\ &\quad + 2[\tilde{b}_+(-\mathbf{k})]^2\frac{1}{(E+\tilde{\omega}_{+,m})^2}\Delta^\dagger(-\mathbf{k})\,(|\mathbf{J}'|\sigma_0 - \mathbf{J}'\cdot\boldsymbol{\sigma})\,(\sigma_0-\sigma_3)\,(|\mathbf{J}'|\sigma_0 - \mathbf{J}'\cdot\boldsymbol{\sigma})\,\Delta(-\mathbf{k})\\ &= 4\,(|\mathbf{J}'| + \mathbf{J}'_3)\left\{[\tilde{a}_+(-\mathbf{k})]^2\frac{1}{(E+\tilde{\omega}_{+,p})^2}\Delta^\dagger(-\mathbf{k})(|\mathbf{J}'|\sigma_0 + \mathbf{J}'\cdot\boldsymbol{\sigma})\Delta(-\mathbf{k})\right.\\ &\quad \left. + [\tilde{b}_+(-\mathbf{k})]^2\frac{1}{(E+\tilde{\omega}_{+,m})^2}\Delta^\dagger(-\mathbf{k})(|\mathbf{J}'|\sigma_0 - \mathbf{J}'\cdot\boldsymbol{\sigma})\Delta(-\mathbf{k})\right\}.\end{aligned} \tag{C45}$$

In order to obtain $v_+(-\mathbf{k})v_+^\dagger(-\mathbf{k})$, we calculate following quantities.

$$\begin{aligned}\Delta_+^\dagger(-\mathbf{k})(|\mathbf{J}'|\sigma_0 \pm \mathbf{J}'\cdot\boldsymbol{\sigma})\Delta_+(-\mathbf{k}) &= -\,i\sigma_2(D_+^* - \mathbf{d}_+^*\cdot\boldsymbol{\sigma})(|\mathbf{J}'|\sigma_0 \pm \mathbf{J}'\cdot\boldsymbol{\sigma})(D_+ - \mathbf{d}_+\cdot\boldsymbol{\sigma})i\sigma_2\\ &= -\,i\sigma_2|\mathbf{J}'|\left(|D_+|^2 + |\mathbf{d}_+|^2 - \mathbf{J}_+\cdot\boldsymbol{\sigma}\right)i\sigma_2\\ &\quad -\,i\sigma_2(D_+^* - \mathbf{d}_+^*\cdot\boldsymbol{\sigma})(\pm\mathbf{J}'\cdot\boldsymbol{\sigma})(D_+ - \mathbf{d}_+\cdot\boldsymbol{\sigma})i\sigma_2,\\ (D_+^* - \mathbf{d}_+^*\cdot\boldsymbol{\sigma})\mathbf{J}'\cdot\boldsymbol{\sigma}(D_+ - \mathbf{d}_+\cdot\boldsymbol{\sigma}) &= |D_+|^2\mathbf{J}'\cdot\boldsymbol{\sigma} - D_+^*\mathbf{J}'\cdot\boldsymbol{\sigma}\mathbf{d}_+\cdot\boldsymbol{\sigma} - D_+\mathbf{d}_+^*\cdot\boldsymbol{\sigma}\mathbf{J}'\cdot\boldsymbol{\sigma} + \mathbf{d}_+^*\cdot\boldsymbol{\sigma}\mathbf{J}'\cdot\boldsymbol{\sigma}\mathbf{d}_+\cdot\boldsymbol{\sigma},\\ \mathbf{J}'\cdot\boldsymbol{\sigma}\mathbf{d}_+\cdot\boldsymbol{\sigma} &= \mathbf{J}'\cdot\mathbf{d}_+\sigma_0 + i(\mathbf{J}'\times\mathbf{d}_+)\cdot\boldsymbol{\sigma}\\ &= -\,\mathbf{F}_+\cdot\mathbf{d}_+\sigma_0 + D_+\mathbf{q}_+\cdot\boldsymbol{\sigma} + [|\mathbf{d}_+|^2\mathbf{d}_+ - (\mathbf{d}_+)^2\mathbf{d}_+^*]\cdot\boldsymbol{\sigma},\\ \mathbf{d}_+^*\cdot\boldsymbol{\sigma}\mathbf{J}'\cdot\boldsymbol{\sigma} &= \mathbf{d}_+^*\cdot\mathbf{J}'\sigma_0 + i(\mathbf{d}_+^*\times\mathbf{J}')\cdot\boldsymbol{\sigma}\\ &= -\,\mathbf{F}_+\cdot\mathbf{d}_+^*\sigma_0 + i(\mathbf{d}_+^*\times\mathbf{J}')\cdot\boldsymbol{\sigma}\\ &= -\,\mathbf{F}_+\cdot\mathbf{d}_+^*\sigma_0 + D_+^*\mathbf{q}_+\cdot\boldsymbol{\sigma} + i(\mathbf{d}_+^*\times\mathbf{q}_+)\cdot\boldsymbol{\sigma}\\ &= -\,\mathbf{F}_+\cdot\mathbf{d}_+^*\sigma_0 + D_+^*\mathbf{q}_+\cdot\boldsymbol{\sigma} + [|\mathbf{d}_+|^2\mathbf{d}_+^* - (\mathbf{d}_+^*)^2\mathbf{d}_+]\cdot\boldsymbol{\sigma},\\ \mathbf{d}_+^*\cdot\boldsymbol{\sigma}\mathbf{J}'\cdot\boldsymbol{\sigma}\mathbf{d}_+\cdot\boldsymbol{\sigma} &= \left[(\mathbf{d}_+^*\cdot\mathbf{J}')\mathbf{d}_+ - |\mathbf{d}|^2\mathbf{J}' + (\mathbf{d}_+\cdot\mathbf{J}')\mathbf{d}_+^*\right]\cdot\boldsymbol{\sigma} + i\mathbf{J}'\cdot(\mathbf{d}_+\times\mathbf{d}_+^*)\sigma_0\\ &= -\left[(\mathbf{d}_+^*\cdot\mathbf{F}_+)\mathbf{d}_+ + |\mathbf{d}|^2\mathbf{J}' + (\mathbf{d}_+\cdot\mathbf{F}_+)\mathbf{d}_+^*\right]\cdot\boldsymbol{\sigma} + \mathbf{q}_+^2\sigma_0,\end{aligned}$$

where the relation

$$\sigma_i\sigma_j\sigma_k = \delta_{ij}\sigma_k - \delta_{ik}\sigma_j + \delta_{jk}\sigma_i + i\varepsilon_{ijk}\sigma_0 \tag{C46}$$

is used. Then, we obtain

$$(D_+^* - \mathbf{d}_+^*\cdot\boldsymbol{\sigma})\mathbf{J}'\cdot\boldsymbol{\sigma}(D_+ - \mathbf{d}_+\cdot\boldsymbol{\sigma}) = |\mathbf{J}'|^2\sigma_0 - (|D_+|^2 + |\mathbf{d}_+|^2)\mathbf{J}_+\cdot\boldsymbol{\sigma}, \tag{C47}$$

$$\begin{aligned}\Delta_+^\dagger(-\mathbf{k})(|\mathbf{J}'|\sigma_0 \pm \mathbf{J}'\cdot\boldsymbol{\sigma})\Delta_+(-\mathbf{k}) =& \sigma_2(|D_+|^2 + |\mathbf{d}_+|^2 \pm |\mathbf{J}_+|)\,(|\mathbf{J}'|\sigma_0 \mp \mathbf{J}_+\cdot\boldsymbol{\sigma})\,\sigma_2 \\ =& (|D_+|^2 + |\mathbf{d}_+|^2 \pm |\mathbf{J}_+|)\,(|\mathbf{J}_+|\sigma_0 \pm \mathbf{J}_+\cdot\boldsymbol{\sigma}^*)\,.\end{aligned} \tag{C48}$$

Finally,we obtain following relation

$$\begin{aligned}v_+(-\mathbf{k})v_+^\dagger(-\mathbf{k}) =& 4\,[|\mathbf{J}_+| + \mathbf{J}'_3]\left\{[\tilde{a}_+(-\mathbf{k})]^2\frac{E-\tilde{\omega}_{+,p}}{E+\tilde{\omega}_{+,p}}\,(|\mathbf{J}_+|\sigma_0 + \mathbf{J}_+\cdot\boldsymbol{\sigma}^*)\right. \\ &\left. + [\tilde{b}_+(-\mathbf{k})]^2\frac{E-\tilde{\omega}_{+,m}}{E+\tilde{\omega}_{+,m}}\,(|\mathbf{J}_+|\sigma_0 - \mathbf{J}_+\cdot\boldsymbol{\sigma}^*)\right\} \\ =& \frac{1}{4|\mathbf{J}_+|}\left[\frac{E-\tilde{\omega}_{+,p}}{E}\,(|\mathbf{J}_+|\sigma_0 + \mathbf{J}_+\cdot\boldsymbol{\sigma}^*) + \frac{E-\tilde{\omega}_{+,m}}{E}\,(|\mathbf{J}_+|\sigma_0 - \mathbf{J}_+\cdot\boldsymbol{\sigma}^*)\right]\end{aligned} \tag{C49}$$

$$\begin{aligned}u_+(\mathbf{k})u_+(\mathbf{k})^\dagger + [v_+(-\mathbf{k})v_+(-\mathbf{k})^\dagger]^* =& \frac{1}{4|\mathbf{J}_+|}\left[\left(\frac{E+\tilde{\omega}_{+,p}}{E} + \frac{E-\tilde{\omega}_{+,p}}{E}\right)(|\mathbf{J}_+|\sigma_0 + \mathbf{J}_+\cdot\boldsymbol{\sigma})\right. \\ &\left. + \left(\frac{E+\tilde{\omega}_{+,m}}{E} + \frac{E-\tilde{\omega}_{+,m}}{E}\right)(|\mathbf{J}_+|\sigma_0 - \mathbf{J}_+\cdot\boldsymbol{\sigma})\right] \\ =& \sigma_0.\end{aligned} \tag{C50}$$

The relation $u_-(\mathbf{k})u_-(\mathbf{k})^\dagger + v_-^*(-\mathbf{k})v_-^{\mathrm{T}}(-\mathbf{k}) = \sigma_0$ is derived similarly.

3. Conductance

Tunneling conductance for general pair potential is obtained by solving following boundary conditions [Eq. (26) and Eq. (27)].

$$e_\sigma + \begin{pmatrix} b_\sigma \\ a_\sigma \end{pmatrix} = \begin{pmatrix} u_+ & v_- \\ v_+ & u_- \end{pmatrix}\begin{pmatrix} c \\ d \end{pmatrix}, \tag{C51}$$

$$ik_z\begin{pmatrix} u_+ & v_- \\ v_+ & u_- \end{pmatrix}\begin{pmatrix} \sigma_0 & 0 \\ 0 & -\sigma_0 \end{pmatrix}\begin{pmatrix} c \\ d \end{pmatrix} - ik_z e_\sigma + ik_z\begin{pmatrix} \sigma_0 & 0 \\ 0 & -\sigma_0 \end{pmatrix}\begin{pmatrix} b_\sigma \\ a_\sigma \end{pmatrix} = \frac{2mU_0}{\hbar^2}\left[e_\sigma + \begin{pmatrix} b_\sigma \\ a_\sigma \end{pmatrix}\right], \tag{C52}$$

with

$$e_\uparrow = (1,0,0,0)^{\mathrm{T}},\ e_\downarrow = (0,1,0,0)^{\mathrm{T}},\ a_\sigma = (a_{\sigma,\uparrow}, a_{\sigma,\downarrow})^{\mathrm{T}},\ b_\sigma = (b_{\sigma,\uparrow}, b_{\sigma,\downarrow})^{\mathrm{T}},\ c = (c_\uparrow, c_\downarrow)^{\mathrm{T}},\ d = (d_\uparrow, d_\downarrow)^{\mathrm{T}}.$$

We define

$$\hat{\Theta}_\pm = v_\pm(u_\pm)^{-1}, \tag{C53}$$

$$Z' = \frac{2mU_0}{k_z\hbar^2}, \tag{C54}$$

$$G = \begin{pmatrix} u_+ & v_- \\ v_+ & u_- \end{pmatrix}. \tag{C55}$$

From Eqs. (C24) and (C25), $\hat{\Theta}_+$ and $\hat{\Theta}_-$ satisfy,

$$\hat{\Theta}_+ = \Delta_+^\dagger u_+(E\sigma_0 + \breve{\omega}_{+,pm})^{-1}u_+^{-1}, \tag{C56}$$

$$\hat{\Theta}_- = \Delta_- u_-(E\sigma_0 + \breve{\omega}_{-,pm})^{-1}u_-^{-1}. \tag{C57}$$

We can check that following $u_\pm^{-1}$ given by Eqs. (C58) and (C59) satisfy $u_\pm u_\pm^{-1} = \sigma_0$.

$$u_+^{-1} = \check{a}_+(\sigma_0+\sigma_3)\left(|\mathbf{J}_+|\sigma_0 + \mathbf{J}_+\cdot\boldsymbol{\sigma}\right) + \check{b}_+(\sigma_0-\sigma_3)\left(|\mathbf{J}_+|\sigma_0 - \mathbf{J}_+\cdot\boldsymbol{\sigma}\right) \tag{C58}$$

$$u_-^{-1} = \check{a}_-(\sigma_0+\sigma_3)\left(|\mathbf{J}_-|\sigma_0 + \mathbf{J}_-\cdot\boldsymbol{\sigma}^*\right) + \check{b}_-(\sigma_0-\sigma_3)\left(|\mathbf{J}_-|\sigma_0 - \mathbf{J}_-\cdot\boldsymbol{\sigma}^*\right) \tag{C59}$$

$$\check{a}_\pm = \sqrt{\frac{1}{4|\mathbf{J}_\pm|[|\mathbf{J}_\pm| + (\mathbf{J}_\pm)_3]}\frac{E}{E+\tilde{\omega}_{\pm,p}}} \tag{C60}$$

$$\check{b}_\pm = \sqrt{\frac{1}{4|\mathbf{J}_\pm|[|\mathbf{J}_\pm| + (\mathbf{J}_\pm)_3]}\frac{E}{E+\tilde{\omega}_{\pm,m}}}$$

$$\tilde{a}_\pm\check{a}_\pm = \tilde{b}_\pm\check{b}_\pm = \frac{1}{8|\mathbf{J}_\pm|[|\mathbf{J}_\pm| + (\mathbf{J}_\pm)_3]} \tag{C61}$$

From Eq. (C36), $\hat{\Theta}_+$ and $\hat{\Theta}_-$ are obtained as

$$\begin{aligned}
\hat{\Theta}_+ =& \Delta_+^\dagger\left[2\tilde{a}_+\check{a}_+\frac{1}{E+\tilde{\omega}_{+,p}}\left(|\mathbf{J}_+|\sigma_0+\mathbf{J}_+\cdot\boldsymbol{\sigma}\right)(\sigma_0+\sigma_3)\left(|\mathbf{J}_+|\sigma_0+\mathbf{J}_+\cdot\boldsymbol{\sigma}\right)\right.\\
&\left.+\,2\tilde{b}_+\check{b}_+\frac{1}{E+\tilde{\omega}_{+,m}}\left(|\mathbf{J}_+|\sigma_0-\mathbf{J}_+\cdot\boldsymbol{\sigma}\right)(\sigma_0-\sigma_3)\left(|\mathbf{J}_+|\sigma_0-\mathbf{J}_+\cdot\boldsymbol{\sigma}\right)\right]\\
=& 4[|\mathbf{J}_+| + (\mathbf{J}_+)_3]\Delta_+^\dagger\left[\tilde{a}_+\check{a}_+\frac{1}{E+\tilde{\omega}_{+,p}}\left(|\mathbf{J}_+|\sigma_0+\mathbf{J}_+\cdot\boldsymbol{\sigma}\right)+\tilde{b}_+\check{b}_+\frac{1}{E+\tilde{\omega}_{+,m}}\left(|\mathbf{J}_+|\sigma_0-\mathbf{J}_+\cdot\boldsymbol{\sigma}\right)\right]\\
=& \frac{\Delta_+^\dagger}{2}\left[\left(\frac{1}{E+\tilde{\omega}_{+,p}}+\frac{1}{E+\tilde{\omega}_{+,m}}\right)+\left(\frac{1}{E+\tilde{\omega}_{+,p}}-\frac{1}{E+\tilde{\omega}_{+,m}}\right)\frac{\mathbf{J}_+}{|\mathbf{J}_+|}\cdot\boldsymbol{\sigma}\right],
\end{aligned} \tag{C62}$$

$$\hat{\Theta}_- = \frac{\Delta_-}{2}\left[\left(\frac{1}{E+\tilde{\omega}_{-,p}}+\frac{1}{E+\tilde{\omega}_{-,m}}\right)+\left(\frac{1}{E+\tilde{\omega}_{-,p}}-\frac{1}{E+\tilde{\omega}_{-,m}}\right)\frac{\mathbf{J}_-}{|\mathbf{J}_-|}\cdot\boldsymbol{\sigma}^*\right]. \tag{C63}$$

If $\mathbf{F}_\pm + \mathbf{q}_\pm = 0$ is satisfied, from Eqs. (C6), (C7), (C24) and (C25), we obtain $\tilde{\omega}_{\pm,p} = \tilde{\omega}_{\pm,m}$ and

$$\hat{\Theta}_+ = \frac{\Delta_+^\dagger}{E+\tilde{\omega}_{+,p}}, \tag{C64}$$

$$\hat{\Theta}_- = \frac{\Delta_-}{E+\tilde{\omega}_{-,p}}. \tag{C65}$$

We solve for c and d from Eqs. (C51) and (C52),

$$\begin{aligned}
\begin{pmatrix} c \\ d \end{pmatrix} =& G^{-1}\left[e_\sigma + \begin{pmatrix} b_\sigma \\ a_\sigma \end{pmatrix}\right]\\
=& \begin{pmatrix} \sigma_0 & 0 \\ 0 & -\sigma_0 \end{pmatrix} G^{-1}\left[(1-iZ')e_\sigma - \begin{pmatrix} (1+iZ')\sigma_0 & 0 \\ 0 & (-1+iZ')\sigma_0 \end{pmatrix}\begin{pmatrix} b_\sigma \\ a_\sigma \end{pmatrix}\right].
\end{aligned}$$

Then we obtain a_σ and b_σ.

$$\begin{pmatrix} b_\sigma \\ a_\sigma \end{pmatrix} = \left[I_4 + G\begin{pmatrix} \sigma_0 & 0 \\ 0 & -\sigma_0 \end{pmatrix} G^{-1}\begin{pmatrix} (1+iZ')\sigma_0 & 0 \\ 0 & (-1+iZ')\sigma_0 \end{pmatrix}\right]^{-1}\left[-I_4 + (1-iZ')G\begin{pmatrix} \sigma_0 & 0 \\ 0 & -\sigma_0 \end{pmatrix} G^{-1}\right] e_\sigma, \tag{C66}$$

where I_4 is the 4×4 identity matrix. From the general relation of $2n\times 2n$ matrix,

$$
\begin{aligned}
&\begin{pmatrix} A & B \\ C & D \end{pmatrix}^{-1} \\
&= \begin{pmatrix} \left(A-BD^{-1}C\right)^{-1} & \left(C-DB^{-1}A\right)^{-1} \\ \left(B-AC^{-1}D\right)^{-1} & \left(D-CA^{-1}B\right)^{-1} \end{pmatrix}, \qquad \text{(C67)} \\
&\begin{pmatrix} A & B \\ C & D \end{pmatrix}\begin{pmatrix} \sigma_0 & 0 \\ 0 & -\sigma_0 \end{pmatrix}\begin{pmatrix} A & B \\ C & D \end{pmatrix}^{-1} \\
&= \begin{pmatrix} A\left(A-BD^{-1}C\right)^{-1}-B\left(B-AC^{-1}D\right)^{-1} & A\left(C-DB^{-1}A\right)^{-1}-B\left(D-CA^{-1}B\right)^{-1} \\ C\left(A-BD^{-1}C\right)^{-1}-D\left(B-AC^{-1}D\right)^{-1} & C\left(C-DB^{-1}A\right)^{-1}-D\left(D-CA^{-1}B\right)^{-1} \end{pmatrix} \\
&= \begin{pmatrix} \left(\sigma_0-BD^{-1}CA^{-1}\right)^{-1}-\left(\sigma_0-AC^{-1}DB^{-1}\right)^{-1} & \left(CA^{-1}-DB^{-1}\right)^{-1}-\left(DB^{-1}-CA^{-1}\right)^{-1} \\ \left(AC^{-1}-BD^{-1}\right)^{-1}-\left(BD^{-1}-AC^{-1}\right)^{-1} & \left(\sigma_0-DB^{-1}AC^{-1}\right)^{-1}-\left(\sigma_0-CA^{-1}BD^{-1}\right)^{-1} \end{pmatrix} \\
&= \begin{pmatrix} \left(\sigma_0-BD^{-1}CA^{-1}\right)^{-1}-\left[\sigma_0-\left(CA^{-1}\right)^{-1}\left(BD^{-1}\right)^{-1}\right]^{-1} & \\ & 2\left[\left(CA^{-1}\right)^{-1}-BD^{-1}\right]^{-1} \\ 2\left[CA^{-1}-\left(BD^{-1}\right)^{-1}\right]^{-1} & \\ & \left[\sigma_0-\left(BD^{-1}\right)^{-1}\left(CA^{-1}\right)^{-1}\right]^{-1}-\left(\sigma_0-CA^{-1}BD^{-1}\right)^{-1} \end{pmatrix} \\
&= \begin{pmatrix} \left(\sigma_0-BD^{-1}CA^{-1}\right)^{-1}\left(\sigma_0+BD^{-1}CA^{-1}\right) & -2\left(\sigma_0-BD^{-1}CA^{-1}\right)^{-1}BD^{-1} \\ 2\left(\sigma_0-CA^{-1}BD^{-1}\right)^{-1}CA^{-1} & -\left(\sigma_0-CA^{-1}BD^{-1}\right)^{-1}\left(\sigma_0+CA^{-1}BD^{-1}\right) \end{pmatrix}, \qquad \text{(C68)}
\end{aligned}
$$

where A, B, C and D are $n\times n$ regular matrices, we obtain the following relation

$$
G\begin{pmatrix} \sigma_0 & 0 \\ 0 & -\sigma_0 \end{pmatrix}G^{-1} = \begin{pmatrix} \left(\sigma_0-\hat{\Theta}_-\hat{\Theta}_+\right)^{-1}\left(\sigma_0+\hat{\Theta}_-\hat{\Theta}_+\right) & -2\left(\sigma_0-\hat{\Theta}_-\hat{\Theta}_+\right)^{-1}\hat{\Theta}_- \\ 2\left(\sigma_0-\hat{\Theta}_+\hat{\Theta}_-\right)^{-1}\hat{\Theta}_+ & -\left(\sigma_0-\hat{\Theta}_+\hat{\Theta}_-\right)^{-1}\left(\sigma_0+\hat{\Theta}_+\hat{\Theta}_-\right) \end{pmatrix}. \qquad \text{(C69)}
$$

Then, within the first brackets of Eq. (C66) becomes

$$
\begin{aligned}
&\left[I_4+G\begin{pmatrix} \sigma_0 & 0 \\ 0 & -\sigma_0 \end{pmatrix}G^{-1}\begin{pmatrix} (1+iZ')\sigma_0 & 0 \\ 0 & (-1+iZ')\sigma_0 \end{pmatrix}\right]^{-1} \\
&= \begin{pmatrix} \sigma_0+(1+iZ')\left(\sigma_0-\hat{\Theta}_-\hat{\Theta}_+\right)^{-1}\left(\sigma_0+\hat{\Theta}_-\hat{\Theta}_+\right) & -2(-1+iZ')\left(\sigma_0-\hat{\Theta}_-\hat{\Theta}_+\right)^{-1}\hat{\Theta}_- \\ 2(1+iZ')\left(\sigma_0-\hat{\Theta}_+\hat{\Theta}_-\right)^{-1}\hat{\Theta}_+ & \sigma_0-(-1+iZ')\left(\sigma_0-\hat{\Theta}_+\hat{\Theta}_-\right)^{-1}\left(\sigma_0+\hat{\Theta}_+\hat{\Theta}_-\right) \end{pmatrix}^{-1} \\
&= \begin{pmatrix} \left(\sigma_0-\hat{\Theta}_-\hat{\Theta}_+\right)^{-1}\left[\left(\sigma_0-\hat{\Theta}_-\hat{\Theta}_+\right)+(1+iZ')\left(\sigma_0+\hat{\Theta}_-\hat{\Theta}_+\right)\right] & \\ & -2(-1+iZ')\left(\sigma_0-\hat{\Theta}_-\hat{\Theta}_+\right)^{-1}\hat{\Theta}_- \\ 2(1+iZ')\left(\sigma_0-\hat{\Theta}_+\hat{\Theta}_-\right)^{-1}\hat{\Theta}_+ & \\ & \left(\sigma_0-\hat{\Theta}_+\hat{\Theta}_-\right)^{-1}\left[\left(\sigma_0-\hat{\Theta}_+\hat{\Theta}_-\right)-(-1+iZ')\left(\sigma_0+\hat{\Theta}_+\hat{\Theta}_-\right)\right] \end{pmatrix}^{-1} \\
&= \begin{pmatrix} \left(\sigma_0-\hat{\Theta}_-\hat{\Theta}_+\right)^{-1}\left[(2+iZ')\sigma_0+iZ'\hat{\Theta}_-\hat{\Theta}_+\right] & -2(-1+iZ')\left(\sigma_0-\hat{\Theta}_-\hat{\Theta}_+\right)^{-1}\hat{\Theta}_- \\ 2(1+iZ')\left(\sigma_0-\hat{\Theta}_+\hat{\Theta}_-\right)^{-1}\hat{\Theta}_+ & \left(\sigma_0-\hat{\Theta}_+\hat{\Theta}_-\right)^{-1}\left[(2-iZ')\sigma_0-iZ'\hat{\Theta}_+\hat{\Theta}_-\right] \end{pmatrix}^{-1} \qquad \text{(C70)}
\end{aligned}
$$

We define 2×2 matrices α_{ij} as

$$
\begin{pmatrix} \alpha_{11} & \alpha_{12} \\ \alpha_{21} & \alpha_{22} \end{pmatrix} = \left[I_4+G\begin{pmatrix} \sigma_0 & 0 \\ 0 & -\sigma_0 \end{pmatrix}G^{-1}\begin{pmatrix} (1+iZ')\sigma_0 & 0 \\ 0 & (-1+iZ')\sigma_0 \end{pmatrix}\right]^{-1}. \qquad \text{(C71)}
$$

From Eq. (C67), α_{11} is obtained,

$$\begin{aligned}\alpha_{11} =& \left(\left(\sigma_0 - \hat{\Theta}_-\hat{\Theta}_+\right)^{-1} \left[(2+iZ')\sigma_0 + iZ'\hat{\Theta}_-\hat{\Theta}_+\right] - \left[-2(-1+iZ')\left(\sigma_0 - \hat{\Theta}_-\hat{\Theta}_+\right)^{-1}\hat{\Theta}_-\right] \right. \\ & \left. \times \left\{ \left(\sigma_0 - \hat{\Theta}_+\hat{\Theta}_-\right)^{-1} \left[(2-iZ')\sigma_0 - iZ'\hat{\Theta}_+\hat{\Theta}_-\right] \right\}^{-1} 2(1+iZ') \left(\sigma_0 - \hat{\Theta}_+\hat{\Theta}_-\right)^{-1} \hat{\Theta}_+ \right)^{-1} \\ =& \left\{ \left[(2+iZ')\sigma_0 + iZ'\hat{\Theta}_-\hat{\Theta}_+\right] - \left[-2(-1+iZ')\hat{\Theta}_-\right] \left[(2-iZ')\sigma_0 - iZ'\hat{\Theta}_+\hat{\Theta}_-\right]^{-1} 2(1+iZ')\hat{\Theta}_+ \right\}^{-1} \left(\sigma_0 - \hat{\Theta}_-\hat{\Theta}_+\right). \end{aligned} \tag{C72}$$

Using the relation

$$\begin{aligned} A(\sigma_0 + BA)^{-1}B =& \left[B^{-1}(\sigma_0 + BA)A^{-1}\right]^{-1} \\ =& \left[(AB)^{-1} + \sigma_0\right]^{-1} \\ =& (\sigma_0 + AB)^{-1}(\sigma_0 + AB - \sigma_0) \\ =& \sigma_0 - (\sigma_0 + AB)^{-1}, \end{aligned} \tag{C73}$$

where A and B are any 2×2 matrices, the second term in the first brackets of Eq. (C72) is given by

$$\begin{aligned} \left[-2(-1+iZ')\hat{\Theta}_-\right] \left[(2-iZ')\sigma_0 - iZ'\hat{\Theta}_+\hat{\Theta}_-\right]^{-1} 2(1+iZ')\hat{\Theta}_+ =& 4\frac{1+Z'^2}{2-iZ'}\hat{\Theta}_- \left(\sigma_0 + \frac{-iZ'}{2-iZ'}\hat{\Theta}_+\hat{\Theta}_-\right)^{-1}\hat{\Theta}_+ \\ =& 4\frac{1+Z'^2}{-iZ'}\left[\sigma_0 - \left(\sigma_0 + \frac{-iZ'}{2-iZ'}\hat{\Theta}_-\hat{\Theta}_+\right)^{-1}\right]. \end{aligned} \tag{C74}$$

Using above equation, Eq. (C72) becomes

$$\begin{aligned}\alpha_{11} =& \left\{ \left[(2+iZ')\sigma_0 + iZ'\hat{\Theta}_-\hat{\Theta}_+\right] - 4\frac{1+Z'^2}{-iZ'}\left[\sigma_0 - \left(\sigma_0 + \frac{-iZ'}{2-iZ'}\hat{\Theta}_-\hat{\Theta}_+\right)^{-1}\right] \right\}^{-1} \left(\sigma_0 - \hat{\Theta}_-\hat{\Theta}_+\right) \\ =& \left\{ \left(\sigma_0 + \frac{-iZ'}{2-iZ'}\hat{\Theta}_-\hat{\Theta}_+\right) \left[(2+iZ')\sigma_0 + iZ'\hat{\Theta}_-\hat{\Theta}_+ - 4\frac{1+Z'^2}{-iZ'}\sigma_0\right] + 4\frac{1+Z'^2}{-iZ'}\sigma_0 \right\}^{-1} \\ & \times \left(\sigma_0 + \frac{-iZ'}{2-iZ'}\hat{\Theta}_-\hat{\Theta}_+\right)\left(\sigma_0 - \hat{\Theta}_-\hat{\Theta}_+\right) \\ =& (2-iZ')\left[Z'^2\hat{\Theta}_-\hat{\Theta}_+ - (4+Z'^2)\sigma_0\right]^{-1} \left(\hat{\Theta}_-\hat{\Theta}_+ - \sigma_0\right)^{-1} \left(\sigma_0 + \frac{-iZ'}{2-iZ'}\hat{\Theta}_-\hat{\Theta}_+\right)\left(\sigma_0 - \hat{\Theta}_-\hat{\Theta}_+\right). \end{aligned} \tag{C75}$$

Also

$$
\begin{aligned}
\alpha_{22} =& \Bigg(\left(\sigma_0 - \hat{\Theta}_+\hat{\Theta}_-\right)^{-1} \left[(2-iZ')\sigma_0 - iZ'\hat{\Theta}_+\hat{\Theta}_-\right] - \left[2(1+iZ')(\sigma_0 - \hat{\Theta}_+\hat{\Theta}_-)^{-1}\hat{\Theta}_+\right] \\
& \times \left\{(\sigma_0 - \hat{\Theta}_-\hat{\Theta}_+)^{-1}[(2+iZ')\sigma_0 + iZ'\hat{\Theta}_-\hat{\Theta}_+]\right\}^{-1} \left[-2(-1+iZ')(\sigma_0 - \hat{\Theta}_-\hat{\Theta}_+)^{-1}\hat{\Theta}_-\right]\Bigg)^{-1} \\
=& \left\{ \left[(2-iZ')\sigma_0 - iZ'\hat{\Theta}_+\hat{\Theta}_-\right] - \left[2(1+iZ')\hat{\Theta}_+\right] \left[(2+iZ')\sigma_0 + iZ'\hat{\Theta}_-\hat{\Theta}_+\right]^{-1} \left[-2(-1+iZ')\hat{\Theta}_-\right] \right\}^{-1} \left(\sigma_0 - \hat{\Theta}_+\hat{\Theta}_-\right) \\
=& \left\{ \left[(2-iZ')\sigma_0 - iZ'\hat{\Theta}_+\hat{\Theta}_-\right] - \frac{4(1+Z'^2)}{2+iZ'}\hat{\Theta}_+ \left[\sigma_0 + \frac{iZ'}{2+iZ'}\hat{\Theta}_-\hat{\Theta}_+\right]^{-1} \hat{\Theta}_- \right\}^{-1} \left(\sigma_0 - \hat{\Theta}_+\hat{\Theta}_-\right) \\
=& \left\{ \left[(2-iZ')\sigma_0 - iZ'\hat{\Theta}_+\hat{\Theta}_-\right] - \frac{4(1+Z'^2)}{iZ'} \left[\sigma_0 - \left(\sigma_0 + \frac{iZ'}{2+iZ'}\hat{\Theta}_+\hat{\Theta}_-\right)^{-1}\right] \right\}^{-1} \left(\sigma_0 - \hat{\Theta}_+\hat{\Theta}_-\right) \\
=& \left\{ \left(\sigma_0 + \frac{iZ'}{2+iZ'}\hat{\Theta}_+\hat{\Theta}_-\right) \left[(2-iZ')\sigma_0 - iZ'\hat{\Theta}_+\hat{\Theta}_- - \frac{4(1+Z'^2)}{iZ'}\right] + \frac{4(1+Z'^2)}{iZ'}\sigma_0 \right\}^{-1} \\
& \times \left(\sigma_0 + \frac{iZ'}{2+iZ'}\hat{\Theta}_+\hat{\Theta}_-\right) \left(\sigma_0 - \hat{\Theta}_+\hat{\Theta}_-\right) \\
=& (2+iZ') \left[Z'^2\hat{\Theta}_+\hat{\Theta}_- - (4+Z'^2)\sigma_0\right]^{-1} \left(\hat{\Theta}_+\hat{\Theta}_- - \sigma_0\right)^{-1} \left(\sigma_0 + \frac{iZ'}{2+iZ'}\hat{\Theta}_+\hat{\Theta}_-\right) \left(\sigma_0 - \hat{\Theta}_+\hat{\Theta}_-\right). \qquad \text{(C76)}
\end{aligned}
$$

Next, we obtain

$$
\begin{aligned}
\alpha_{12} =& \Bigg\{ 2(1+iZ') \left(\sigma_0 - \hat{\Theta}_+\hat{\Theta}_-\right)^{-1} \hat{\Theta}_+ - \left(\sigma_0 - \hat{\Theta}_+\hat{\Theta}_-\right)^{-1} \left[(2-iZ')\sigma_0 - iZ'\hat{\Theta}_+\hat{\Theta}_-\right] \\
& \times \left[-2(-1+iZ') \left(\sigma_0 - \hat{\Theta}_-\hat{\Theta}_+\right)^{-1} \hat{\Theta}_-\right]^{-1} \left(\sigma_0 - \hat{\Theta}_-\hat{\Theta}_+\right)^{-1} \left[(2+iZ')\sigma_0 + iZ'\hat{\Theta}_-\hat{\Theta}_+\right] \Bigg\}^{-1} \\
=& \left\{ 2(1+iZ')\hat{\Theta}_+ - \left[(2-iZ')\sigma_0 - iZ'\hat{\Theta}_+\hat{\Theta}_-\right] \left[-2(-1+iZ')\hat{\Theta}_-\right]^{-1} \left[(2+iZ')\sigma_0 + iZ'\hat{\Theta}_-\hat{\Theta}_+\right] \right\}^{-1} \left(\sigma_0 - \hat{\Theta}_+\hat{\Theta}_-\right) \\
=& 2(-1+iZ') \left\{ -4(1+Z'^2)\hat{\Theta}_+ + \left[(2-iZ')\sigma_0 - iZ'\hat{\Theta}_+\hat{\Theta}_-\right] \hat{\Theta}_-^{-1} \left[(2+iZ')\sigma_0 + iZ'\hat{\Theta}_-\hat{\Theta}_+\right] \right\}^{-1} \left(\sigma_0 - \hat{\Theta}_+\hat{\Theta}_-\right) \\
=& 2(-1+iZ') \left[-4(1+Z'^2)\hat{\Theta}_+ + (4+Z'^2)\hat{\Theta}_-^{-1} + 2Z'^2\hat{\Theta}_+ + Z'^2\hat{\Theta}_+\hat{\Theta}_-\hat{\Theta}_+ \right]^{-1} \left(\sigma_0 - \hat{\Theta}_+\hat{\Theta}_-\right) \\
=& 2(-1+iZ') \left[-2(2+Z'^2)\hat{\Theta}_-\hat{\Theta}_+ + (4+Z'^2) + Z'^2\hat{\Theta}_-\hat{\Theta}_+\hat{\Theta}_-\hat{\Theta}_+ \right]^{-1} \hat{\Theta}_- \left(\sigma_0 - \hat{\Theta}_+\hat{\Theta}_-\right) \\
=& 2(-1+iZ') \left[(4+Z'^2)\sigma_0 - Z'^2\hat{\Theta}_-\hat{\Theta}_+\right]^{-1} \left(\sigma_0 - \hat{\Theta}_-\hat{\Theta}_+\right)^{-1} \hat{\Theta}_- \left(\sigma_0 - \hat{\Theta}_+\hat{\Theta}_-\right), \qquad \text{(C77)}
\end{aligned}
$$

$$
\begin{aligned}
\alpha_{21} =& \Bigg\{ -2(-1+iZ') \left(\sigma_0 - \hat{\Theta}_-\hat{\Theta}_+\right)^{-1} \hat{\Theta}_- - \left(\sigma_0 - \hat{\Theta}_-\hat{\Theta}_+\right)^{-1} \left[(2+iZ')\sigma_0 + iZ'\hat{\Theta}_-\hat{\Theta}_+\right] \\
& \times \left[2(1+iZ') \left(\sigma_0 - \hat{\Theta}_+\hat{\Theta}_-\right)^{-1} \hat{\Theta}_+\right]^{-1} \left(\sigma_0 - \hat{\Theta}_+\hat{\Theta}_-\right)^{-1} \left[(2-iZ')\sigma_0 - iZ'\hat{\Theta}_+\hat{\Theta}_-\right] \Bigg\}^{-1} \\
=& \left\{ -2(-1+iZ')\hat{\Theta}_- - \left[(2+iZ')\sigma_0 + iZ'\hat{\Theta}_-\hat{\Theta}_+\right] \left[2(1+iZ')\hat{\Theta}_+\right]^{-1} \left[(2-iZ')\sigma_0 - iZ'\hat{\Theta}_+\hat{\Theta}_-\right] \right\}^{-1} \left(\sigma_0 - \hat{\Theta}_-\hat{\Theta}_+\right) \\
=& 2(1+iZ') \left\{ 4(1+Z'^2)\hat{\Theta}_- - \left[(2+iZ')\sigma_0 + iZ'\hat{\Theta}_-\hat{\Theta}_+\right] \hat{\Theta}_+^{-1} \left[(2-iZ')\sigma_0 - iZ'\hat{\Theta}_+\hat{\Theta}_-\right] \right\}^{-1} \left(\sigma_0 - \hat{\Theta}_-\hat{\Theta}_+\right) \\
=& -2(1+iZ') \left[(4+Z'^2)\sigma_0 - Z'^2\hat{\Theta}_+\hat{\Theta}_-\right]^{-1} \left(\sigma_0 - \hat{\Theta}_+\hat{\Theta}_-\right)^{-1} \hat{\Theta}_+ \left(\sigma_0 - \hat{\Theta}_-\hat{\Theta}_+\right). \qquad \text{(C78)}
\end{aligned}
$$

Then in the second brackets of Eq. (C66) becomes

$$
\begin{aligned}
&\left[-I_4+(1-iZ')G\begin{pmatrix}\sigma_0 & 0\\ 0 & -\sigma_0\end{pmatrix}G^{-1}\right]\\
=&\begin{pmatrix}
-\sigma_0+(1-iZ')\left(\sigma_0-\hat{\Theta}_-\hat{\Theta}_+\right)^{-1}\left(\sigma_0+\hat{\Theta}_-\hat{\Theta}_+\right) & -2(1-iZ')\left(\sigma_0-\hat{\Theta}_-\hat{\Theta}_+\right)^{-1}\hat{\Theta}_-\\
2(1-iZ')\left(\sigma_0-\hat{\Theta}_+\hat{\Theta}_-\right)^{-1}\hat{\Theta}_+ & -\sigma_0-(1-iZ')\left(\sigma_0-\hat{\Theta}_+\hat{\Theta}_-\right)^{-1}\left(\sigma_0+\hat{\Theta}_+\hat{\Theta}_-\right)
\end{pmatrix}\\
=&\begin{pmatrix}
\left(\sigma_0-\hat{\Theta}_-\hat{\Theta}_+\right)^{-1}\left[-iZ'\sigma_0+(2-iZ')\hat{\Theta}_-\hat{\Theta}_+\right] & -2(1-iZ')\left(\sigma_0-\hat{\Theta}_-\hat{\Theta}_+\right)^{-1}\hat{\Theta}_-\\
2(1-iZ')\left(\sigma_0-\hat{\Theta}_+\hat{\Theta}_-\right)^{-1}\hat{\Theta}_+ & -\left(\sigma_0-\hat{\Theta}_+\hat{\Theta}_-\right)^{-1}\left[(2-iZ')\sigma_0+-iZ'\hat{\Theta}_+\hat{\Theta}_-\right]
\end{pmatrix}.
\end{aligned}
\tag{C79}
$$

Finally, b_σ and a_σ are obtained

$$
\begin{aligned}
b_\sigma =&(2-iZ')\left[Z'^2\hat{\Theta}_-\hat{\Theta}_+-(4+Z'^2)\sigma_0\right]^{-1}\left(\hat{\Theta}_-\hat{\Theta}_+-\sigma_0\right)^{-1}\left(\sigma_0+\frac{-iZ'}{2-iZ'}\hat{\Theta}_-\hat{\Theta}_+\right)\left(\sigma_0-\hat{\Theta}_-\hat{\Theta}_+\right)\\
&\times\left(\sigma_0-\hat{\Theta}_-\hat{\Theta}_+\right)^{-1}\left[-iZ'\sigma_0+(2-iZ')\hat{\Theta}_-\hat{\Theta}_+\right]\tilde{e}_\sigma\\
&+2(-1+iZ')\left[(4+Z'^2)\sigma_0-Z'^2\hat{\Theta}_-\hat{\Theta}_+\right]^{-1}\left(\sigma_0-\hat{\Theta}_-\hat{\Theta}_+\right)^{-1}\hat{\Theta}_-\left(\sigma_0-\hat{\Theta}_+\hat{\Theta}_-\right)2(1-iZ')\left(\sigma_0-\hat{\Theta}_+\hat{\Theta}_-\right)^{-1}\hat{\Theta}_+\tilde{e}_\sigma\\
=&(2-iZ')\left[Z'^2\hat{\Theta}_-\hat{\Theta}_+-(4+Z'^2)\sigma_0\right]^{-1}\left(\hat{\Theta}_-\hat{\Theta}_+-\sigma_0\right)^{-1}\left(\sigma_0+\frac{-iZ'}{2-iZ'}\hat{\Theta}_-\hat{\Theta}_+\right)\left[-iZ'\sigma_0+(2-iZ')\hat{\Theta}_-\hat{\Theta}_+\right]\tilde{e}_\sigma\\
&+2(-1+iZ')\left[(4+Z'^2)\sigma_0-Z'^2\hat{\Theta}_-\hat{\Theta}_+\right]^{-1}\left(\sigma_0-\hat{\Theta}_-\hat{\Theta}_+\right)^{-1}\hat{\Theta}_-2(1-iZ')\hat{\Theta}_+\tilde{e}_\sigma\\
=&\left[(4+Z'^2)\sigma_0-Z'^2\hat{\Theta}_-\hat{\Theta}_+\right]^{-1}\left(\sigma_0-\hat{\Theta}_-\hat{\Theta}_+\right)^{-1}\\
&\times\left\{(2-iZ')\left(\sigma_0+\frac{-iZ'}{2-iZ'}\hat{\Theta}_-\hat{\Theta}_+\right)\left[-iZ'\sigma_0+(2-iZ')\hat{\Theta}_-\hat{\Theta}_+\right]+2(-1+iZ')\hat{\Theta}_-2(1-iZ')\hat{\Theta}_+\right\}\tilde{e}_\sigma\\
=&-iZ'(2-iZ')\left[(4+Z'^2)\sigma_0-Z'^2\hat{\Theta}_-\hat{\Theta}_+\right]^{-1}\left(\sigma_0-\hat{\Theta}_-\hat{\Theta}_+\right)^{-1}\left(\sigma_0-\hat{\Theta}_-\hat{\Theta}_+\right)^{2}\tilde{e}_\sigma\\
=&\frac{-iZ'}{2+iZ'}\left(\sigma_0-\hat{\Theta}_-\hat{\Theta}_+\right)\left[\sigma_0-(1-\sigma_{\rm N})\hat{\Theta}_-\hat{\Theta}_+\right]^{-1}\tilde{e}_\sigma,
\end{aligned}
\tag{C80}
$$

$$
\begin{aligned}
a_\sigma =&-2(1+iZ')\left[(4+Z'^2)\sigma_0-Z'^2\hat{\Theta}_+\hat{\Theta}_-\right]^{-1}\left(\sigma_0-\hat{\Theta}_+\hat{\Theta}_-\right)^{-1}\hat{\Theta}_+\left(\sigma_0-\hat{\Theta}_-\hat{\Theta}_+\right)\\
&\times(\sigma_0-\hat{\Theta}_-\hat{\Theta}_+)^{-1}\left[-iZ'\sigma_0+(2-iZ')\hat{\Theta}_-\hat{\Theta}_+\right]\tilde{e}_\sigma\\
&+(2+iZ')\left[Z'^2\hat{\Theta}_+\hat{\Theta}_--(4+Z'^2)\sigma_0\right]^{-1}\left(\hat{\Theta}_+\hat{\Theta}_--\sigma_0\right)^{-1}\left(\sigma_0+\frac{iZ'}{2+iZ'}\hat{\Theta}_+\hat{\Theta}_-\right)\left(\sigma_0-\hat{\Theta}_+\hat{\Theta}_-\right)\\
&\times 2(1-iZ')(\sigma_0-\hat{\Theta}_+\hat{\Theta}_-)^{-1}\hat{\Theta}_+\tilde{e}_\sigma\\
=&\left[(4+Z'^2)\sigma_0-Z'^2\hat{\Theta}_+\hat{\Theta}_-\right]^{-1}\left(\sigma_0-\hat{\Theta}_+\hat{\Theta}_-\right)^{-1}\\
&\times\left\{-2(1+iZ')\left[-iZ'\sigma_0+(2-iZ')\hat{\Theta}_+\hat{\Theta}_-\right]+(2+iZ')\left(\sigma_0+\frac{iZ'}{2+iZ'}\hat{\Theta}_+\hat{\Theta}_-\right)2(1-iZ')\right\}\hat{\Theta}_+\tilde{e}_\sigma\\
=&4\left[(4+Z'^2)\sigma_0-Z'^2\hat{\Theta}_+\hat{\Theta}_-\right]^{-1}\left(\sigma_0-\hat{\Theta}_+\hat{\Theta}_-\right)^{-1}\left(\sigma_0-\hat{\Theta}_+\hat{\Theta}_-\right)\hat{\Theta}_+\tilde{e}_\sigma\\
=&\sigma_{\rm N}\hat{\Theta}_+\left[\sigma_0-(1-\sigma_{\rm N})\hat{\Theta}_-\hat{\Theta}_+\right]^{-1}\tilde{e}_\sigma,
\end{aligned}
\tag{C81}
$$

where $\tilde{e}_\sigma$ is defined by $e_\sigma^{\rm T}=(\tilde{e}_\sigma^{\rm T},0,0)$. Here, we define 2×2 matrices a and b as

$$
a=\begin{pmatrix}a_\uparrow & a_\downarrow\end{pmatrix},
\tag{C82}
$$

$$
b=\begin{pmatrix}b_\uparrow & b_\downarrow\end{pmatrix}.
\tag{C83}
$$

Then a general formula of tunneling conductance is expressed compactly by using $\hat{\Theta}_+$ and $\hat{\Theta}_-$.

$$\begin{aligned}
\sigma_{\rm S} =&\frac{1}{2}\sum_{\sigma}\left[1+a_\sigma^\dagger a_\sigma - b_\sigma^\dagger b_\sigma\right]\\
=&\frac{1}{2}{\rm Tr}\left[\sigma_0 + a^\dagger a - b^\dagger b\right]\\
=&\frac{1}{2}{\rm Tr}\Big\{\sigma_0+\sigma_{\rm N}^2\left[\sigma_0-(1-\sigma_{\rm N})\hat{\Theta}_+^\dagger\hat{\Theta}_-^\dagger\right]^{-1}\hat{\Theta}_+^\dagger\hat{\Theta}_+\left[\sigma_0-(1-\sigma_{\rm N})\hat{\Theta}_-\hat{\Theta}_+\right]^{-1}\\
&-(1-\sigma_{\rm N})\left[\sigma_0-(1-\sigma_{\rm N})\hat{\Theta}_+^\dagger\hat{\Theta}_-^\dagger\right]^{-1}\left(\sigma_0-\hat{\Theta}_+^\dagger\hat{\Theta}_-^\dagger\right)\left(\sigma_0-\hat{\Theta}_-\hat{\Theta}_+\right)\left[\sigma_0-(1-\sigma_{\rm N})\hat{\Theta}_-\hat{\Theta}_+\right]^{-1}\Big\}\\
=&\frac{1}{2}{\rm Tr}\Big(\left[\sigma_0-(1-\sigma_{\rm N})\hat{\Theta}_+^\dagger\hat{\Theta}_-^\dagger\right]^{-1}\\
&\times\Big\{\left[\sigma_0-(1-\sigma_{\rm N})\hat{\Theta}_+^\dagger\hat{\Theta}_-^\dagger\right]\left[\sigma_0-(1-\sigma_{\rm N})\hat{\Theta}_-\hat{\Theta}_+\right]+\sigma_{\rm N}^2\hat{\Theta}_+^\dagger\hat{\Theta}_+-(1-\sigma_{\rm N})\left(\sigma_0-\hat{\Theta}_+^\dagger\hat{\Theta}_-^\dagger\right)\left(\sigma_0-\hat{\Theta}_-\hat{\Theta}_+\right)\Big\}\\
&\times\left[\sigma_0-(1-\sigma_{\rm N})\hat{\Theta}_-\hat{\Theta}_+\right]^{-1}\Big)\\
=&\frac{\sigma_{\rm N}}{2}{\rm Tr}\left\{\left[\sigma_0-(1-\sigma_{\rm N})\hat{\Theta}_+^\dagger\hat{\Theta}_-^\dagger\right]^{-1}\left[\sigma_0+\sigma_{\rm N}\hat{\Theta}_+^\dagger\hat{\Theta}_+ +(\sigma_{\rm N}-1)\hat{\Theta}_+^\dagger\hat{\Theta}_-^\dagger\hat{\Theta}_-\hat{\Theta}_+\right]\left[\sigma_0-(1-\sigma_{\rm N})\hat{\Theta}_-\hat{\Theta}_+\right]^{-1}\right\}. \qquad \text{(C84)}
\end{aligned}$$

4. Spin rotation

In this subsection, we explain that the conductance is invariant under the spin rotation. Under the spin rotation ($\Psi\to U\Psi$),

$$U=\begin{pmatrix}R&0\\0&R^*\end{pmatrix}, \qquad \text{(C85)}$$

$$R=e^{-i\boldsymbol{\theta}\cdot\boldsymbol{\sigma}/2}, \qquad \text{(C86)}$$

pair potential $\Delta_\pm$ and $\mathbf{J}_\pm$ are transformed as

$$\Delta_\pm \to R\Delta_\pm R^{\rm T} \qquad \text{(C87)}$$

$$\mathbf{J}_+\cdot\boldsymbol{\sigma}\to R\mathbf{J}_+\cdot\boldsymbol{\sigma}R^\dagger, \qquad \text{(C88)}$$

$$\mathbf{J}_-\cdot\boldsymbol{\sigma}^*\to R^*\mathbf{J}_-\cdot\boldsymbol{\sigma}^*R^{\rm T}. \qquad \text{(C89)}$$

These relations come from following relations.

$$D_\pm\to D_\pm, \qquad \text{(C90)}$$

$$\mathbf{d}_\pm\cdot\boldsymbol{\sigma}\to R\mathbf{d}_\pm\cdot\boldsymbol{\sigma}R^\dagger, \qquad \text{(C91)}$$

$$\mathbf{d}_\pm^*\cdot\boldsymbol{\sigma}=(\mathbf{d}_\pm\cdot\boldsymbol{\sigma})^\dagger\to R\mathbf{d}_\pm^*\cdot\boldsymbol{\sigma}R^\dagger, \qquad \text{(C92)}$$

$$i\mathbf{d}_\pm\times\mathbf{d}_\pm^*\cdot\boldsymbol{\sigma}=(\mathbf{d}_\pm\cdot\boldsymbol{\sigma})(\mathbf{d}_\pm^*\cdot\boldsymbol{\sigma})-|\mathbf{d}_\pm|^2\sigma_0\to R(i\mathbf{d}_\pm\times\mathbf{d}_\pm^*\cdot\boldsymbol{\sigma})R^\dagger. \qquad \text{(C93)}$$

It is noted that R does not depend on the subscript $\pm$.

$\hat{\Theta}_\pm$ is transformed as

$$\begin{aligned}
\hat{\Theta}_+\to&\frac{R^*\Delta_+^\dagger R^\dagger}{2}\left[\left(\frac{1}{E+\omega_{+,p}}+\frac{1}{E+\omega_{+,m}}\right)+\left(\frac{1}{E+\omega_{+,p}}-\frac{1}{E+\omega_{+,m}}\right)\frac{R\mathbf{J}_+\cdot\boldsymbol{\sigma}R^\dagger}{|\mathbf{J}_+|}\right]\\
=&R^*\hat{\Theta}_+R^\dagger, \qquad \text{(C94)}\\
\hat{\Theta}_-\to&\frac{R\Delta_-R^{\rm T}}{2}\left[\left(\frac{1}{E+\omega_{-,p}}+\frac{1}{E+\omega_{-,m}}\right)+\left(\frac{1}{E+\omega_{-,p}}-\frac{1}{E+\omega_{-,m}}\right)\frac{R^*\mathbf{J}_-\cdot\boldsymbol{\sigma}^*R^{\rm T}}{|\mathbf{J}_-|}\right]\\
=&R\hat{\Theta}_-R^{\rm T}. \qquad \text{(C95)}\\
& \qquad \text{(C96)}
\end{aligned}$$

Then the conductance is invariant under the spin rotation.

$$\begin{aligned}\sigma_{\mathrm{S}} \to & \mathrm{Tr}\left[\sigma_0-(1-\sigma_{\mathrm{N}})R\hat{\Theta}_+^\dagger R^{\mathrm{T}}R^*\hat{\Theta}_-^\dagger R^\dagger\right]^{-1}\left[1+\sigma_{\mathrm{N}}R\hat{\Theta}_+^\dagger R^{\mathrm{T}}R^*\hat{\Theta}_+R^\dagger+(\sigma_{\mathrm{N}}-1)R\hat{\Theta}_+^\dagger R^{\mathrm{T}}R^*\hat{\Theta}_-^\dagger R^\dagger R\hat{\Theta}_-R^{\mathrm{T}}R^*\hat{\Theta}_+R^\dagger\right]\\ &\left[\sigma_0-(1-\sigma_{\mathrm{N}})R\hat{\Theta}_-R^{\mathrm{T}}R^*\hat{\Theta}_+R^\dagger\right]^{-1}\\ =&\mathrm{Tr}R\left[\sigma_0-(1-\sigma_{\mathrm{N}})\hat{\Theta}_+^\dagger\hat{\Theta}_-^\dagger\right]^{-1}R^\dagger R\left[1+\sigma_{\mathrm{N}}\hat{\Theta}_+^\dagger\hat{\Theta}_++(\sigma_{\mathrm{N}}-1)\hat{\Theta}_+^\dagger\hat{\Theta}_-^\dagger\hat{\Theta}_-\hat{\Theta}_+\right]R^\dagger R\left[\sigma_0-(1-\sigma_{\mathrm{N}})\hat{\Theta}_-\hat{\Theta}_+\right]^{-1}R^\dagger\\ =&\sigma_{\mathrm{S}}. \end{aligned} \tag{C97}$$